THE
PHYSICAL REVIEW
*A Journal of Experimental and Theoretical Physics Established by E. L. Nichols in 1893*
VOL. 51, NO. 1 JANUARY 1, 1937 SECOND SERIES

# The Beta-Ray Spectra of Radium E and Radioactive Phosphorus

ERNEST M. LYMAN, *Radiation Laboratory, Department of Physics, University of California, Berkeley*
(Received October 27, 1936)

The beta-ray spectra of Ra E and $P^{32}$ were obtained by means of a magnetic spectrometer of high resolution. The observed end points of the spectra of Ra E and $P^{32}$ are at $5280 \pm 20\ H\rho$ (1.15 Mev) and $7150 \pm 100\ H\rho$ (1.69 Mev), respectively. The end points obtained by extrapolating the Konopinski-Uhlenbeck plots are in each case about 17 percent greater than the observed ones, indicating that for some spectra these plots should not be used to determine the upper limits.

## INTRODUCTION

SEVERAL attempts have been made to formulate a theory of beta-decay which would predict closely the observed form of the continuous momentum distribution spectrum of electrons emitted from a radioactive substance. One of the recent and most successful ones is due to Konopinski and Uhlenbeck[1] and is a modification of Fermi's theory.[2] Many observers have found that the shape of the distribution obtained from the K–U theory was in fair accord with the experimentally determined shape over the major portion of the spectrum. By assuming that the K–U theory was correct over the whole spectrum, it was then possible to extrapolate data taken over the middle portion of the spectrum to give the end point of the spectrum. In order to test the validity of the K–U prediction of the end point, a study of the spectra of radium E and radioactive phosphorus, $P^{32}$, both emitting electrons only, was undertaken by means of a spectrometer of high resolution.[3]

[1] E. J. Konopinski and G. E. Uhlenbeck, Phys. Rev. **48**, 7 (1935).
[2] E. Fermi, Zeits. f. Physik **88**, 161 (1934).
[3] E. M. Lyman, Phys. Rev. **50**, 385 (1936).

## APPARATUS AND EXPERIMENTAL METHOD

A diagram of the magnetic spectrometer is shown in Fig. 1. The radioactive material, deposited on a plate or foil, was placed inside an aluminum box at $O$, and tipped at an angle of 45° to the plane of $AD$. Beta-particles passing through the incident slit, $AB$ (2 mm wide, 8 mm long) into the evacuated chamber, were acted upon by a magnetic field, $H$, perpendicular to the chamber, so that their paths became circular. Particles of the proper momentum (proportional to $H\rho$) arrived at the counter slit, $CD$ (4 mm wide, 8 mm long). The distance $BD$ was 30.00 cm, making the minimum radius of curvature, $\rho$, of particles admitted to the counter slit 14.80 cm. The maximum radius of curvature, defined by the stops, $E$, $F$, was 15.20 cm. The separation of the aluminum-lined flat sides of the chamber was 14 mm. Auxiliary aluminum stops were located on the sides and on the top, $BEC$, and bottom, $AFD$, to prevent particles outside the proper $\delta\rho$ interval from being scattered from the walls into the counter slit. The stops were constructed so as to present a minimum of scattering material to the beam, coupled with a thickness sufficient to absorb completely 2 Mev electrons. The depth of

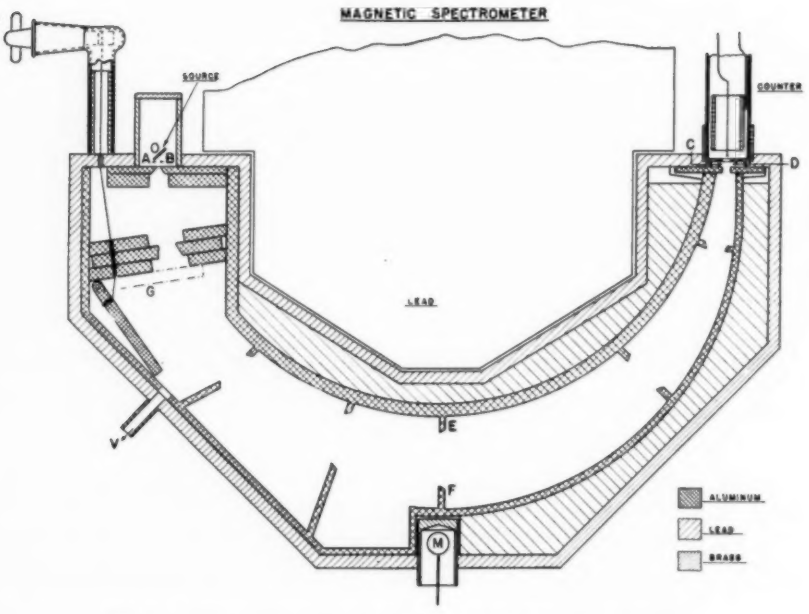


FIG. 1. Magnetic spectrometer for obtaining the beta-ray spectrum.

the beam was 8 mm. The particles passing through *CD* entered a Geiger counter which was connected to a three stage amplifier and a recording circuit capable of recording 60 counts per second. An aluminum gate, *G*, could be raised to cut off the beam in order to obtain the background count. Since the spectrometer was designed for use with a source emitting $\gamma$-rays as well as electrons, lead shielding was placed as shown to protect the counter from direct and scattered radiation. The chamber was evacuated through the outlet, *V*, by a Cenco Hyvac pump kept running continuously throughout the experiments.

In order to measure the magnetic field, a small flip coil, connected to a ballistic galvanometer, was inserted into the cavity, *M*. The system was calibrated by connecting the secondary of a standard Leeds and Northrup 50 millihenry mutual inductance in series and obtaining galvanometer deflections due to reversing measured currents in the primary. Then, from the dimensions of the flip coil, the value of *H* corresponding to any deflection produced by flipping the coil through 180° in a field could be computed. As a check upon this calibration, deflections of the galvanometer were compared with the expected deflections when the coil was flipped in the field at the center of a long solenoid through which a measured current flowed. For an absolute calibration, both methods required a knowledge of the absolute values of the currents. In this case it was considered sufficiently reliable to measure the currents by passing them through a standard resistance and comparing the potential differences produced with the e.m.f.'s of several Weston standard cells. A further check was made by comparing the expected deflections with those produced in strong fields previously calibrated by a bismuth spiral. All three methods agreed to within 0.3 percent. The magnetic field was measured for each point on the following curves, and the probable error is estimated to be well within $\pm 0.25$ percent of *H*.

The field, produced by a half-ton electromagnet, was mapped over all the region traversed by the particles and found to be homogeneous to within 0.5 percent up to a distance of 1 cm below the incident and exodus slits. At the slit position it was 4 percent lower than at *M*. By applying

Hartree's[4] correction to the nonhomogeneous field, it was found that the effective correction, $DH_0$, to be applied to $H$, the value of the field measured at $M$, was $-0.23$ percent. Furthermore, it was observed that the relative inhomogeneities in the field-map were constant for all values of $H$ in the range employed; therefore, this correction applied throughout.

The counter above $CD$ was in a weak part of the magnetic field due to the fringing flux at the edges of the poles. By varying the magnetic field and observing that the counting rate due to a nearby $\gamma$-ray source remained constant, it was concluded that the variations in the field had no effect upon the counter. The field-map showed that the beta-particles always traversed the same region of the counter regardless of the value of the field. The counter and counting system were operated in a "plateau" region and were tested for variation in counting efficiency at different observed counting rates. For some counters used this variation was as high as 15 percent of the observed rate, while for others it was negligible at the high counting rates. The ordinates of the curves have been reduced to a standard efficiency.

Correction for the absorption and scattering of the mica window (0.002 cm thick) of the counter was made by adding, successively, two extra sheets of mica to it, observing a spectrum in each case, and then extrapolating to a spectrum corresponding to zero thickness of mica. This was done by plotting the three ordinates at various values of $H\rho$ against the thickness of the mica, and extrapolating linearly to an ordinate corresponding to zero thickness. The ratios between ordinates of the extrapolated spectrum and the spectrum corresponding to the window alone presented a method whereby the ordinates of any observed spectrum could be corrected for the effect of the window. In this case, the probable errors of the extrapolation were rather large, resulting in large probable errors in the ordinates of the following curves for values of $H\rho$ less than 2800 $H\rho$. The window had no effect upon the spectrum above 2800 $H\rho$. There was no material between the source and the initial slit; hence the initial distribution was undistorted when it reached the counter slit, and the above correction eliminated the distortion due to the mica window.

[4] D. R. Hartree, Proc. Camb. Phil. Soc. **21**, 746 (1923).

Each point of the following spectra is the result of about 1000 counts. When the background is very small compared to the counting rate, the probable error in the points is about $\pm 3$ percent of the value of the ordinates: $\pm 2$ percent due to statistical fluctuations alone, and $\pm 1$ percent additional, estimated from the other sources of error involved (chiefly the variation of the counting efficiency due to fluctuations in the high voltage supply). However, as the counting rate approaches the background level, the relative probable errors in the ordinates become very large because the ordinates are small differences between two very nearly equal counting rates. This difficulty, and the fact that there is no *a priori* knowledge of the shape of the distribution near the end point obviously make it impossible to assign a definite upper limit to a spectrum.

There was no appreciable scatterng from the stops or walls of the spectrometer chamber. This was shown, first, by increasing $H\rho$ to a point slightly beyond the upper limit of the spectrum and observing that there was no noticeable count above background. If there had been scattering of the high velocity particles from the walls or stops, some of them would have been scattered into the counter slit, resulting in a long tail on the end of the spectrum. Next, the field was decreased to a value so low that the particles arriving at $CD$ were unable to penetrate the mica window. Here again, no count above background was observed, although the multitude of particles with slightly greater penetrating power would certainly have been scattered into the counter, had such scattering existed. It was concluded therefore, that the scattering from the walls and stops of the chamber was negligibly small. As a further indication that this was true, an entirely different slit system, involving more auxiliary stops and defining slits at $G$, gave within the limits of error the same distribution for the $P^{32}$ spectrum.

The radio-phosphorus sample was prepared by bombarding, in vacuum, a red phosphorus target backed by a copper plate, with 30 microampere-hours of 5 Mev deuterons produced in the cyclotron.[5] The copper plate was cooled by a

[5] E. O. Lawrence and M. S. Livingston, Phys. Rev. **45**, 608 (1934).

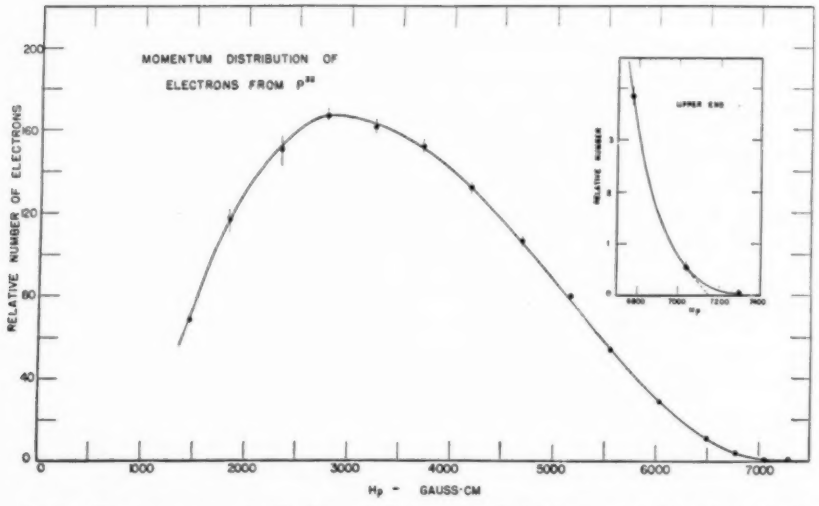


FIG. 2. The momentum distribution of $P^{32}$ electrons. Probable errors in the points due to statistical fluctuations and experimental sources are indicated by the crosses through the points. The $H\rho$ of the last point is computed using the minimum radius of curvature.

liquid air flask in order to minimize evaporation of the phosphorus.[6] The sample obtained was approximately 2 millicuries in strength. It was placed about 1 cm above the incident slit and tipped at an angle of 45° to the plane of $AD$.

The Ra E sample was prepared from old radon tubes by deposition of the Ra E and F from 0.1 $N$ HCl solution at 80°C onto a nickel plate. The strength was about 2.5 millicuries.

## RESULTS

To obtain the momentum distribution (or distribution with respect to $H\rho$) from the observed data, namely, the number of counts per minute for various values of $H$, the values of $H$ were multiplied by the mean radius of curvature of the particles entering the counter slit, $CD$, and the numbers of counts per minute were divided by the corresponding values of $H$. To find the mean radius of curvature, $\rho$, it was observed that particles of radii ranging from 14.80 cm to 15.20 cm could enter the counter slit, and if the source were uniformly homogeneous in beta-particles of all radii, a maximum number would enter for $\rho=15.00$ cm. By applying the geometrical method due to Wooster[7] to obtain the graph of distribution with radius of curvature of beta-particles entering $CD$ from such a source, it was shown that the mean radius of curvature was 14.99 cm, and that the distribution was more nearly symmetrical about this radius than about that of the maximum ($\rho=15.00$ cm). Thus, $\rho=14.99$ cm was regarded as the center of the $\delta\rho$ interval and $H\times14.99$ gauss-cm was therefore the mean value of $H\rho$ of the particles throughout a $\delta(H\rho)$ interval.

In computing the $H\rho$ value of the last point of each spectrum, the minimum radius of curvature (14.80 cm) was used. This procedure implies that the last observed positive count (above background) was due to particles which had radii just great enough to allow them to enter the counter slit, and this, in turn, involves the assumption that the distribution actually ended at this last observed point, or very close to it.

In any magnetic spectrometer, distortion of the true momentum distribution always occurs due to the finite dimensions of the slits. The amount of distortion depends upon the resolution of the spectrometer: in general, the better the resolution, the less the observed spectrum will be distorted. In this case, the fractional resolution, that is, the difference in $H\rho$ of two resolvable monochromatic lines divided by their mean $H\rho$, was 0.014. The amount of distortion introduced

[6] I am indebted to Mr. H. C. Paxton for the use of this target.

[7] W. A. Wooster, Proc. Roy. Soc. **A114**, 729 (1927).

by this spectrometer was investigated by the method suggested by Henderson,[8] in which one constructs, by the trial and error process, a distribution curve which, when scanned by the finite-sized counter slit, reproduces the observed spectrum. The distribution curve thus invented is not unique, but at least it is one step closer to the true distribution curve than the observed curve. In the cases of Ra E and $P^{32}$, the distribution curves thus obtained were identical with those observed, well within the limits of the probable errors of the ordinates, showing that the distortion present in the observed spectra (*after* having corrected the end points by using the minimum radius of curvature) was negligible.

The evaluation of the end points and estimation of the probable errors in them was accomplished by considering the probable errors in the last two points of the spectrum. For example, the last point of the Ra E spectrum, at $H\rho=5290\pm13$ (using the minimum radius of curvature) was obtained by subtracting the background counting rate, $14.84\pm0.46$, obtained with the gate closed, from $15.37\pm0.64$, the rate with it open. Thus the counting rate at $H\rho=5290\pm13$ was $0.53\pm1.10$. At $H\rho=5274\pm13$ (using the mean $\rho$), the rate was $1.61\pm1.30$. These observations indicate that the end point probably lies between $5290\pm13$ and $5274\pm13$, or, roughly, it is at $5280\pm20$ $H\rho$.

The momentum distribution curves for $P^{32}$ and Ra E electrons are shown in Figs. 2 and 3. The lower ends of the spectra have not been investigated. The data from the two distributions have been applied to the Fermi and K–U theories in order to test their validity near the upper ends. As has already been observed,[9, 10] the attempt to fit the Fermi theory to data of this type has been unsuccessful, while the K–U modification has fit somewhat better. According to the two theories, the momentum distribution of electrons may be expressed as

$$(N/(\eta_e)^2)^{1/\alpha}=K[(1+(\eta_e)_{\max.}{}^2)^{\frac{1}{2}}-(1+(\eta_e)^2)^{\frac{1}{2}}] \quad (1)$$

for light elements, and

$$(N/\eta_e(1+0.355\eta_e))^{1/\alpha}=K[(1+(\eta_e)_{\max.}{}^2)^{\frac{1}{2}}-(1+(\eta_e)^2)^{\frac{1}{2}}] \quad (2)$$

for heavy elements, where $N$ is the number of electrons in small, equal momentum intervals, $\eta_e=H\rho/1700$ is the mean momentum of the electrons in the interval, $(\eta_e)_{\max.}$ is the maximum momentum of the electrons, i.e., the value at the end point, $K$ is a constant of proportionality, and $\alpha=2$ for the Fermi theory and 4 for the K–U theory.

Thus plots of

$$(N/(\eta_e)^2)^{1/\alpha} \quad \text{or} \quad (N/\eta_e(1+0.355\eta_e))^{1/\alpha}$$

against $(1+(\eta_e)^2)^{\frac{1}{2}}$ should be linear and strike the $(1+(\eta_e)^2)^{\frac{1}{2}}$ axis at $(1+(\eta_e)_{\max.}{}^2)^{\frac{1}{2}}$ when $\alpha=2$ if the Fermi theory is correct and when $\alpha=4$ if the K–U theory is correct.

The data have been plotted according to the two theories in Fig. 4 for $P^{32}$ and Fig. 5 for Ra E. As may be seen, neither of the two theories is in agreement with the data. A straight line may be drawn through the central portion of the K–U plot, or the final portion of the Fermi plot in each case, but in neither instance are the data fitted throughout. It thus appears that neither the Fermi nor the K–U curves of Eqs. (1) and (2) can serve to determine the end points of spectra when

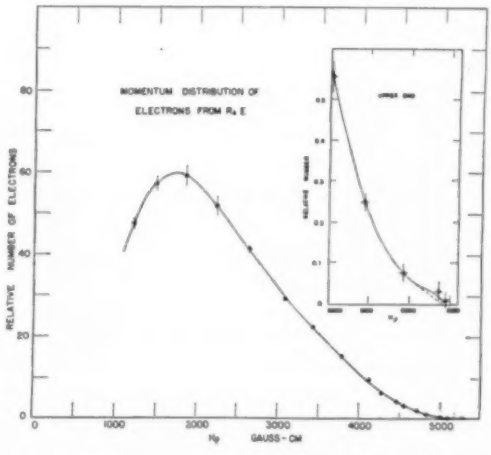


FIG. 3. The momentum distribution of Ra E electrons. The $H\rho$ of the final point is computed using the minimum radius of curvature.

[8] W. J. Henderson, Proc. Camb. Phil. Soc. **31**, 285 (1935).
[9] F. N. D. Kurie, J. R. Richardson and H. C. Paxton, Phys. Rev. **49**, 368 (1936).
[10] W. A. Fowler, L. A. Delsasso and C. C. Lauritsen, Phys. Rev. **49**, 561 (1936).

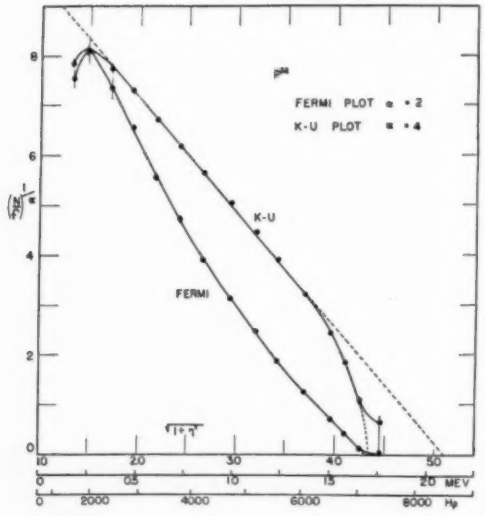


FIG. 4. The Fermi and K–U treatment of the data for $P^{32}$ (Eq. (1)). The solid lines are drawn through the data, assuming that the distributions continue on beyond the observed end points. The curved, broken line at the end of the K–U plot is drawn, assuming that the distribution ends at the observed end point. The extrapolated Fermi end point is at $(1+(\eta_e)^2)^{\frac{1}{2}}=4.32$, the K–U, at 5.10, and the observed, at 4.33.

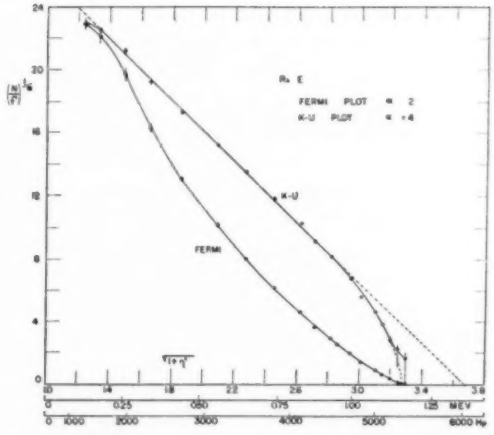


FIG. 5. The Fermi and K–U treatment of the data for Ra E (Eq. (2)). The lines are drawn as in Fig. 4. The extrapolated Fermi end point is at $(1+(\eta_e)^2)^{\frac{1}{2}}=3.26$, the K–U, at 3.69 and the observed at 3.25.

data are taken throughout the central portions alone. However, for purposes of comparison, straight lines have been drawn through the points of the central portions of the two K–U plots and the end portions of the Fermi plots. The "extrapolated end points" corresponding to the intercepts of these straight lines on the $(1+(\eta_e)^2)^{\frac{1}{2}}$ axis are shown in Table I, along with the observed end points obtained from the data given in Figs. 2 and 3:

In plotting the final points in Figs. 4 and 5, the mean radius of curvature was used to compute the values of $(1+(\eta_e)^2)^{\frac{1}{2}}$ because the central portions of the K–U plots indicate that the distributions should not end at the observed end points, but rather, should continue on out considerably further than was experimentally observed. In addition, however, the trend of the K–U points, assuming that the distributions do end at the observed end points, have been indicated by the broken lines in each case. The Fermi points have been plotted in the same manner.

It may be observed that the deviations from the K–U straight lines, as drawn, are far greater than the experimental errors involved. For example, in the case of $P^{32}$ at $H\rho=7000$, the number of particles that should be observed according to the K–U straight line is $(2/1.1)^4$ or 11 times that actually obtained, while at $H\rho=7200$, the number is 26 times that observed.

The deviations at the lower ends of the K–U plots are probably due in part to the inability of the extrapolation method to compensate completely for the absorption and scattering of the mica window.

The ratios of the extrapolated K–U to the observed end points are the same for the two substances, within the limits of error: the K–U limits are about 17 percent higher than the observed ones.

The shape and value for the end point of the Ra E spectrum are in essential agreement with what has been found by some other experimenters. Among these, Alichanow, Alichanian, and Dzelepow,[11] Madgwick[12] and Champion[13] found end points at 5200, 5000 and 5500 $H\rho$, respectively. However, neither the shape nor the end point agrees with Scott's results.[14] On the other hand, many observers working with cloud

[11] Alichanow, Alichanian and Dzelepow, Nature **137**, 314 (1936).
[12] Madgwick, Proc. Camb. Phil. Soc. **23**, 982 (1927).
[13] Champion, Proc. Roy. Soc. **A134**, 672 (1932).
[14] F. A. Scott, Phys. Rev. **48**, 391 (1935).

chambers find agreement with the K–U formula near the upper limit for $P^{32}$ or other radioactive substances, but, as shown by Fowler, Delsasso and Lauritsen[10] and by Paxton,[15] this agreement is only apparent, due to the large probable errors inherent in cloud chamber technique.

## Discussion

In the light of the results, it must be concluded that the K–U distribution as expressed in (1) and (2) does not fit the data throughout the spectrum. The fact that the K–U plot drops to the axis long before the extrapolated end point has suggested the possibility that a neutrino mass different from zero should be considered in applying formulas (1) and (2). The correction to the formulas for this case was given to me by Mr. W. E. Lamb, Jr., of this department. Application of the correction to the data showed that no positive neutrino mass, of any magnitude whatever, was capable of bringing about agreement.

Table I. *Extrapolated end points given by theories and experiment.*

| | Observed | | Fermi | K-U | Obs/K-U | Maximum |
|---|---|---|---|---|---|---|
| | $H\rho$ | Mev | $H\rho$ | $H\rho$ | | $H\rho$ |
| $P^{32}$ | 7150 ±100 | 1.69 | 7140 | 8500 | 0.84 | 2800 |
| Ra E | 5280 ±20 | 1.15 | 5300 | 6950 | 0.87 | 1750 |

[15] H. C. Paxton, Phys. Rev. (in press).

Furthermore, it may be pointed out that the formulas (1) and (2) apply to the so-called "allowed" beta-transitions, whereas, Ra E is a "singly forbidden" transition and $P^{32}$, judging from its position on the Sargent curves, is probably "doubly forbidden." There are a number of forms that can be chosen for the coupling of heavy and light particles, all of which lead essentially to the K–U plots for the allowed transitions, but give substantially different curves for the forbidden ones. The simplest forms of the coupling, including the one actually suggested by Konopinski and Uhlenbeck, have been investigated by Mr. Lamb and only partially remove the discrepancy at the upper limit, giving, however, a much better fit for Ra E than for radiophosphorus. It is not yet clear how these experimental curves can be fitted by a suitable and more complicated choice of the coupling, but here it must be emphasized that the failure of the K–U plots to fit these data need not be regarded as an argument against their applicability to allowed beta-spectra. A formula of the form (1) or (2), but with $\alpha$ taken equal to 3, represents the data very closely, although it has no theoretical foundation.

It is a pleasure to express my appreciation to Professor E. O. Lawrence and Professor J. R. Oppenheimer and to other members of the department for their helpful suggestions and advice during the course of the experiments, and to Mr. W. E. Lamb, Jr., who so kindly made the theoretical calculations.

# Alpha-Particle Bombardment of Neon, Calcium and Argon and Masses of Light Nuclei

ERNEST POLLARD* AND CHARLES J. BRASEFIELD, *Sloane Physics Laboratory, Yale University, New Haven, Connecticut*

(Received October 20, 1936)

Under bombardment by ThC′ alpha-particles neon and calcium have been found to emit protons while argon does not. The maximum energies of the protons have been measured: the nuclear energy changes are for the neon reaction $-2.6_4$ Mev and for calcium $-4.2_2$ Mev. In each case only one group was found. Using Aston's recent value for the mass of $Ne^{20}$ we deduce that the mass of $Na^{23}$ is 22.9972. Data from a number of transmutations are used together with mass spectrographic values to give a table of isotopic masses from $Ne^{20}$ to $A^{40}$ with four exceptions.

IN two recent papers[1, 2] we have described experiments on the protons ejected from the elements sulphur, phosphorus, chlorine and potassium under bombardment by ThC′ alpha-particles. In this paper we give the results of similar work on neon, calcium and argon. These elements are of interest as the preponderant isotopes are of the type $4n$ and might be expected to give groups similar to those from the elements $Mg^{24}$, $Si^{28}$, $S^{32}$ studied by Haxel.[3] Argon and calcium are of added interest as they are isobars differing in charge by two and the properties of any emitted proton groups might have significance in a theoretical interpretation. The transmutation of neon, and those of the elements previously investigated enable use to be made of Aston's recent mass determinations and several independently studied reactions to give values for the isotopic masses from $Ne^{20}$ to $A^{40}$ with the exceptions of $Ne^{21}$, $Mg^{25}$, $S^{33}$ and $K^{39}$.

None of these elements has been investigated in this way since the early work of Rutherford and Chadwick[4] who reported particles were emitted from neon and argon but not from calcium.

## Experimental Arrangement and Results

For the two gaseous elements neon and argon we used "source boxes" n which the bombardment was carried on as illustrated in Fig. 1. The design (a) was intended to test the presence or absence of a yield and no care was taken to limit the geometrical conditions to favor resolution. It happens that a fair estimate of the nuclear energy change (or $Q$ value) can be made from the maximum range of any protons observed since an error of 20° in the angle chosen as the least effective angle between proton- and alpha-ray introduces a relatively small change in the $Q$ value. This arrangement is very bad for the separation of groups. The design (b) in which an annular space of gas is bombarded has better geometrical conditions and was intended for a subsequent analysis into groups. In both cases the effective range of the alpha-particles depends on the gas pressure. We checked our estimate of the alpha-particle range and maximum angle between proton and alpha-ray by preliminary experiments on nitrogen in each case. Taking this angle for the design (a) to be 43°, for design (b) 37°, the calculated $Q$ values for nitrogen were found to be $-1.48$ and $-1.40$ Mev, in agreement with the accepted value $-1.4\pm0.2$ Mev. With design (b) we found two groups, ranges 22 and 48 cm of roughly equal yield: the short range group is probably a composite of protons due to the 4.9 cm particles present in the source and a second $Q$ value discovered by

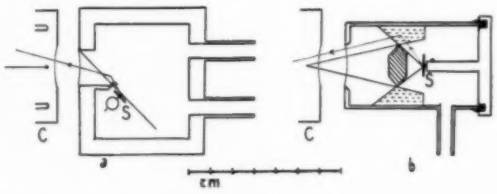


FIG. 1. The two arrangements for bombarding gases. (a) is intended to detect protons, (b) to resolve them into groups. In (b) diagonal shading indicates the lead screen and horizontal shading the annular volume of gas which is bombarded. $S$ is the source, $C$ the counter.

* Sterling Fellow.

[1] C. J. Brasefield and E. Pollard, Phys. Rev. **50**, 296 (1936).

[2] E. Pollard and C. J. Brasefield, Phys. Rev. **50**, 890 (1936).

[3] O. Haxel, Phys. Zeits. **36**, 804 (1935).

[4] Rutherford and J. Chadwick, Proc. Phys. Soc. London **36**, 417 (1924).

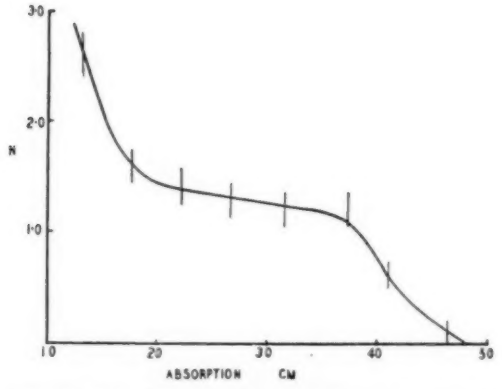


FIG. 2. Absorption curve for protons from nitrogen using arrangement (b). $N$ is the number of protons counted per minute per millicurie, the absorption is in centimeters air equivalent.

Fischer Colbie.[5] The curve we obtain (Fig. 2) in which the number per minute per millicurie ($N$) is plotted against absorption, is very similar to that reported by Haxel.[6]

For calcium, bombarded as $Ca(OH)_2$, we used the arrangements described in our previous papers,[1, 2] one a large yield arrangement with poorly defined angles, another giving a low yield but having better geometrical conditions.

## EXPERIMENTAL RESULTS

### Neon

With the (a) design this gas gave a yield which was roughly two-thirds that from nitrogen. An absorption curve was plotted which appears in Fig 3(a). The maximum range is estimated to be 32 cm for a bombarding alpha-particle range of 7.9 cm. No attempt was made to resolve the curve into several groups as the geometrical conditions render this impossible. The (b) design was then used with gas at an average pressure of 60 cm: the absorption curve found is shown in Fig. 3(b). The maximum range is 32 cm, for an effective alpha-particle range 7.5 cm. It will be seen that it is uncertain whether more than one group occurs, there being a possibility that a short range group is present. We therefore repeated the curve at a lower average pressure (38 cm) which should reduce the spread due to

[5] E. Fischer Colbie: see G. Stetter, Zeits. f. Physik **100**, 652 (1936).
[6] O. Haxel, Zeits. f. Physik **93**, 400 (1935).

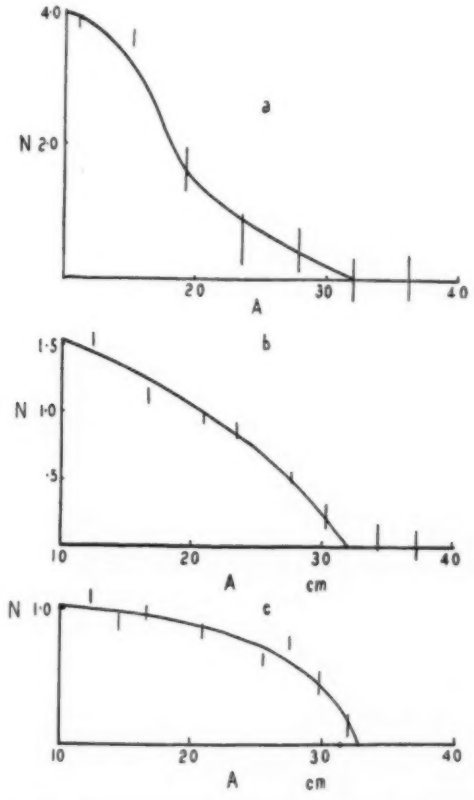


FIG. 3. Absorption curves for protons from neon using arrangements (a) and (b), the latter at two pressures. $N$ is the number of protons counter per minute per millicurie and $A$ is the absorption in centimeters air equivalent.

the absorption in the neon and so sharpen up the discontinuities if any. This curve appears as in Fig. 3(c). It will be seen that any rise at small absorptions is less prominent than before and we conclude that neon gives only one group of protons with a range beyond 10 cm. The maximum range for curve 3(c) is 32.5 cm for an effective alpha-particle range of 7.9 cm. Since calculation shows that protons should just be detectable beyond the natural protons from the source if emitted in the same direction as the alpha-particles (forward direction) we used a box similar to design (b) but with no central lead screen, closed by gold and aluminum foils. The yield from neon was just picked up beyond the natural protons and had a range of 41 cm which was checked by comparison with the

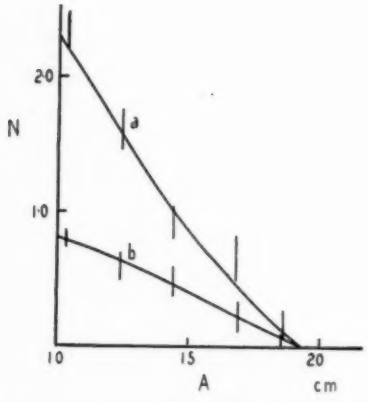


FIG. 4. Absorption curve for protons from calcium using high yield (a) and low yield (b) arrangement. $N$ and $A$ are as in the previous figure.

protons projected forward from methane at a pressure arranged to give the same absorption as the neon. Some yield was found of range about 50 cm but this was ascribed to nitrogen—an impurity of 3 percent would suffice to explain it.

**Argon**

Using the large yield design (a) we made several runs in which the box was alternately filled with argon and evacuated. With argon present we found a very small increase over the vacuum at low absorptions, amounting to less than 0.05 per minute per millicurie. Nitrogen gave 3.0 per minute per millicurie under identical conditions in counts interspersed with the argon runs. The yield we found is almost small enough to be explainable by the $A^{36}$ isotope though we consider it more likely that it is due to either neon or nitrogen impurity. We conclude that $A^{40}$ gives no yield of protons.

**Calcium**

Curves (a) and (b) of Fig. 4 show the results obtained with calcium in the large yield and low yield arrangements respectively. Both show definite yields with a maximum range of 19 cm. We made careful tests to find a group of greater range than this without success. We do not think it likely that any analysis of the observed protons into more than one group can be made.

In all the curves the lengths of the lines at each point are intended to give some idea of the precision in N. If $n$ is the number of particles counted at a point, the line extends a distance $1/\sqrt{n}$ of the plotted value on each side. This is not a limit of error but enables the numbers counted to be inferred and a judgment of the validity of the line drawn through the points to be made accordingly.

The average strength of our sources was 2 millicuries.

## DISCUSSION

We ascribe the protons we find to the two reactions:

$$Ne^{20}+He^{4}\rightarrow Na^{23}+H^{1}(+Q), \qquad (1)$$

$$Ca^{40}+He^{4}\rightarrow Sc^{43}+H^{1}(+Q). \qquad (2)$$

The greatness of the yield from neon and the fact that only one group is found render it likely that the most abundant isotope is responsible for the emitted particles. The same reasoning applies to calcium where the fact that $Ca^{40}$ has an abundance of 97 percent renders it nearly certain that the above reaction is right.

We deduce the following values for the nuclear energy change in Mev:

*Reaction (1)—Neon*

| Design (*a*) | Design (*b*) | Forward | Recommended Value |
|---|---|---|---|
| −2.64 | −2.56; −2.67 | −2.51 | $-2.6_4\pm0.20$ |

*Reaction (2)—Calcium*

From both curves $-4.2_3\pm.20$.

The result we get for neon is in good agreement with Rutherford and Chadwick's early experiments.[4] They found a range of 16 cm in the right angle direction using Ra (B+C) alpha-particles. Calling the effective alpha-particle range 6.4 cm (i.e. allowing 0.5 cm for absorption in the gas) this gives a nuclear energy change value of −2.8 Mev which is in agreement within the errors of experiment.

Our results for argon and calcium differ from their conclusions as we do not observe protons from argon and do from calcium. Their negative result from calcium would be expected since the yield is undoubtedly very small or zero if the less energetic particles from Ra C′ are used and so would not have been detected in their experiments. If the argon they used contained neon or nitrogen their positive result could be explained. It is of some interest that this is the only case

in which their early experiments, made with a method of detection that taxes the observer's freedom from bias very seriously, have not been verified substantially by later work.

Both neon and calcium appear to give only one group of protons. Since both elements contain an equal number of neutrons and protons they are similar to the elements $Mg^{24}$, $Si^{28}$, $S^{32}$ for which three groups spaced by roughly a million volts are found. Such a spacing might occur for $Ca^{40}$ but be undetected in our experiments as our minimum detected range is 10 cm. This is not the case for $Ne^{20}$ where a group lying just short of our minimum would have a $Q$ value of $-4.8$ Mev so that the least spacing between the ground and first excited state of $Na^{23}$ must exceed 2.2 Mev. It therefore appears that neon does not fit in to the scheme of $Mg^{24}$, $Si^{28}$ and $S^{32}$.

The lack of emission from argon is not surprising. $A^{40}$ already contains four neutrons in excess of its proton content. A transmutation of the type here studied would give a product nucleus containing five excess neutrons. Since there is an increase of mass proportional to the square of this surplus[7] (the isotopic number) there will be an addition of mass which is considerable and which renders the energy required to cause proton emission much greater. The greater the isotopic number the more energy is required to achieve the transmutation. It seems likely that this factor, and not the difficulty of penetration through the barrier, is effective in preventing alpha-particle disintegration of elements beyond calcium.

## Masses of Elements from Neon to Calcium

When subjected to alpha-particle bombardment all the nuclei from $F^{19}$ to $Ca^{40}$ of the type either $4n$ (e.g. $Mg^{24}$) or $4n+3$ (e.g. $Al^{27}$) with the exception of $A^{36}$ have been observed to emit protons whose maximum energies have been measured. Aston[8] has recently given figures for the masses of $Ne^{20}$, $Al^{27}$, $Si^{28}$, $Si^{29}$ and $A^{40}$ while Bainbridge[9] had previously determined $Cl^{35}$ and $Cl^{37}$. These data, together with the transmutation energies, permit the deduction of all the masses from $Ne^{20}$ to $A^{40}$ with the exception of $Ne^{21}$, $Mg^{25}$, $S^{33}$, $A^{36}$ and $K^{39}$. For $A^{36}$ there is an old value of Aston's[10] so that we have information about all but four mass numbers. In a letter to "Nature"[11] we used all the then available figures to derive most of these masses: the present work enables two more to be added by reason of the neon reaction giving $Na^{23}$ and

$$Na^{23}+He^4 \rightarrow Mg^{26}+H^1(+Q)^{12}$$

studied by König giving $Mg^{26}$. We give below the list of reactions used and the resulting masses derived. (Energies are given in mass units $\times 10^3$.)

$$F^{19}+He^4 \rightarrow Ne^{22}+H^1+1.5^{13}$$
$$Ne^{20}+He^4 \rightarrow Na^{23}+H^1-2.8$$
$$Na^{23}+He^4 \rightarrow Mg^{26}+H^1+2.2^{12}$$
$$Mg^{24}+He^4 \rightarrow Al^{27}+H^1-1.2^{3,\,14}$$
$$Al^{27}+He^4 \rightarrow Si^{30}+H^1+2.3^{14}$$
$$Si^{28}+He^4 \rightarrow P^{31}+H^1-2.6^3$$
$$P^{31}+He^4 \rightarrow S^{34}+H^1+0.0^{13,\,15,\,2}$$
$$S^{32}+He^4 \rightarrow Cl^{35}+H^1-2.6^{3,\,1}$$
$$Cl^{35}+He^4 \rightarrow A^{38}+H^1=0.1^2$$

| | | | |
|---|---|---|---|
| $Ne^{20}$ | 19.9986 ($A$) | $P^{31}$ | 30.9844 |
| $Ne^{21}$ | ——— | $S^{32}$ | 31.9812 |
| $Ne^{22}$ | 21.9989 | $S^{33}$ | ——— |
| $Na^{23}$ | 22.9972* | $S^{34}$ | 33.9802 |
| $Mg^{24}$ | 23.9939 | $Cl^{35}$ | 34.9796 ($B$) |
| $Mg^{25}$ | ——— | $A^{36}$ | 35.976 ($A'$) |
| $Mg^{26}$ | 25.9908* | $Cl^{37}$ | 36.9777 ($B$) |
| $Al^{27}$ | 26.9909 ($A$) | $A^{38}$ | 37.9753 |
| $Si^{28}$ | 27.9860 ($A$) | $K^{39}$ | ——— |
| $Si^{29}$ | 28.9864 ($A$) | $A^{40}$ | 39.9754 ($A$) |
| $Si^{30}$ | 29.9844 | $Ca^{40}$ | ——— |

Aston's early value is indicated by ($A'$), his recent values by ($A$), Bainbridge's by ($B$) while the remainder are derived from transmutations.

We would like to thank Professor A. F. Kovarik for his interest and encouragement.

[7] H. Bethe and R. F. Bacher, Rev. Mod. Phys. **8**, 165 (1936).
[8] F. W. Aston, Nature **137**, 613 (1936).
[9] K. T. Bainbridge, Phys. Rev. **43**, 378 (1933).
[10] F. W. Aston, Proc. Roy. Soc. **115**, 505 (1927).
[11] E. Pollard and C. J. Brasefield, Nature **137**, 943 (1936).
[12] A. König, Zeits. f. Physik **90**, 197 (1934).
[13] A. N. May and R. Vaidyanathan, Proc. Roy. Soc. **155**, 519 (1936).
[14] W. E. Duncanson and H. Miller, Proc. Roy. Soc. **146**, 396 (1934).
[15] R. F. Paton, Zeits. f. Physik **90**, 586 (1934).
* New values.

# Vibrational Analysis of the Emission Bands of Germanous Oxide

R. WILLIAM SHAW, *Department of Physics, Cornell University, Ithaca, N. Y.*

(Received October 22, 1936)

Twenty-one bands degraded to the red and associated with GeO have been observed in the region λ2500 to λ2900. The wave numbers of the band heads are expressed by the equation

$$\nu = 37763.7 + 649.4\,(v'+\tfrac{1}{2}) - 3.81\,(v'+\tfrac{1}{2})^2 - 985.0\,(v''+\tfrac{1}{2}) + 4.36\,(v''+\tfrac{1}{2})^2.$$

Attention is called to the regular variation of the dissociation energies for the normal states of the monoxides and monosulphides of the fourth periodic column. It is shown that the electronic transition $^1\Pi \rightarrow {}^1\Sigma$ for the GeO system seems to agree best with the available evidence. It is found that the quantity $\omega_e'' r_e^2 \cdot 10^{-16}$ cm is very nearly constant for the fourth column monoxides. From this it is concluded that $1.65 \pm 0.06$A is a good value of $r_e$ for GeO. The dense structure due to overlapping bands and isotope effect makes rotational analysis extremely difficult.

ABSORPTION bands arising from black germanous oxide were observed by Shapiro[1] in certain experiments on the isotopes of germanium. These bands, which are degraded towards the longer wave-lengths, lie in the spectral region λ2500 to λ2900. Because of the tendency of hot GeO vapor to attack the quartz windows of the absorption tube with the formation of a non-transparent glaze, it was impossible to obtain spectrograms of sufficient intensity for precise measurement.

Somewhat later a preliminary report was made by the author[2] concerning emission bands, lying in the same spectral region and degraded toward the red, which were observed in a flaming arc charged with the dioxide of germanium. Similar results in experiment and analysis were obtained by W. F. G. Ferguson[3] of New York University. The present paper is concerned with the details of the observations on the emission bands.

## EXPERIMENTAL PART

The flaming arc used for the excitation of the emission bands consisted of a vertical positive electrode of graphite, cored with germanium dioxide, and a horizontal negative electrode also of graphite. The horizontal electrode was ground to a long point by means of a pencil sharpener. This pointed electrode was found advantageous in causing the arc (8–10 amp.) to play on the oxide in the positive electrode. When the pointed electrode was drawn well away from the vertical one there resulted a high flame in which the GeO bands were well developed—an essential result since very limited quantities of the oxide were available. Light from only the higher portions of the flame was used. The spectrograms were obtained by means of a Hilger E I Littrow quartz spectrograph with an iron arc for the standard comparison. Inasmuch as the rotational structure of the GeO bands is extremely dense due to overlapping and isotope effect it seemed inadvisable to attempt a rotational analysis. Hence the measurements were confined to the *R* heads of the bands. Measurements were made both by comparator and by microphotometer tracings.

TABLE I. *Band heads in the GeO system. Last column is the difference between observed and calculated wave numbers.*

| $v'$ | $v''$ | $\nu$ (VAC) | INTENSITY | O−C |
|---|---|---|---|---|
| 7 | 1 | 40954.9 | 0 | +2.6 |
| 5 | 0 | 40729.2 | 2 | +0.3 |
| 4 | 0 | 40117.9 | 2 | +0.3 |
| 5 | 1 | 39752.1 | 2 | −0.5 |
| 3 | 0 | 39498.9 | 5 | +0.2 |
| 2 | 0 | 38872.0 | 8 | −0.4 |
| 1 | 0 | 38237.4 | 5 | −0.5 |
| 2 | 1 | 37897.0 | 2 | −0.1 |
| 0 | 0 | 37596.1 | 4 | 0.0 |
| 1 | 1 | 37261.3 | 10 | −0.3 |
| 2 | 2 | (36928.6)* | | |
| 0 | 1 | 36619.0 | 8 | −0.8 |
| 1 | 2 | (36294.1)* | | |
| 2 | 3 | 35968.7 | 2 | −1.1 |
| 0 | 2 | 35651.5 | 10 | −0.8 |
| 1 | 3 | (35335.3)* | | |
| 2 | 4 | 35018.2 | 0 | −1.0 |
| 0 | 3 | 34692.6 | 10 | −0.9 |
| 1 | 4 | 34384.8 | 4*d* | +0.1 |
| 0 | 4 | 33742.9 | 4*d* | 0.0 |
| 1 | 5 | 33443.4 | 6*d* | −0.5 |

* Present but with head obscured by atomic line.

[1] Shapiro, Gibbs and Laubengayer, Phys. Rev. **40**, 354 (1932).
[2] R. W. Shaw, Phys. Rev. **43**, 104 (1933).
[3] Private communication.

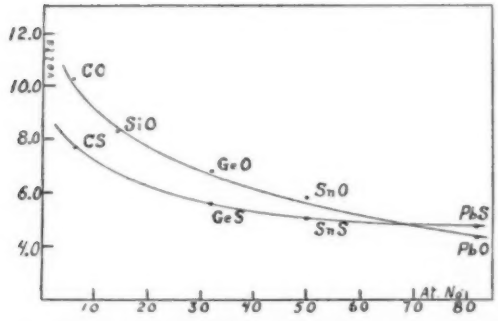


FIG. 1. Heats of dissociation of the diatomic oxides and sulphides of the fourth periodic column.

The latter were especially helpful in the cases of the fainter bands.

## OBSERVATIONS AND DISCUSSION

Twenty-one bands were observed of which three heads were obscured by atomic germanium lines. The wave numbers, vibrational assignments and intensities are given in Table I. Analysis of these data leads to the following vibrational equation for the $R$ heads of the bands.

$$\nu = 37763.7 + 649.4(v'+\tfrac{1}{2}) - 3.81(v'+\tfrac{1}{2})^2 - 985.0(v''+\tfrac{1}{2}) + 4.36(v''+\tfrac{1}{2})^2.$$

The column of observed minus calculated wave numbers (O−C) in Table I shows that this equation expresses the observations satisfactorily.

The intensities are eye estimates and are perhaps none too reliable because of excessive overlapping of the bands. However the intensity distribution indicates a wide Condon curve in keeping with similar observations of the typical

TABLE II. *Heats of dissociation.*

| MOLECULE | AT. NO. | $D_e''$ (VOLTS) | SOURCE |
|---|---|---|---|
| CO | 6+8 | 10.3 | Kaplan[1] |
| SiO | 14 | 8.4 | Saper[2] |
| GeO | 32 | 6.8 | Present work |
| SnO | 50 | 5.8 | Connelly[3] |
| PbO | 82 | 4.3 | Shawhan-Morgan[4] |
| CS | 6+16 | 7.7 | Crawford-Shurcliff[5] |
| GeS | 32 | 5.6 | Shapiro[6] |
| SnS | 50 | 5.0 | Shawhan[7] |
| PbS | 82 | 4.7 | Rochester-Howell[8] |

[1] Kaplan, Phys. Rev. **35**, 957 (1930).
[2] Saper, Phys. Rev. **42**, 498 (1932).
[3] Connelly, Proc. Phys. Soc. London **46**, 571 (1934).
[4] Shawhan and Morgan, Phys. Rev. **47**, 377 (1935).
[5] Crawford and Shurcliff, Phys. Rev. **45**, 860 (1934).
[6] Shapiro, Phys. Rev. **40**, 354 (1932).
[7] Shawhan, Phys. Rev. **48**, 521 (1935).
[8] Rochester and Howell, Proc. Roy. Soc. **A148**, 157 (1935).

TABLE III. *Internuclear distances.*

| MOLECULE | $\omega_e''$ | $r_e''$. $10^{-8}$ CM | $\omega_e'' r_e''^2$. $10^{-16}$ CM |
|---|---|---|---|
| CO | 2169.3 | 1.13 | 2770.2 |
| SiO | 1242.0 | 1.50 | 2794.5 |
| GeO | 985.0 | (1.69) | |
| SnO | 821.9 | (1.82) | |
| PbO | 722.3 | 1.92 | 2662.4 |
| | | *Mean* | 2742.3 |

and $B$ sub-group monoxides of the fourth periodic column and with the observed harmonic constants, $\omega_e'' > \omega_e'$.

The coincidence of wave-lengths and the direction of degradation of the present bands with those observed by Shapiro in the absorption spectrum of germanous oxide indicate clearly that the emission bands are due to the monoxide and, moreover, that the observed lower state is the normal state of the molecule. That it is the normal state which is observed is demonstrated further by the heats of dissociation. While it is generally unsatisfactory to use the Birge-Sponer[4] extrapolation of vibrational levels for heats of dissociation in cases with few observed vibrational states, values of the correct order of magnitude may often be obtained. Values of dissociation energies for the normal states of the typical and type $B$ group monoxides of the fourth periodic column are given in Table II. These values, when plotted against atomic number as in Fig. 1, give a remarkably smooth curve. Similar data[5] for the corresponding monosulphides are included for the sake of comparison.

The normal state of GeO is then a $^1\Sigma$ state since the molecule has an even number of electrons and sub-shells are all closed. From analogy with similar molecules the normal state should be considered as arising from Ge ($^3P$) and O ($^3P$) states. When allowance is made for the fact that linear extrapolations of vibrational levels for heats of dissociation usually give values which are too large, it appears that the GeO molecule dissociates in the excited state with the products

[4] Birge and Sponer, Phys. Rev. **28**, 259 (1926).
[5] All the data included in Table II have been computed on the same basis. The recent value, 8.41 volts for CO by Brons, Nature **136**, 796 (1935) and others, does not agree well with the data given unless the value for SiO be changed to 7.8 volts, which is a more probable value for SiO at least as compared with its isoelectronic molecules. The CO value has been arrived at by a detailed study of perturbations in the various CO band systems. These studies are difficult or impossible in the other less complete molecular systems.

Ge ($^1D$) and O ($^3P$). The electronic transitions $^1\Pi \rightarrow {}^1\Sigma$ and $^1\Sigma \rightarrow {}^1\Sigma$, are therefore possibilities. A comparison of the values of $\nu_e$ of the fourth column monoxides shows that the $^1\Pi \rightarrow {}^1\Sigma$ transition is the more likely. The observed band system of GeO is then similar to the fourth positive system of CO.

It is interesting to note that the quantity, $\omega_e'' r_e^2 \cdot 10^{-16}$ cm, as evaluated from the data on CO, SiO and PbO, is very nearly a constant. The essential data, which are given in Table III, show that the deviations of individual values from the mean, 2742.3 cm, are less than three percent. This produces in the case of a calculated value of $r_e$ for PbO a deviation of 0.02 unit or about one percent which is within usual experimental error in determinations of $r_e$. The corresponding calculated values of $r_e$ for GeO and SnO are 1.69A and 1.82A, respectively. The internuclear distance 1.69A for GeO is in good agreement with the Ge−O distance, 1.65A, observed by Warren[6] in $GeO_2$.

[6] B. E. Warren, Phys. Rev. **45**, 657 (1934).

It is well known[7] that there is only a small change in the C−O distance[8] in $CO_2$ (1.05−1.2A depending on the physical state) and CO (1.13A) and in $SiO_2$ (1.60A) and SiO (1.50A). Moreover, while the character of binding gradually changes as one goes downward in a periodic column as is shown by chemical properties, it has not varied so greatly at germanium that one would expect any pronounced peculiarities of internuclear distance. It seems reasonable, therefore, to consider 1.65±0.06A as a good value of $r_e$ for GeO pending the possibility of a rotational analysis of some of the individual bands.

The author wishes to express appreciation to Professor R. C. Gibbs for his interest in the problem and to Professor A. W. Laubengayer of the Chemistry Department for supplying the $GeO_2$ and for many helpful discussions on the properties of the oxides of the fourth periodic column.

[7] R. Kronig, *Optical Basis of the Theory of Valency* (1935), p. 164.
[8] H. A. Stuart, *Molekulstruktur* (1934), p. 77.

JANUARY 1, 1937 PHYSICAL REVIEW VOLUME 51

# Helium I Like Spectra

HOWARD A. ROBINSON,* *University of Uppsala, Sweden*
(Received October 17, 1936)

New measurements of the $1s^2\ {}^1S_0 - 1s \cdot np\ {}^1P_1$ series of the Helium I isoelectronic sequence for Be III, B IV and C V together with previously published data on He I, Li II, N VI and O VII are critically examined and values for the $1s^2\ {}^1S_0$ terms for these spectra obtained. A slightly modified Hylleraas type extrapolation formula is used to calculate these same values. When relativity, spin, mass and mass polarization corrections are applied the agreement between observed and calculated values is very good for the heavier elements. A small discrepancy appears in the case of Li II.

IT has been possible for some time to calculate the ground states of the helium I like spectra by means of the formulae first given by Hylleraas.[1] The experimental data have, however, been meager due mainly to the inaccessibility of the region below 100A where most of the necessary lines lie. A new 4° grazing incidence spectrograph designed by Professor Siegbahn[2] and built in the workshops of this institute has proved unusually well suited to this region and it is now possible for the first time to measure lines below 100A with an accuracy of a few thousandths of an angstrom. The spectra Li II, Be III, B IV, and C V are, in addition, useful as wave-length

TABLE I. *Data for* Li II.

| n | 2 | 3 | 4 |
|---|---|---|---|
| λ (A) | 199.280±0.003 | 178.014±0.003 | 171.575±0.004 |
| $\nu$ cm$^{-1}$ | 501,807±5 | 561,754±10 | 582,835±14 |
| $T$ cm$^{-1}$ | 108,263±10 | 48,330±3 | 27,247±4 |
| $1s^2\ {}^1S_0$ = | 610,070±15 | 610,084±13 | 610,082±18 |

$1s^2\ {}^1S_0$ = 610,079±25 cm$^{-1}$ I.P. = 75,2593±0.0031 volts

* Irving Langmuir Fellow, American Scandinavian Foundation. Now at Ohio State University.
[1] E. Hylleraas, Zeits. f. Physik **65**, 209 (1930).
[2] B. Edlén, Zeits. f. Physik **100**, 621 (1936).

standards between 200A and 33A, particularly when used in conjunction with the hydrogen like spectra of the same elements the lines of which may be calculated exactly by means of Penney's[3] formula. The wave-lengths as presented in this paper have been measured in several orders using the hydrogen like spectra or known oxygen lines as standards. The beryllium III measurements have been described separately.[4] The measurements for boron IV are from unpublished data of B. Edlén and are included here for completeness through the kindness of Docent Edlén. The measurements for carbon V are the averages of measurements made by Docent Edlén and the author on a series of individual plates. While in all cases the maximum deviation from the mean of the higher orders and all measurements on the individual lines was in the maximum case $\pm 0.003$A it is nevertheless felt that the higher series measurements may be in error by $\pm 0.005$A. The error in the first two members should, however, be less than this latter value due to the many high order measurements involved. The higher series lines are furthermore apt to be diffuse, but this effect appears to be less marked as the atomic number increases.

The discussion which follows should be considered as supplementary to that of Bethe[5] the notation used here being the same as in that article. Several small numerical errors have been corrected. Most of these are in Bethe's Table 7 (page 363) where the relativity corrections for Li II, Be III, B IV and C V are incorrectly given. The calculated energies for the ground state are therefore also in error. Bethe's Table 11 (page 384) is essentially correct except for small deviations in the last unit in certain cases. This deviation, however, is beyond the accuracy of the calculation and therefore of no importance.

TABLE II. *Data for Be III.*

| $n$ | λ (A) | $\nu$ cm$^{-1}$ | $1s\cdot np\ ^1P_1$ | $n^*$ |
|---|---|---|---|---|
| 2 | 100.254 ± 0.001 | 997,466 ± 10 | 243,759 | 2.01282 ± 0.00037 |
| 3 | 88.314 ± .002 | 1,132,323 ± 25 | 108,902 | 3.0114 |
| 4 | 84.758 ± .003 | 1,179,830 ± 40 | 61,395 | 4.0107 |
| 5 | 83.202 ± .003 | 1,201,894 ± 43 | 39,331 | 5.0109 |
| 6 | 82.377 ± .004 | 1,213,931 ± 60 | 27,294 | 6.0107 |
| 7 | 81.891 ± .005 | 1,221,135 ± 75 | 20,090 | 7.0103 |

$1s^2\ ^1S_0 = 1{,}241{,}225 \pm 100$ cm$^{-1}$ I.P. $= 153.118 \pm 0.012$ volts

[3] W. G. Penney, Phil. Mag. **9**, 661 (1930).
[4] H. A. Robinson, Phys. Rev. **50**, 99 (1936).
[5] H. Bethe, *Handbuch der Physik*, Vol. 24/1, p. 324 et seq.

TABLE III. *Data for B IV.*

| $n$ | λ (A) | $\nu$ cm$^{-1}$ | $1s\cdot np\ ^1P_1$ | $n^*$ |
|---|---|---|---|---|
| 2 | 60.313 ± 0.002 | 1,658,017 ± 60 | 433,943 | 2.01145 ± 0.00051 |
| 3 | 52.679 ± .002 | 1,898,290 ± 72 | 193,670 | 3.0109 |
| 4 | 50.435 ± .003 | 1,982,750 ± 120 | 109,210 | 4.0096 |
| 5 | 49.456 ± .005 | 2,021,999 ± 205 | 69,961 | 5.0095 |

$1s^2\ ^1S_0 = 2{,}091{,}960 \pm 300$ cm$^{-1}$ I.P. $= 258.064 \pm 0.034$ volts

TABLE IV. *Data for C V.*

| $n$ | λ (A) | $\nu$ cm$^{-1}$ | $1s\cdot np\ ^1P_1$ | $n^*$ |
|---|---|---|---|---|
| 2 | 40.270 ± 0.001 | 2,483,238 ± 65 | 679,212 | 2.00972 ± 0.00089 |
| 3 | 34.973 ± .002 | 2,859,347 ± 165 | 303,101 | 3.0085 |
| 4 | 33.426 ± .003 | 2,991,683 ± 275 | 170,677 | 4.0081 |
| 5 | 32.754 ± .005 | 3,053,062 ± 500 | 109,388 | 5.0079 |

$1s^2\ ^1S_0 = 3{,}162{,}450 \pm 600$ cm$^{-1}$ I.P. $= 390.120 \pm 0.074$ volts

## THE EXPERIMENTAL DATA

### Helium I

The ground state of this spectrum has been treated by Paschen.[6] The higher states are well known because of accurate measurements in more accessible regions and Paschen was able by means of a spectrogram taken by Kruger to evaluate the ground state by means of its eleven combinations with the lowest eleven $1s\cdot np\ ^1P_1$ terms ($n=2$ to 12) already known. Paschen's[7] final value is $1s^2\ ^1S_0 = 198{,}305$ cm$^{-1}$. Since the values are consistent to within $\pm 10$ cm$^{-1}$ we may assume that the value is accurate to $\pm 15$ cm$^{-1}$ (especially if we consider that the absolute value of the terms may also be in error by a few centimeters$^{-1}$).

$$1s^2\ ^1S_0 = 198{,}305 \pm 15 \text{ cm}^{-1},$$
$$I.P. = 24.4633 \pm 0.0019 \text{ volts}.$$

### Lithium II

The higher states for Li II are known from the work of Schüler and Werner,[8] as in the He I case, but with much less accuracy. The $1s^2\ ^1S_0 - 1s\cdot np\ ^1P_1$ series appears to be difficult to excite as several long exposures have failed to reveal more than the first three or four members. The values in Table I are from the data of Docent Edlén but differ somewhat from his previously published values.[9] The term values are those of Werner.

[6] F. Paschen, Preussische Akad. der Wiss. Sitzungsber. Seite 662 (1929).
[7] Data from correspondence between Professor Paschen and the author. I am extremely indebted to Professor Paschen for his kindness in this matter.
[8] S. Werner, *Studier over Spektroskopiske Lyskilder* (Copenhagen, Dissertation 1927).
[9] B. Edlén, *Nova Acta Regiae Soc. Scient.* Vol. 9, No. 6 (Uppsala, 1933).

The errors in the latter are those assigned by that author.

**Beryllium III**

Data for the higher terms have never been published and as a result one must depend on the $1s^2\ ^1S_0-1s\cdot np\ ^1P_1$ series for an evaluation of the limit. The data are given in Table II.

The error in the absolute value of the ground state has been calculated as in the following spectra by assuming the maximum error in each wave-length and recalculating the limit under these new conditions: The error in $n^*$ is that due to the error in the limit.

**Boron IV**

The only available data are those for the $1s^2\ ^1S_0-1s\cdot np\ ^1P_1$ series. The measurements are given in Table III.

**Carbon V**

The $1s^2\ ^1S_0-1s\cdot np\ ^1P_1$ series of carbon V is given in Table IV.

This series has been measured by F. Tyrén[10] in this institute using a 5-meter concave grating and a plate perpendicular to the diffracted rays. The measurements made by this method are inherently less accurate than those made by the grazing incidence method, primarily because the dispersion is about six times as large in this latter case. For the lines given the check between Tyrén's values and these is satisfactory. The three higher members as measured by Tyrén alone show, however, rather considerable variation in the quantum defect, as calculated using the above limit, as follows:

| | |
|---|---|
| $n=6$ | $n^*=6.0069$ |
| 7 | 7.0178 |
| 8 | 7.7924. |

Since the accuracy of these latter three lines is so much below that of the first four members of the series they have not been considered in calculating the limit.

**Nitrogen VI and oxygen VII**

Tyrén[10] has observed the first lines in these series ($1s^2\ ^1S_0-1s\cdot 2p\ ^1P_1$) at 28.787A and 21.615A, respectively. In order to obtain an estimate of the accuracy of these measurements we may extrapolate $\nu-RZ^2\cdot\frac{3}{4}$ for this line as follows:

| | $\nu$ measured | | $\nu$ extrapolated | |
|---|---|---|---|---|
| He I | 88,292 | | | |
| | | 89,795 | | |
| Li II | 172,615 | | | |
| | | 84,169 | | |
| Be III | 256,784 | | | |
| | | 84,449 | | |
| B IV | 341,233 | | 341,233 | |
| | | 84,608 | | 84,608 |
| C V | 425,841 | | 425,841 | |
| | | 85,152 | | [84,900] |
| N VI | 510,993 | | [510,740] | |
| | | 82,713 | | [85,200]. |
| O VII | 593,706 | | [595,940] | |

We thus see that the N VI line $\nu$ value is possible 250 cm$^{-1}$ too large, but that the O VII line $\nu$ value is in error by approximately 2000 cm$^{-1}$. The extrapolation in this latter case is rather more accurate because of the position of the line itself with respect to standards. We may therefore take for N VI

$$\nu^1{}_{S_0-{}^1P_1}=3{,}473{,}790\pm400\ \text{cm}^{-1}\quad \lambda=28.787\pm0.004$$

and for O VII

$$\nu^1{}_{S_0-{}^1P_1}=4{,}627{,}900\pm1500\ \text{cm}^{-1}$$
$$\lambda=21.608\pm0.007$$

where the latter value refers to a weighted mean between extrapolation and observed values. We may furthermore extrapolate by Moseley's law to obtain a value for $1s\cdot 2p\ ^1P_1$ as follows:

| | $\nu$ | $\sqrt{\nu}$ | $\Delta\sqrt{\nu}$ |
|---|---|---|---|
| He I | 27,176 | 164.85 | |
| | | | 164.19 |
| Li II | 108,268 | 329.04 | |
| | | | 164.68 |
| Be III | 243,759 | 493.72 | |
| | | | 165.02 |
| B IV | 433,943 | 658.74 | |
| | | | 165.40 |
| C V | 679,212 | 824.14 | |
| | | | [165.82] |
| N VI | [979,880] | [989.89] | |
| | | | [166.28] |
| O VII | [1,336,320] | [1155.99] | |

Using these values we get for the ground states:

N VI $1s^2\ ^1S_0=4{,}453{,}670\pm1500$, I.P. $=549.41\pm0.18$ volts.
O VII $1s^2\ ^1S_0=5{,}964{,}200\pm2500$, I.P. $=735.74\pm0.31$ volts.

## The Calculation of the Ground States

The Hylleraas calculation for the gound states of these ions consists essentially of two parts. Calculations were first made of the absolute value of the ionization potential for the negative

[10] F. Tyrén, Zeits. f. Physik **98**, 768 (1936).

hydrogen ion ($H^-$) and for He I by means of the Ritz variational method carried to high approximations. The Schrödinger equation was then solved by means of a perturbation calculation involving the energies in terms of a series in powers of $1/Z$. Hylleraas succeeded in calculating the first three coefficients of this series. Because the values for the first two members ($H^-$ and He I) of the isoelectronic sequence were known (from the first part of the Hylleraas calculation) it was possible to solve for two more coefficients. A recent, as yet unpublished, calculation of the Li II ionization potential by Mr. H. A. S. Eriksson of this university shows in the 12th approximation a small deviation in the last place from the value calculated by means of the Hylleraas formula. If we use the Eriksson value for Li II it is now possible to find one more coefficient in the expansion of $1/Z$ and thus to slightly modify the Hylleraas formula. The final result is

$$J=\left[Z^2-\frac{5}{4}Z+.31488-\frac{.01710}{Z}+\frac{.00422}{Z^2}+\frac{.00084}{Z^3}\right]R_Z. \quad (1)$$

This formula, which gives slightly larger values for the ground state than does the original Hylleraas formula, has been used in this paper.

The values obtained from (1) are to be corrected for several effects not considered in the original derivation. The first of these $H_1$ arises from the relativistic change of mass with velocity. The second of these $H_4$ arises from a characteristic term in the Dirac Theory and in the one electron problem is known as the spin correction for $s$ terms. These corrections can be calculated when the respective wave functions are known. They have been calculated by Bethe[11] using the simple first approximation wave functions $u=e^{-(Z-5/16)(r_1+r_2)}$. The results are for a *two* electron case

$$H_1=-5/2(Z-5/16)^4\alpha^2R, \quad (2)$$

$$H_4=+2(Z-5/16)^3(Z-1/8)\alpha^2R. \quad (3)$$

Since we are considering calculations of ionization potentials (which are the differences in energy between the $z$th and the $(z-1)$ ion) $H_1$ and $H_4$ must have subtracted from them, in order to be applicable to our problem, the corresponding correction for the ion with one electron ($H_i$).

$$H_i=-\tfrac{1}{4}Z^4\cdot\alpha^2\cdot R. \quad (4)$$

These three corrections taken together must be considered as only first approximations due to the simple manner of their calculation. The values are listed in Table V.

In addition to the previously discussed relativity correction we have certain mass corrections to be considered. Deviating from Bethe's treatment we shall here use the value of $R_Z$[12] corresponding to each individual element instead of multiplying by $R_\infty$ and applying a correction. There is, however, very small polarization mass correction $\epsilon_3$ which as Bethe[13] has shown amounts to 5.2 $cm^{-1}$ in the case of helium. In an effort to approximate this correction for the higher ions a calculation has been made by using the Hylleraas wave function with eight terms. (Bethe, Eqs. (18.9), (18.24) and (18.30)) and evaluating the integral given by Bethe on page 375. The result is

$$\epsilon_3=\frac{m}{M}Z^2\left[\frac{0.03359Z-0.20054}{0.77539+0.56283Z+0.12499Z^2}\right]. \quad (5)$$

[11] Reference 5, page 384.
[12] Values of $R_Z$ taken from White, *Introduction to Atomic Spectra*, p. 38.
[13] Reference 5, page 375.

TABLE V. *Relativity corrections.*

| | He I | | Li II | Be III | B IV | C V | N VI | O VII |
|---|---|---|---|---|---|---|---|---|
| | A. | B. | | | | | | |
| $H_1$ relativity | +19.4 | +20.3 | +130.4 | +462.2 | +1207.0 | +2615.9 | +5000.3 | +8731.3 |
| $H_4$ spin | −20.1 | −18.0 | −111.6 | −388.6 | −1004.2 | −2161.7 | −4112.4 | −7155.4 |
| $H_i$ ion | − 4 | − 4 | − 20.3 | − 64.0 | − 156.3 | − 324.0 | − 600.3 | −1024.0 |
| Total ($\alpha^2R$) | − 4.7 | − 1.7 | − 1.5 | + 9.6 | + 46.5 | + 130.2 | + 287.6 | + 551.9 |
| Total ($cm^{-1}$) | −27 | −10 | − 8 | + 56 | + 272 | + 760 | +1680 | +3223 |

TABLE VI. *Mass polarization corrections.*

| | He I | | Li II | | Be III | B IV | C V | N VI | O VII |
|---|---|---|---|---|---|---|---|---|---|
| $\epsilon_2$ | A. $-0.17\,m/M$ | B. $-0.22\,m/M$ | A. $-0.10\,m/M$ | B. $-0.25\,m/M$ | $-0.21\,m/M$ | $-0.12\,m/M$ | $+0.005\,m/M$ | $+0.16\,m/M$ | $+0.33\,m/M$ |
| ($cm^{-1}$) | −5.2 | −6.6 | −1.7 | −4.3 | −2.7 | −1.4 | + .07 | +1.3 | +2.4 |

TABLE VII. *Compilation of results for various spectra.*

| ELEMENT | HYLLERAAS MOD. | RELATIVITY CORRECTION | MASS POLARIZ. CORRECTION | TOTAL | | TOTAL* | |
|---|---|---|---|---|---|---|---|
| | | | | CALCULATED | EXPERIMENTAL | VOLTS (CALCULATED) | VOLTS (EXPERIMENTAL) |
| He I | 198,322 $cm^{-1}$ | (A) −27 $cm^{-1}$ | −5 $cm^{-1}$ | 198,290 $cm^{-1}$ | | (A) 24.4611 | |
| | | (B) −10 | −5 | 198,307 | 198,305 ± 15 $cm^{-1}$ | (B) 24.4632 | 24.4633 ± 0.0019 |
| Li II | 610,057 | −8 | −4 | 610,045 | 610,079 ± 25 | 75.2552 | 75.2593 ± .0031 |
| Be III | 1,241,151 | +56 | −3 | 1,241,204 | 1,241,225 ± 100 | 153.1149 | 153.118 ± .012 |
| B IV | 2,091,672 | +272 | −1 | 2,091,943 | 2,091,960 ± 300 | 258.0621 | 258.064 ± .034 |
| C V | 3,161,629 | +760 | 0 | 3,162,389 | 3,162,450 ± 600 | 390.1124 | 390.120 ± .074 |
| N VI | 4,451,055 | +1680 | +1 | 4,452,736 | 4,453,700 ± 1500 | 549.2895 | 549.41 ± .18 |
| O VII | 5,959,945 | +3223 | +2 | 5,963,170 | 5,964,200 ± 2500 | 735.6168 | 735.74 ± .31 |

* In all calculations in this paper the factor $1.2336 \times 10^{-4}$ has been used in changing $cm^{-1}$ to electron volts.

The values are listed in Table VI.[14] It will be seen that with the possible exception of the values for He I and Li II these corrections are unimportant.

## FINAL RESULTS

In Table VII the final results are shown. The two relativity corrections for He I are (A) calculated by Bethe using Hartree eigenfunctions and (B) calculated using Eqs. (2), (3) and (4).

The final results show, on the whole, remarkably good agreement but the following points should be noticed.

I. In the case of Li II there appears to be a small but real difference between the theoretical and observed value for $1s^2\ {}^1S_0$.

II. The experimental values lie without exception slightly higher than do the calculated values. This difference is to be expected from a variation method as the latter should lead to slightly too low a value for the ionization potential.

III. The Eriksson calculation shows that the Hylleraas extrapolation formula cannot be markedly changed by the calculation of higher members of the isoelectronic series. As a result a more exact calculation of the relativity and mass corrections should be carried through at least for the Li II case in order to determine if there be in reality a small, as yet unaccounted for, residual effect.[15]

I wish to take the opportunity to thank Professor Siegbahn for his extreme kindness in placing the necessary apparatus at my disposal and for the generous manner with which he has met every request. Professor Ivar Waller has been extremely kind in discussing the latter part of the paper with me.

Docent Bengt Edlén, aside from allowing me to publish part of his own data, has critically examined the whole of the experimental results while Mr. Eriksson has allowed me free use of his own calculations on lithium II prior to their publication. I should also like to thank the American Scandinavian Foundation for its part in making my stay in Uppsala possible.

*Note added in proof:* Since writing the above Mr. Eriksson has kindly forwarded his complete results on the relativity corrections for Li II. The values given in Table V may now be replaced by the following

| $H_1$ | $H_4$ | $H_5$ | Total ($\alpha^2 R$) | Total ($cm^{-1}$) |
|---|---|---|---|---|
| +153.8 | −125.1 | −20.3 (calc. from (4)) | +8.4 | +49 |

The calculated value for the ground state is thus 610,102 $cm^{-1}$ which checks with the experimental result within the limit of error. It should be noted, however, that this case is an exception to conclusion II stated above.

[14] In this table the two values for He and Li refer (A) to the evaluation of $\epsilon_2$ using the helium (Li) eigenfunction (Bethe, page 375) and (B) to the evaluation of $\epsilon_2$ using 5. A more careful calculation should be made before one can decide whether the change in sign beginning with C V is real.

[15] This is now being done by Mr. Eriksson. Since the total correction in this case is the difference of two practically equal quantities the rough calculation made using Eqs. (2) and (3) would not be expected to be at all accurate. From the experimental data one should expect the correction to be positive instead of negative. Mr. Eriksson's preliminary results show that $H_1$ is given in Table V is actually too small, with the result that the discrepancy is probably due to the error in the "correction."

# The Nuclear Spin and Magnetic Moment of $Li^6$

J. H. MANLEY AND S. MILLMAN,* *Columbia University, New York, N. Y.*

(Received October 27, 1936)

The spin of the $Li^6$ nucleus and the h.f.s. separation of the $^2S_{\frac{1}{2}}$ normal state have been measured by the atomic beam method of zero moments. The evaluation of the contribution of $Li^7$ to the intensity in the neighborhood of the $Li^6$ zero moment peak was made by an extension of the method of analysis previously used in determining the spin of $K^{41}$ and $Rb^{87}$. The spin of $Li^6$ was found to be 2/2 and the h.f.s. separation $0.0077 \pm 0.0001$ $cm^{-1}$ on the basis of the value of Fox and Rabi for $Li^7$. The ratio of the magnetic moments of the isotopes is $\mu_6/\mu_7 = 0.258 \pm 0.5$ percent. From the value calculated by Breit and Doerman for $Li^7$, the moment of $Li^6$ is 0.85 nuclear magneton.

## INTRODUCTION

APPROXIMATE determination of the magnetic moment of the $Li^6$ nucleus has been made by Schüler[1] from hyperfine structure measurements and an assumption of the nuclear spin. The resolution was insufficient for an accurate determination of the separation and completely inadequate for a determination of the spin. The measurements of Fox and Rabi[2] on $Li^7$ by the atomic beam method indicated that this method could also be used for the less abundant isotope. They were able to conclude that the spin of $Li^6$ is 2/2 or greater and that the moment ratio $\mu_6/\mu_7$ lies between 0.15 and 0.25. The results of the measurements described in this paper have been previously summarized.[3]

## APPARATUS AND PROCEDURE

With a few modifications the apparatus was that used in the investigation of $K^{41}$.[4] The resolution was increased by reducing the height of the beam to 1.5 mm which gave a variation of the field over this height of less than two percent. Further resolution was obtained by the insertion of a slit 0.01 mm wide before a four-mil tungsten detecting filament. This arrangement eliminated the fragileness of small diameter filaments necessary to secure comparable resolution. For good detection of lithium it was found convenient to supply a continuous oxygen flow to the surface of the filament. A small jet directed at the filament and connected through a capillary with an oxygen reservoir maintained the necessary high work-function surface at all times.

As in all measurements by this method, the beam intensity at the undeflected position is obtained as a function of the current which produces the inhomogeneous magnetic field. Sufficient intensity for accurate measurements was obtained with an oven temperature of about 750°C.

## RESULTS

A typical curve showing the variation of beam intensity with field current is given in Fig. 1. The zero moment peak due to $Li^6$ occurs at about 22 amperes, that due to $Li^7$ near 116 amperes. The intensity in the 40–105 ampere region is constant, and therefore this portion of the curve has been omitted. The insert, *A*, of Fig. 1 is a portion

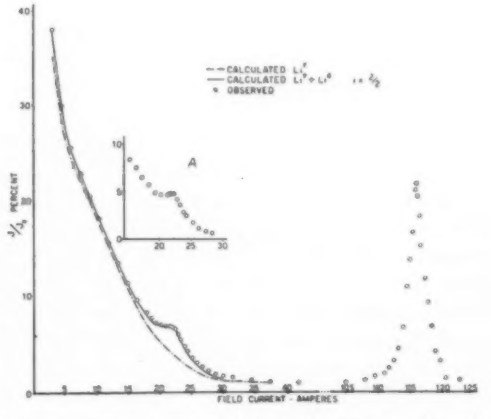


FIG. 1. A typical curve of the beam intensity at the undeflected position as a function of the current producing the magnetic field. The insert, *A*, is a portion of a similar curve taken with slightly higher resolution.

* Barnard Fellow.

[1] Schüler, Zeits. f. Physik **99**, 285 (1935); **66**, 431 (1930).

[2] Fox and Rabi, Phys. Rev. **48**, 746 (1935).

[3] Manley and Millman, Phys. Rev. **50**, 380 (1936).

[4] Manley, Phys. Rev. **49**, 921 (1936).

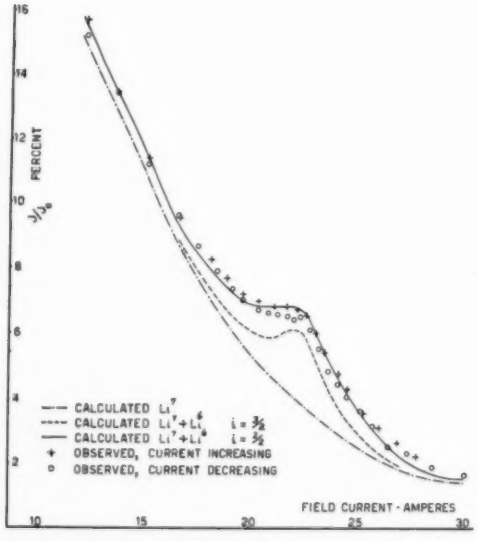


FIG. 2. The $Li^6$ peak region of Fig. 1 plotted to a larger scale to show the calculated curves for spins of 2/2 and 3/2.

of a curve taken with higher resolution but at some sacrifice of accuracy of intensity measurements. The spin calculations are therefore based on results with less than the maximum possible resolution.

For an unambiguous determination of the spin of $Li^6$ it is essential to evaluate the $Li^7$ background in the 22 ampere region. The necessary data for this calculation is furnished by the course of the curve in the neighborhood of the $Li^7$ zero moment peak. This calculation can be carried out by an extension of the method already applied in the determination of the nuclear spin of $K^{41}$ and $Rb^{87}$.[5]

For the purposes of these deflection experiments the property which distinguishes the atoms of one isotope from those of another, or atoms of different magnetic quantum states of either isotope, is the effective magnetic moment of the atom. Since the force on an atom in an inhomogeneous magnetic field of the type used is proportional to the product of the magnetic moment of the atom and the current in the field, the fraction of atoms of a given magnetic state remaining at the position of zero deflection depends on this product. All other quantities such as beam shape, energy-distribution, etc., which enter an intensity expression are common to atoms of any state of either isotope. Hence a knowledge of the variation of intensity with respect to this moment-current product for any one state of either isotope permits the evaluation of the contribution of any other state to the total intensity at any current, provided the nuclear spin is known. The proviso is necessary because of the dependence of the atomic moment on the spin of the nucleus. In the region of the $Li^7$ zero moment peak the intensity is due solely to atoms of the $m=-1$ states of $Li^7$. Since the nuclear spin of this atom is known, the moment may be calculated for any value of the field current from the Breit-Rabi formula.[6] The observed intensity due to these states plotted as a function of the moment-current product yields the desired calibration curve. At any current the moment-current product for each magnetic state of $Li^7$ is then calculated and the corresponding intensity read from the calibration curve. The sum of these intensities is the total contribution of $Li^7$ to the intensity at the current chosen. The result of this procedure is shown in the dot-dash curve of Fig. 1 and Fig. 2.

In a similar manner, the same calibration curve can be used to calculate the contribution of $Li^6$ to the intensity at any current. A spin is assumed, the moment-current product calculated, and the intensity contribution read from the curve. The reading gives the fraction of atoms of any state which remain at the position of zero deflection. The absolute intensity is obtained by using the mass-spectrographic abundance ratio 11.6.[7] The total intensity of all states of $Li^6$ is then added to the calculated $Li^7$ background. The solid curve of Figs. 1 and 2 is the result for an assumed spin of 2/2 for $Li^6$, and the dotted curve of Fig. 2 for a spin of 3/2. The two sets of experimental points are in good agreement with the 2/2 curve but deviate considerably from the curve for 3/2 in the region of the $Li^6$ peak where the comparison is particularly significant. The departure from the 2/2 curve occurs at the values of the moment-current product for which the calibration curve is less accurate.

A careful search was made to determine the

[5] Millman and Fox, Phys. Rev. **50**, 220 (1936).

[6] Breit and Rabi, Phys. Rev. **38**, 2082 (1931).

[7] Brewer, Phys. Rev. **49**, 635 (1936).

possible presence of additional zero moment peaks. It is certain that none exist at currents greater than 22 amperes. While no peaks or breaks in the curve were found at currents less than this value, there is a slight possibility that the large $Li^7$ intensity would mask their presence. However, if the spin is greater than 3/2 the peak which is evident would have to be the high-current peak. For such cases this peak can be calculated by the method described and would lie between the 3/2 curve and the $Li^7$ background in the 22 ampere region (Fig. 2). It would therefore deviate more markedly from the observed points than the curve obtained for an assumed spin of 3/2. It is concluded from this analysis that the spin of the $Li^6$ nucleus is 2/2.

The ratio of the h.f.s. separations of the two isotopes follows from the ratio of the currents at the zero moment peaks. Several determinations of this ratio have been made under various conditions with the result,

$$I_p(Li^6)/I_p(Li^7)=0.193\pm0.5 \text{ percent},$$
$$\Delta\nu(Li^6)/\Delta\nu(Li^7)=0.290\pm0.5 \text{ percent}.$$

This ratio and the value 0.0267 $cm^{-1}$ for $\Delta\nu(Li^7)$ from the results of Fox and Rabi[2] yield

$$\Delta\nu(Li^6)=0.0077\pm0.0001 \text{ cm}^{-1}.$$

The ratio of the nuclear magnetic moments is given by

$$\mu_6/\mu_7=[\Delta\nu(Li^6)/\Delta\nu(Li^7)]$$
$$[\{2i/2i+1\}_6/\{2i/2i+1\}_7]=0.258\pm0.5 \text{ percent}.$$

On the basis of the value 3.28 calculated by Breit and Doerman,[8] the nuclear moment of $Li^6$ is 0.85 nuclear magneton.

## Conclusion

$Li^6$ is one of the small group of four nuclei (D, $Li^6$, $B^{10}$, $N^{14}$) of odd atomic number which are composed of equal numbers of protons and neutrons. Three of these (D, $Li^6$, $N^{14}$) are now known to have a spin 1. The nuclear moment of the deuteron as measured by Kellogg, Rabi and Zacharias[9] and that of $Li^6$ are the same. This equality lends support to the argument of Bethe and Bacher[10] that the normal state of the $Li^6$ nucleus, like that of D, is $^3S_1$. If perturbations due to other nuclear configurations are of minor importance in their effect on the $Li^6$ moment, one may now say that the intrinsic moments of the proton and neutron are the same in the two nuclei to within the experimental error of a few percent.

We are very much indebted to Prof. I. I. Rabi for suggesting the problem and for many helpful suggestions. We also wish to acknowledge the assistance of Mr. J. E. Gorham in the measurements and calculations.

[8] Breit and Doerman, Phys. Rev. **36**, 1262 (1930).
[9] Kellogg, Rabi, Zacharias, Phys. Rev. **50**, 472 (1936).
[10] Bethe and Bacher, Rev. Mod. Phys. **8**, 182 (1936).

# The Magnetic Scattering of Slow Neutrons

L. JACKSON LASLETT, *Radiation Laboratory, Department of Physics, University of California, Berkeley, California*

(Received October 15, 1936)

To determine whether the large cross sections for the scattering of slow neutrons by iron and nickel arise in part from the ferromagnetic nature of these materials, a comparison of the scattering at room temperature and above the Curie point was made. As no significant change in scattering was found, the conclusion is drawn that the largeness of these cross sections is not of magnetic origin. It is pointed out, however, that this result does not preclude the neutron possessing a magnetic moment of the order of magnitude of a nuclear magneton.

## 1. INTRODUCTION

THE scattering of slow neutrons by non-hydrogenous substances has been investigated by several authors.[1–7] The last results of Mitchell,[4] as well as those of Pontecorvo and Wick,[6] show greater scattering (measured in the backward direction) for iron and nickel than for neighboring elements in the periodic table. As iron and nickel are ferromagnetic substances and as the neutron is believed to possess a magnetic moment, it might be thought that this increase in scattering is chiefly of magnetic origin and would disappear, at least in part, if these scatterers should be raised above their Curie temperatures.

That the scattering cross sections apparently do not differ markedly[4, 6] for the various slow neutron groups is evidence against this explanation. Bloch[8] has published a formula for the magnetic scattering to be expected in a ferromagnetic substance; the substitution of reasonable values in this formula indicates the change in scattering as the material is raised from room temperature to above the Curie point would be small (very likely less than ten percent and probably less than one percent), even for thermal neutrons. The experiment reported here was undertaken at the suggestion of Professor Bloch, however, in the hope of finding some effect, which could, then, be regarded as due to the neutron possessing a magnetic moment. A negative result, within ordinary limits of error, would not, of course, constitute evidence against a magnetic moment for the neutron equal in order of magnitude to a nuclear magneton, but would show without reference to any theory that the high values for the scattering by iron and nickel are primarily due to other causes.

## 2. EXPERIMENTAL ARRANGEMENT

The primary source of neutrons was a beryllium target in the Berkeley cyclotron.[9] This target was bombarded with some ten microamperes of $5\frac{1}{2}$ Mev deuterons and produced fast neutrons, with a large spread in energy, according to the reaction[10, 11]

$$_4Be^9 + _1H^2 = _5B^{10} + _0n^1.$$

The scattering material and detector were located about one meter from this target at the end of a tunnel in a large water-box (see Fig. 1). Within the tunnel was placed either a block of paraffin ten centimeters thick (at *A*) or a container for water twelve centimeters thick (at *A or B*). The location of this hydrogenous material, which had the purpose of producing slow neutrons from the primary fast ones, did not seem to make any important change in the scattering measurements.

[1] A. C. G. Mitchell and E. J. Murphy, Phys. Rev. **48**, 653 (1935).
[2] A. C. G. Mitchell, E. J. Murphy and L. M. Langer, Phys. Rev. **49**, 400 (1936).
[3] A. C. G. Mitchell, E. J. Murphy and M. D. Whitaker, Phys. Rev. **49**, 401 (1936).
[4] A. C. G. Mitchell, E. J. Murphy and M. D. Whitaker, Phys. Rev. **50**, 133 (1936).
[5] D. Budnitzky and I. Kurtschatow, Physik. Zeits. Sowjetunion **8**, 170 (1935).
[6] B. Pontecorvo and G. C. Wick, Ricerca Scient. II, **1**, 134 and 220 (1936).
[7] R. Fleischmann, Zeits. f. Physik **100**, 307 (1936).
[8] F. Bloch, Phys. Rev. **50**, 259 (1936).
[9] E. O. Lawrence and D. Cooksey, Phys. Rev. **50**, 1131 (1936).
[10] H. R. Crane, C. C. Lauritsen and A. Soltan, Phys. Rev. **44**, 692(1933); Comptes rendus **197**, 913 (1933).
[11] M. S. Livingston, M. C. Henderson and E. O. Lawrence, Phys. Rev. **44**, 782 (1933).

A thin silver piece (0.15 mm thick, 3.2 cm diameter) was used as a detector of the incident and reflected neutrons, for much of the previous work[4, 6] was carried out with a similar detector. Because it was found that two-thirds of the activity produced in this silver arose from neutrons readily absorbed in cadmium, it was not thought desirable to introduce the complication of calculating *C* group intensities from runs made with and without cadmium filtering. A second silver sample, similar to the first, was in every run placed in a definite position beside the water-box and used as a control to integrate the effective neutron intensity; if the anisotropy of the neutron distribution about the cyclotron changed markedly during a series of runs, it thus introduced some error in the measurements, but this error was not a systematic one, for the temperature of the scatterer was alternated from cold to hot every few runs. The samples, after activation for a definite time (usually six minutes), were rushed to a Lauritsen electroscope and the activities read alternately for some ten minutes. The decay curves plotted logarithmically from these activities (consisting of two periods) were drawn with the same template and the intensity ratio of detector to control then obtained from them.

With the scatterer located at the end of the water-box, a larger percentage of the slow neutrons reaching it came directly from the hydrogenous material in the tunnel than if the experiment had been performed closer to the beryllium target, for, with the latter arrangement, a large fraction of the neutrons striking the scatterer and detector would arise from the large oil tanks of the magnet. However, even at the end of the water-box, a considerable percentage of the neutrons arriving at the scatterer would have come from the back and sides (probably after being scattered by the walls of the room) had not fairly complete shielding been accomplished for the *C* group neutrons by surrounding the scatterer on all sides but the front with sheet cadmium metal (approximately 1 mm thick). This shielding was in place in every series of runs except the first series made with nickel; as will be seen it had the effect of raising the scattering observed from approximately twelve percent to forty percent—a value still not to be regarded as an accurate estimate of the scattering percentage.

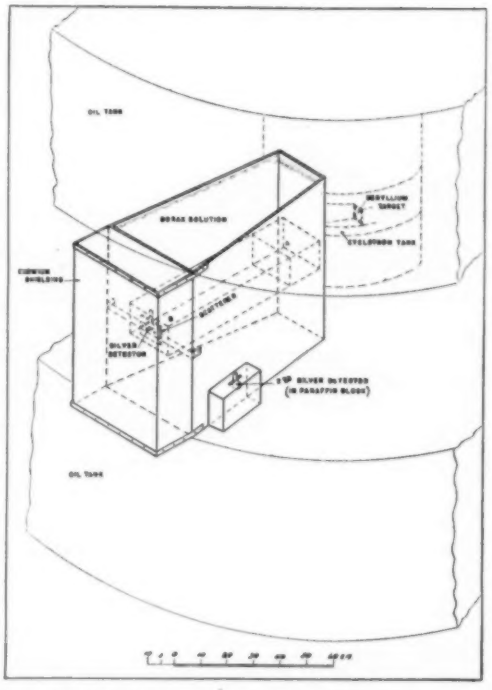


FIG. 1. Sketch showing arrangement of detector, scatterer and water-box between the oil tanks of the cyclotron.

The scatterers were mounted on an iron support left in place even when no scatterer was present. This support did not scatter much itself (perhaps three percent), but was fairly rigid in order to resist the pull of the magnetic field from the cyclotron on the nickel and iron samples when they were below their Curie temperatures. The heating was accomplished by use of one to three oxygen torches always left in place and lit when needed; due to the presence of the magnetic field (approximately 170 gauss at this point), the attainment of the Curie temperature was directly manifested by the scatterer ceasing to attract a small test piece of iron or steel.

## 3. RESULTS

Because the present experiment was concerned chiefly with *changes* in scattering, the neutron intensity without scatterer present was not investigated as carefully as when the scatterers

were in place. For this reason the scattering percentages found for a given element varied somewhat from one series of runs to another. The values may differ considerably from those of other workers for the additional reasons that the shielding with sheet cadmium could be expected to be complete only for *C* group neutrons and that scattering is known to depend markedly upon geometrical conditions, e g., decreasing with increased parallelism of the incident neutrons.[1] In every series of runs, however, at least one or two runs without scatterer would be introduced in the series to verify that scattering was actually taking place; in the second series made with nickel, a pair of runs was inserted in which a copper scatterer was used in order to verify that the difference in scattering by these two materials was easily detectable with the arrangement described above.

The results of four series of runs are tabulated in Table I. The errors attached are probable errors, calculated in all cases of two or more runs by the usual formula involving the deviations from the mean. No attempt was made to discard runs deviating from the mean by several times the probable error, for it was felt that, as the intensity for each run was calculated from decay curves each determined by several points, the possibility of huge, accidental errors could not be admitted. The order in which the runs of a series were made is indicated in the table, using the following abbreviations: n, cold nickel; N, hot nickel; f, cold iron; F, hot iron; c, cold copper; and o, no scatterer.

TABLE I. *Scattering of slow neutrons by various elements below and above their Curie temperatures (Ag detector).*

| Series | I | II | III | IV |
|---|---|---|---|---|
| No Scatterer | 100±2 | 100±2 | 100±2 | 100±14 |
| Cold Nickel | 112±2 | 139±1 | 136±4 | |
| Hot Nickel | 112±2 | 141±2 | | |
| Cold Iron | | | 139±2 | 153±1 |
| Hot Iron | | | 134±2 | 152±1 |
| Cold Copper | | 128±2 | | |
| Order of Runs | oonnNNn | oonnNNnceo | offFFFffon | fffFFFfffFFFfo |
| Dimensions (cm) | | | | |
| Nickel | 10.2×7.7×1.3 | 10.2×7.7×1.3 | 10.2×7.7×1.3 | |
| Iron | | | 10.2×7.7×1.6 | 8.4×8.1×1.6 |
| Copper | | 10.2×7.7×1.3 | | |

## 4. Conclusions

From Table I one may conclude that, with a probable error of 5½ percent for nickel and 2½ percent for iron, there is no change in the scattering of slow neutrons by these elements as they are raised above their Curie temperatures. Recalling that two-thirds the activity of the silver detector was found to arise from *C* group neutrons, one may draw a similar conclusion for thermal neutrons, but with a somewhat higher probable error—8 percent and 4 percent for nickel and iron, respectively. As was pointed out in the introduction, this shows the large slow neutron scattering cross sections found by Mitchell and co-workers[2-4] for nickel and iron are not of magnetic origin; in view of the calculations of Bloch,[8] it does not, however, constitute evidence against a magnetic moment for the neutron equal, in order of magnitude, to a nuclear magneton.

An experiment similar to the one here reported but which eliminates the annoyance of heating the samples would be to compare the scattering of a Heusler alloy with that of its nonalloyed constituents.

## 5. Acknowledgments

The author is deeply indebted to Professor Bloch for suggesting this experiment and for many helpful discussions, as well as to Professors J. R. Oppenheimer, E. O. Lawrence, and members of the laboratory staff for their active interest in the problem. This investigation was aided by grants from the Research Corporation, the Chemical Foundation, and the Josiah Macy, Jr. Foundation.

# On the Cross Sections of $Cl_2$ and $N_2$ for Slow Electrons

J. B. FISK,* *George Eastman Laboratory, Massachusetts Institute of Technology, Cambridge, Massachusetts*

(Received October 9, 1936)

Measurements of total cross section for collision of slow electrons between 2 and 40 volts have been carried out in $N_2$ and $Cl_2$ by use of a Brode type apparatus. The results for $N_2$ compare well with those of previous investigators and with the theory of elastic scattering. The cross section of $Cl_2$ is of order 2000 sq. atomic units with a maximum at $2.65\sqrt{V}$, the curve being similar to those for Na, K, Cs and Rb. Application of the theory of elastic scattering indicates that only a small portion of these collisions can be elastic.

## 1. INTRODUCTION

A NUMBER of researches have been made during the past few years by a variety of methods to determine the "effective cross section for collisions" of atoms and molecules when subject to electron bombardment.[1] This paper concerns itself chiefly with measurements of the total cross section for slow electrons in chlorine. The purpose in undertaking this experiment was several-fold: (i) for completeness, as no cross-sectional measurements for halogen molecules have been reported; (ii) to put the theory of elastic collisions for diatomic molecules[2] to further test, inasmuch as $Cl_2$ is one of the few molecules for which calculations can be carried through; (iii) to discover whether or not any correlation could be made between the cross sections of $H_2$ and $Cl_2$, and that of HCl, as suggested by Brüche;[3] (iv) and, finally, to obtain any further insight into the nature of molecular fields, and the habits of $Cl_2$, which the experiment might choose to reveal.

## 2. APPARATUS AND METHOD OF MEASUREMENT

The method adopted was essentially that developed by Brode[4] and used subsequently by Normand[5] and others. The scattering chamber consisted of a cylindrical box constructed of tantalum in which a number of slits on the circumference of a 3.0 cm diameter circle served to define a narrow beam of electrons, focused by means of Helmholtz coils, from the source to the collector (Fig. 1). The source was a 3 mil tungsten filament parallel to the axis of a long 7.0 mm diameter cylinder in which a 0.1 mm slit was made, 5 mm in height. The return lead for the filament came back through this cylinder as close as possible to the filament in order to minimize the magnetic field of the straight wire. The current to the collector, $I$, was measured by means of a sensitive galvanometer. This current then passed through a second galvanometer which measured the total current from the source slit, assumed to be equal to some constant times $I_0$. That is

$$I = I_0 e^{-\alpha p x},$$

$p$ being the pressure, $x$ the path length. The absorption coefficient, $\alpha$, is then related to $Q$, the total cross section for collision, by $Q = 1.02\ \alpha$ where $Q$ is in square atomic units.

The scattering chamber was mounted in a Pyrex tube, in which precaution was taken against electrical leakage. Provision was made for the gas, first $N_2$, and later $Cl_2$, to flow continuously through the tube from a large reservoir.

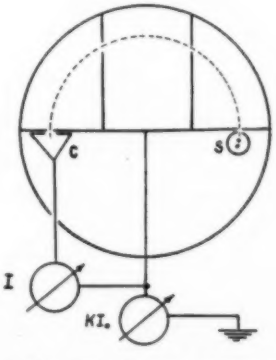


FIG. 1. Schematic diagram of apparatus.

* Now at Harvard University, Society of Fellows.

[1] Ramsauer and Kollath, *Handbuch der Physik*, XXII/2, 243 *et seq.*; R. B. Brode, Rev. Mod. Phys. **5**, 257 (1933).

[2] J. B. Fisk, Phys. Rev. **49**, 167 (1936).

[3] E. Brüche, Ann. d. Physik **82**, 25 (1927).

[4] R. B. Brode, Proc. Roy. Soc. **125**, 134 (1929).

[5] C. E. Normand, Phys. Rev. **35**, 1217 (1930).

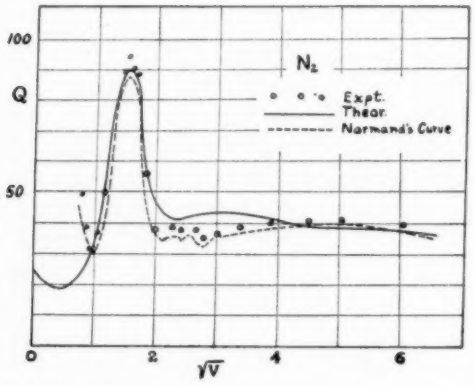


FIG. 2. Total cross section for scattering, $Q$, as a function of electron velocity in $\sqrt{V}$ for $N_2$. Circles are expt. points. Solid line is elastic cross section calculated. Dotted line is experimental curve of Normand.

The reservoir pressure, and that in the tube itself, was adjusted by means of ungreased, sealed $L$ stopcocks on which long grooves were filed. Auxiliary pressure control was had by use of a mercury cutoff near the diffusion pump whose inner sleeve was punctured by a series of holes of decreasing diameter ordered vertically.

Pressure was measured by means of a MacLeod gauge. While Boyle's law does not hold accurately to within a few percent for $Cl_2$, this method of measurement seemed, nevertheless, to be the best available. Great care must be taken, however, that the entire system is free from water vapor. When this is done the reaction of $Cl_2$ with the Hg of the gauge is only noticeable after several weeks of use, and consistent readings can be made. In the preliminary measurements with $N_2$, the capillary leaks were calibrated against the MacLeod gauge, thereby offering an auxiliary test of consistency of pressure readings when $Cl_2$ was used.

Before any measurements were made the tube was thoroughly baked at 450°C. The filament was aged at 2600° for 24 hours. At the end of this aging process a copious emission of electrons was obtained, and reproducible measurements could be made.

The earth's magnetic field was balanced out by a second Helmholtz coil, the electron velocities then calculated directly in terms of the current through the focusing coils and the geometry of the apparatus. This current would be set to focus a particular velocity electron beam, the accelerating potential between filament and source slit then increased until a very sharp maximum was observed from the collector galvanometer. Measurements were taken at several pressures, then plots made of $\ln (KI_0/I)$ *vs.* pressure to determine the validity of the assumption concerning $I_0$. The slope of the resulting line is $-\alpha x$, from which $Q$ is immediately obtainable.

## 3. Results of Measurements

The aggressive nature of $Cl_2$, and the uncertainty occasioned thereby concerning the life of the filament, made it desirable to carry through measurements first with some relatively inert gas. Nitrogen was used for this purpose. The results for $N_2$ compare very favorably with those of previous investigators, and with the theory of elastic scattering, as will be discussed later. These results are shown in Fig. 2.

Chlorine was then introduced into the system. The procedure followed in filament aging and in measurement was exactly that used for $N_2$. The

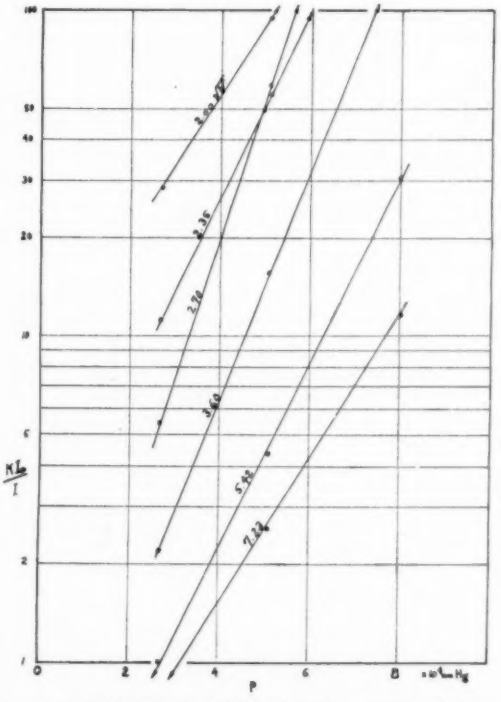


FIG. 3. Logarithmic plot of $(KI_0/I)$ against pressure for $Cl_2$.

filament evaporated somewhat more rapidly in an atmosphere of $Cl_2$ than in $N_2$. It was immediately obvious that the cross sections were very large thereby necessitating the use of a much smaller pressure range for the measurements.

The assumption that the total current leaving the source slit was proportional to $I_0$ (the current which would be collected at zero pressure or with zero path length) was then put to test. Fig. 2 shows that the assumption is justified inasmuch as the plot of $\ln (KI_0/I)$ against pressure results in straight lines. With $Cl_2$ it was found very difficult to obtain any results below 1.5 $\sqrt{V}$. Fig. 4 shows the total cross section calculated directly from such plots as Fig. 3. The crosses and circle represent two entirely independent sets of data.

## 4. Interpretation of Results

### A. Theory of elastic scattering

The theory of elastic scattering of slow electrons by diatomic molecules has been developed previously[2] and has been applied with considerable success to $N_2$, $O_2$ and $H_2$. The molecular field is assumed to be confined within a spheroid. Solutions of the wave equation inside and outside the molecule are then joined at the boundary, these boundary conditions determining the "phase-defects," $\delta_{ml}$, from which the cross section $Q$ may be calculated:

$$Q=4\pi(d/2)^2\sum_{m,\,l} q_{ml}=(4\pi/k^2)\sum_{m,\,l}(2-\delta_{0m})\sin^2\delta_{ml},$$

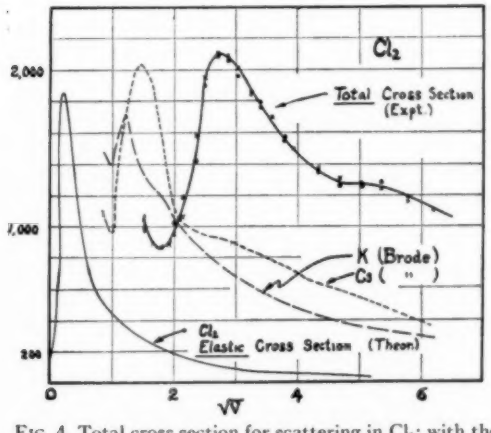


Fig. 4. Total cross section for scattering in $Cl_2$; with the experimental results of Brode for K and Cs for comparison. The solid line is the theoretical elastic cross section for $Cl_2$.

where $\delta_{0m}=0$ if $m\neq 0$; $d$ is the internuclear distance; and $k=2\pi/\lambda$. The "phase-defects," $\delta_{ml}$, are given by

$$\tan\delta_{ml}=(-1)^m\left[\frac{R'e^{(1)}_{m,\,l}(c,\,\xi_0)-g_{ml}\cdot Re^{(1)}_{m,\,l}(c,\,\xi_0)}{g_{ml}Re^{(2)}_{m,\,l}(c,\,\xi_0)-R'e^{(2)}_{m,\,l}(c,\,\xi_0)}\right],$$

where the $Re_{m,\,l}{}^{(1)\text{ or }(2)}(c,\,\xi_0)$ are spheroidal functions, solutions of the wave equation for $V=0$; and

$$g_{ml}=f'(\xi_0)/f(\xi_0)-(\alpha-c^2)^{\frac{1}{2}},$$

$f(\xi_0)$ being the "radial" part of the solution for $\xi<\xi_0$, i.e., $V\neq 0$, $\alpha$ being $2Zd\xi_0/(\xi_0-1)^2$, $\xi_0$ the spheroidal boundary and $c$ being $\pi d/\lambda$.

The cross sections may be obtained in terms of a parameter $\beta^2=Z^*\cdot d\cdot\xi_0/4$ where $Z^*$ is an "effective" charge number determined for a given molecule from Slater's rules on shielding constants. For each symmetrical diatomic molecule there is then a unique value of $\beta$ to determine its elastic cross section. For $N_2$ the value of $\beta$ is 1.32, for $Cl_2$ it is 2.10. Referring to previous calculations of "partial cross sections" as functions of $\beta$, the total cross sections for elastic scattering may be obtained as a sum of partial cross sections.

### B. Relation of theory to experiment

The solid line of Fig. 2 is the theoretical cross section calculated as above for $N_2$. The agreement here is excellent. It seems that up to electron velocities of 50 volts nearly all of the scattering is elastic. The experimental curve of Normand[5] is given for comparison.

For $Cl_2$, however, it is quite a different matter. Theory predicts a very high maximum below 0.5 $\sqrt{V}$, falling rapidly as the velocity approaches zero. This peak is contributed by the $q_{m=0,\ l=1}$ "partial cross section." For fluorine theory gives a similar result. This result is not unlike that obtained for scattering in Na, K, Cs, Rb by Allis and Morse[6] and experimentally by Brode.[1] It is obvious then that either the theory breaks down for $Cl_2$, or the extremely large cross section ($Q=2100$ at 2.65 $\sqrt{V}$) is due chiefly to several possible types of inelastic collisions. The theory for Na, etc., gives no account for the extremely high maxima observed. Similarity between the cross sections of those elements with one electron

[6] Allis and Morse, Zeits. f. Physik **70**, 567 (1931).

outside a closed shell, the alkali metals, and those with an almost completed shell, the halogens, is not surprising. The fields of both of these groups of elements must spread out much farther than those of any of the other elements. The ratio of the energies at which the high maxima occur in K and in $Cl_2$ corresponds roughly to the ratio of their ionization potentials. Here, however, any conclusion is difficult inasmuch as the process in $Cl_2$ is much more complicated than in K.

Even at very low velocities one would hardly expect to check with the theory of elastic scattering for here the probability of capture to form a negative ion would be large. The remainder of the cross section curve must be accounted for by a number of probable events: dissociation (the energy required being but 2.47 $V$) with the formation of negative ions, ionization, excitation, and excitation of vibration and rotation. It would be interesting to explain by a direct calculation these high and unexplained peaks in the Na, K, Cs, Rb and $Cl_2$ curves. These involved calculations require approximate wave functions, which at present are not available.

Comparison of the cross section curves of $H_2$, HCl, and $Cl_2$ is interesting. $H_2$ has a maximum of about 60 of these atomic units at 1.5 $\sqrt{V}$, whereas $Cl_2$ has the value of $Q=2100$ at 2.65 $\sqrt{V}$. HCl, on the other hand, has a peak at 3.5 $\sqrt{V}$ of some 80 sq. atomic units. This comparison only lends weight to the previous conclusion of Brüche[3] that the cross section is determined by the nature of the external shell of electrons; HCl being very like argon.

The author is indebted to Professor E. S. Lamar and to Doctors R. P. Johnson and P. T. Smith for teaching him the technique of experiment. Professor W. B. Nottingham and Dr. E. B. Jordan have kindly supplied the author with clues to the overcoming of several difficulties.

---

JANUARY 1, 1937 PHYSICAL REVIEW VOLUME 51

# Probe Measurements on High Pressure Arcs

R. C. MASON, *Research Laboratories, Westinghouse Electric and Manufacturing Company, East Pittsburgh, Pennsylvania*

(Received October 16, 1936)

The introduction of a probe in a carbon arc in air at atmospheric pressure has been found to increase the arc voltage by several volts, the increase being almost independent of the velocity with which the probe is moved, but being a function of probe perimeter. Observation showed that the probe was surrounded by a dark space, with a fairly definite boundary several times the diameter of the probe, which was uninfluenced by the potential applied to the probe. The gas temperature fell from several thousand degrees at the outer boundary of the dark space to a few hundred degrees at the probe surface. The rate of flow of energy to the probe was measured to be about 50 watts per cm length of probe, for a 0.03 cm diameter probe at the center of a 6-amp. arc; calculations show about half the energy was carried by thermal conduction across the dark space, and about half came from recombination of dissociated molecules upon the probe surface.

The interpretation of the probe current voltage characteristic, valid at low pressures, does not apply at high pressures because ions reaching the probe must travel from the arc through the dark space. An insulated probe must have a potential several volts negative with respect to the cathode side of the dark space boundary; from this interpretation, the cathode fall of the arc lies above 10 volts, and the anode fall is about 20 volts. In a 6-amp. arc, the current density in the positive column is about 20 amp. per $cm^2$; the gradient, 33 volts per cm; and the ion density, above $10^{14}$.

KNOWLEDGE of low pressure gas discharges has been greatly advanced by numerous investigations in the dozen years since Langmuir showed how the current voltage characteristics of probes could be made to yield information about the distribution of potential, ion density, and electron temperature in such discharges. In attempting to apply the Langmuir probe methods, however, to the study of high pressure positive columns (pressure of a few millimeters or greater) one encounters experimental difficulties at once: the melting of the probe used, or the attainment of a temperature sufficient for thermionic emission. Nottingham overcame these by moving a probe through the arc at a speed so great that the probe never attained a high temperature. Meas-

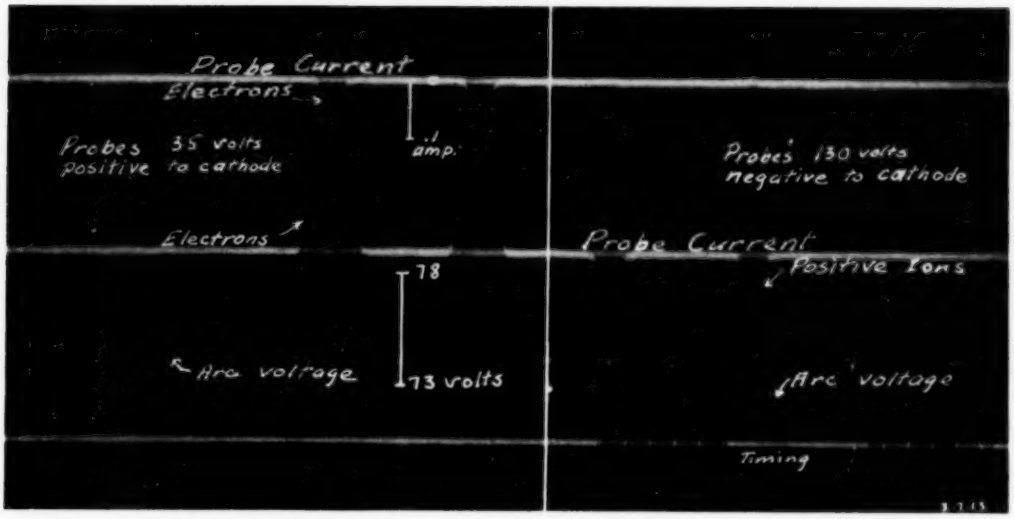


FIG. 1. Passage of two 0.025 cm diameter probes through 6-amp. arc.

uring the charge collected by the probe for different voltages, he applied the usual Langmuir theory, and from his results believed he had obtained the electron temperature and the potential distribution in a number of arcs at atmospheric pressure.[1] Following Nottingham, Bramhall[2] and Myer[3] used essentially the same methods in studying other arcs, obtaining results not always in agreement.

Experiments with a moving probe in a carbon arc at atmospheric pressure, in which an oscillograph was used to record currents and voltages, revealed a large change in arc voltage when the probe passed through the arc.[4] Since so great a change must have been due to a profound disturbance of the arc by the probe, which might vitiate the usual interpretation placed upon the probe characteristics, extensive experiments have been undertaken to find the cause of the disturbance, and to determine its effect upon probe measurements at high pressures.

This paper, in reporting the results of these experiments, first describes the effect of probes of different geometries and speeds. Photographs, made with a special design of probe, show the probe to be surrounded by a large dark space. Primarily, the origin of the disturbance seems to lie in the cooling of the arc by the probe. Next, this idea is advanced further by actual measurements of the energy received by a probe in the arc. Rough calculations show that about half this energy is conveyed by thermal conduction; the remainder must come from the recombination of dissociated molecules on the probe surface.

With the nature of the disturbing effect of the probe in mind, the difficulties of interpretation of the probe current voltage characteristic, and the contrast with the low pressure case, are discussed fully. It is shown that the presence of the dark space around the probe makes an exact description of the motion of ions to the probe almost impossible, but a qualitative explanation of the

TABLE I.

| PROBE SECTION | MAXIMUM INCREASE IN ARC VOLTAGE |
|---|---|
| 0.01×0.046 cm | |
| Broad side parallel to arc axis | 8.25 |
| Broad side perpendicular to arc axis | 8.24 |
| 0.02×0.09 cm | |
| Broad side parallel to arc axis | 10.57 |
| Broad side perpendicular to arc axis | 10.64 |
| 0.0056×0.092 cm | |
| Broad side parallel to arc axis | 9.17 |
| Broad side perpendicular to arc axis | 9.39 |

[1] Nottingham, J. Frank. Inst. **206**, 43 (1928); **207**, 299 (1929).
[2] Bramhall, Proc. Camb. Phil. Soc. **27**, 421 (1931); Phil. Mag. **13**, 682 (1932).
[3] Myer, Zeits. f. Physik **87**, 1 (1933).
[4] Mason, Phys. Rev. **40**, 1045 (1932).

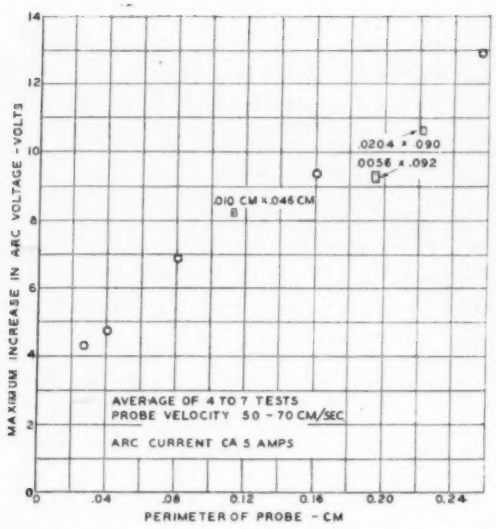
MAXIMUM INCREASE IN ARC VOLTAGE - VOLTS
PERIMETER OF PROBE - CM
.0204 x .090
.0056 x .092
.010 CM x .046 CM
AVERAGE OF 4 TO 7 TESTS
PROBE VELOCITY 50 - 70 CM/SEC
ARC CURRENT CA 5 AMPS

FIG. 2. Increase in arc voltage caused by probe swinging through arc.

nature of the probe characteristic is developed from the form of the potential and ion distributions which must set up about the probe. In this way, a rough idea of the potential distribution in the arc is secured, but no information about the electron temperature results. Finally, a critique of earlier investigations with probes at high pressures is given, and general conclusions about the use of probes are drawn.

## I. Disturbance Caused by a Probe

### Effect on arc voltage

In these investigations electrodes, 13 mm in diameter, of Siemens "E Homogenkohle E" brand carbon,[3] were mounted so that the arc axis was vertical, with the cathode below. A fine copper probe wire, on a long radius arm revolved in a plane perpendicular to the arc axis. On one of the probe passages through the arc, an oscillographic record of currents and voltages was made. A typical oscillogram is shown in Fig. 1, upon which are recorded two separate exposures, the first being represented in the part to the right of the vertical line, and the second in the part to the left. Two 0.025 cm diameter probes followed one another in rapid succession, through a 6-amp.

[3] The electrodes were kindly furnished by the Siemens Planiawerke.

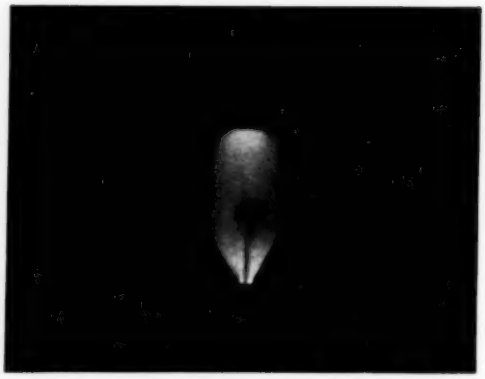

FIG. 3. Photograph of 6-amp., 0.89 cm long, arc with 0.025 cm probe wire 0.38 cm from cathode (lower) electrode.

arc 0.89 cm long. The first probe, reading from left to right, was 0.38 cm from the cathode and the second, 0.13 cm from the cathode. The upper trace in the left picture shows the electron current collected by the probes when they were about 35 volts positive with respect to the cathode. The next trace gives the probe current on a much larger scale, obtained by a vacuum tube amplifying circuit. In the left half of the figure, the saturation of one tube for large probe currents resulted in a constant deflection during most of the probe passage. When the probes were 130 volts negative with respect to the cathode, in the right half of the figure, the positive ion current collected is given, on an arbitrary scale. The third trace shows the arc voltage, and the bottom trace records the closing of timing contacts on the probe arm from which the probe velocity can be obtained. The arc length and arc voltage were slightly greater on the second exposure. It will be noted that the arc voltage increased as the probe moved into the arc, and the maximum increase, when the probe was in the center, amounted to about 6 volts. In addition, the increase in arc voltage was the same when the probes were negative as when they were positive.

One cause of the increase in arc voltage which suggested itself was mixing in of cold gas carried along by the rapid motion of the probe. In order to test this point, the probe velocity was varied between wide limits, and probes of different sizes and shapes were used. No consistent effect of

probe speed was found: for 0.025 and 0.051 cm diameter probes, the maximum increase in arc voltage was about 20 percent smaller at 120 than at 10 cm per sec., while for a 0.081 cm probe, the increase was 10 percent greater at the high velocity.

Next, probes of rectangular cross section were tried, both with the broad side of the probe parallel to the arc axis, and with it perpendicular. Very nearly the same increase in arc voltage was noted in either case. The averages of several tests for different probes are tabulated in Table I. As any turbulent gas flow would be expected to be influenced by probe velocity, or in particular by the orientation of the flat, rectangular probes, it must be concluded that such effects are not responsible for the increase in arc voltage.

When the increase in arc voltage is plotted against probe perimeter as in Fig. 2, a direct correlation is seen, the voltage rise being almost directly proportional to probe perimeter. The values for round wires are indicated by circles, and the points for the rectangular probes, by rectangles. Thus it is strongly suggested that conduction of heat to the probe, or some other diffusion phenomenon, is primarily responsible for the increase in arc voltage.

In order to see distinctly any change in appearance of the arc produced by the probe, and as well to obtain current voltage characteristics more conveniently, a different type of probe was devised. A small copper wire was wound from one spool to another, passing horizontally through V grooves in maple guides mounted on a movable carriage. Then with the wire moving along its own axis at a speed sufficient to prevent melting when in the arc, the carriage could be moved so as to introduce the probe into the vertical arc. In this way, it was possible to move the probe wire very slowly through the arc, or even to hold it at any desired position in the arc. With this type of probe, which produced only a few tenths of a volt greater change in arc voltage than the revolving probe, it was observed that the arc voltage increased markedly only after the probe entered the central intense core of the arc.

Though the increase in arc voltage was virtually independent of the probe potential, very large negative potentials resulted in an additional few tenths of a volt increase. The type of supply circuit had a considerable effect on the increase of arc voltage with a revolving probe: if no inductance was included in the circuit, the increased arc voltage produced by the entrance of the probe caused a reduction in the arc current; the reduced current through the undisturbed parts of the arc required a higher arc voltage, so the measured increase in arc voltage included the effects of both factors. From the extensive data collected, it was possible to construct a volt-ampere curve for an arc with a 0.025 cm probe passing through its center, and to compare it with the characteristic of an undisturbed arc. The increase in arc voltage caused by the probe alone was larger the smaller the current, being 3.5 volts at 11 amps. and 7 volts at 3 amps.

### Visual observations

When the continuous wire probe was used, it was seen that a large dark space surrounded the probe. The boundary of the dark space was quite sharp, being as definite as the outer boundary of the arc itself. The diameter of the dark space, within the accuracy with which it could be measured, was independent of the potential applied to the probe within very wide limits. In photographs, the dark region appeared exactly the same, whether the probe was over a hundred

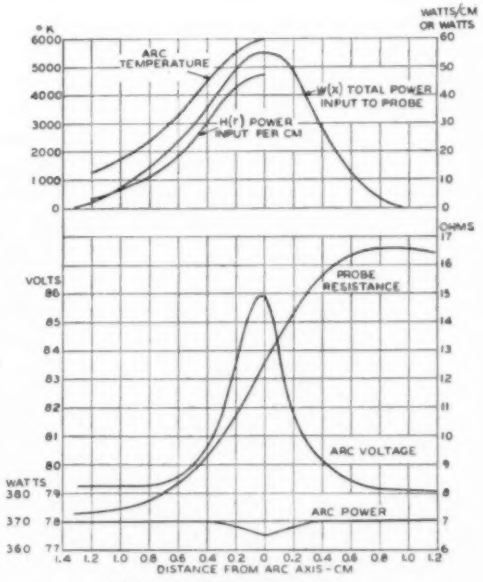


FIG. 4. Thermal probe in arc.

volts negative and collecting several milliamperes of positive ion current, or was sufficiently positive to receive several hundred milliamperes of electrons; but for very large negative voltages, above 200 say, a distinct bluish spark passed from the probe to the arc. The dark space surrounding the probe is thus nothing like the dark space at the cathode of glow discharges, or that surrounding negatively charged Langmuir probes in low pressure discharges; but because of its descriptive character, the term "dark space" will be used herein to apply to the region devoid of light which has been found about cold wires in atmospheric arcs.

A photograph of the arc and probe is shown in Fig. 3. A continuously moving 0.025 cm copper wire was held in the center of a 6-amp. arc, 0.38 cm from the cathode (lower) terminal. The lower part of the arc is hidden by the guide, the V groove in which can be seen.

From photographs, the following dark space diameters were found for a 0.025 cm diameter insulated probe at different positions in a 6-amp. arc: 0.086 cm diameter dark space at 0.13 cm from the arc cathode; 0.112 cm, at 0.25 cm; 0.128 cm, at 0.38 cm; and 0.168 cm, at 0.51 cm. Approximately the same dimensions were obtained when the dark space was measured by projecting an enlarged image on a screen, and by observing through a measuring telescope. Substantially the same results were found for currents up to 12 amps. The dark space size was independent of the velocity of the probe wire, which was usually between 20 and 50 cm per sec., and of the radial position of the probe in the arc core. Some measurements of the projected image of the dark space surrounding other sizes of probes were made, but with not as great accuracy as the above determinations. The results are: for a 0.013 cm diameter probe, a dark space 0.083 cm diameter; for a 0.051 cm probe, a dark space 0.143 cm, at 0.38 cm from the cathode.

At the center of the arc, or near the cathode, it was possible to make the continuous wire run perfectly steadily through the axis of the arc, with no motion of the arc core; but near the anode, such a position was one of unstable equilibrium, the arc moving quickly to one side or the other. Presumably, the arc behaved similarly when the revolving probe was used; so, near the anode, the relative velocity of the probe and the arc core varied widely as the probe passed through the arc, even though the probe velocity may have been constant. For other positions of the probe in the arc, the relative velocity was probably always nearly equal to the probe velocity; some nonuniformity occurred as may be seen from the slight dissymmetry in Figs. 1 and 4.

## II. Heating of Probe

### Experimental

As the increase in arc voltage caused by the introduction of a probe has been clearly shown to be unaffected by turbulent gas flow around the probe, but to be a function of probe perimeter, loss of energy from the arc by diffusion of particles through the dark space to the probe could explain the increased power input required. In order to test the idea quantitatively, an experiment was arranged to measure directly the heat input to a probe. Consider a revolving probe passing once through an arc. Since the arc is circular in section, different parts of the probe will be in the arc different lengths of time and will attain different temperatures. If $W(t)$ represents the power input to the probe at any time $t$, then the total energy input up to $t$, measured from $t=0$ at some time prior to the entrance of the probe into the arc, will be

$$\int_0^t W(t)dt = c\delta A \int_0^l T ds, \qquad (1)$$

where $c$ is the specific heat; $\delta$, the density; and $A$, the cross section of the probe; $s$ is measured along the probe; and $T$, the temperature rise of the probe at time $t$, is a function of $s$. The integral on the right must be taken not over the length of the probe in the arc, but over the total length, as there will be conduction of heat along the probe. It is assumed, however, that there is no loss of energy *from* the wire. Likewise, the *increase* in resistance of the probe due to the change in temperature is

$$\Delta R = ((\rho_0 \alpha_0)/A) \int_0^l T ds, \qquad (2)$$

where $\rho_0$ is the resistivity at room temperature, and $\alpha_0$ its temperature coefficient. It will be more

convenient later to express $W$ as a function of $x$, the distance of the probe from the axis of the arc at any time $t$; thus, from (1) and (2), if $v$ is the probe velocity

$$W(x) = (c\delta A^2/\rho_0\alpha_0)v(d/dx)\Delta R. \qquad (3)$$

As a probe, a one-inch length of the filament from a 60-watt Mazda lamp, seasoned by several hours burning, was chosen. The filament was a coil, 0.0297 cm outside diameter, wound of 0.0046 cm tungsten wire, 145 turns per cm. The probe was placed in one arm of a wheatstone bridge, which was approximately balanced with the probe out. The unbalance in current when the probe was in the arc was obtained by an oscillograph. The cold resistance of the probe was about 8 ohms; the bridge current through it was a little over 1 ma. An oscillogram, showing the resistance of the probe, the arc voltage, and the power input to the arc is reproduced in the lower part of Fig. 4 with time translated into distance from the arc axis; the probe was midway between the electrodes. It was found that the decrease of resistance after the probe emerged from the arc was very slow, so it is proper to neglect the cooling of the probe while it is in the arc. From the slope of the resistance curve, the total power input to the probe, $W(x)$, was calculated as above.

Before any calculations can be made on heat flow, it is necessary to find the heat input per unit length of the probe. This may vary from point to point in the arc, so it would not be correct merely to divide the total power by the arc diameter. Fig. 4 gives further evidence on this point; one sees that the probe is being heated before it enters the core of the arc at about $r=0.3$; in fact almost half the total input comes from regions about the arc in which the presence of the probe causes almost no change in the arc voltage. If the power input per cm length of the probe, $H(r)$, is expressed as a function of the distance from the center of the arc, then

$$W(x) = 2\int_x^\infty H(r)\frac{rdr}{(r^2-x^2)^{\frac{1}{2}}}. \qquad (4)$$

Eq. (4) is very similar to Abel's equation, so a solution for $H(r)$ may be found readily.[6]

[6] Cf. Bocher, *Integral Equations*, second edition, p. 8.

$$H(r) = -\frac{1}{\pi}\int_r^\infty W'(x)\frac{dx}{(x^2-r^2)^{\frac{1}{2}}}. \qquad (5)$$

From Fig. 4, and similar curves, $W(x)$ was obtained, and Eq. (5) solved for chosen values of $r$ by mechanical integration. In the upper part of Fig. 4, $H(r)$ is plotted for the experimental data given below it. Considerable variability was exhibited in the values of $H(r)$ obtained, as might be expected since a double graphical differentiation of an experimental curve was involved. For $r>0.3$ all tests gave about the same $H(r)$, but values of $H(0)$ between 44 and 138 watts per cm were obtained. The most reliable gave approximately 50 watts per cm for the power input at the center of the arc. Likewise the maximum total power inputs to the probe, $W(0)$ were scattered, values between 55 and 90 watts being found; probably the best figure is 55.

**Effect of probe on arc energy**

In Fig. 4, it will be seen that where the arc voltage increase was about 10 percent of the maximum, corresponding to a probe position just outside the central core, the power input to the probe was $\frac{1}{3}$ to $\frac{1}{2}$ the maximum. Most of the arc energy is developed within the central core and lost from it to the surrounding medium. Parts of the probe lying outside the core, though receiving a large amount of heat from the hot gas, do not cause any additional energy loss from the arc; what they receive would be lost from the core even if the probe were not present. Energy given to the portion of the probe inside the core represents an additional loss which must be made up by an increase energy input to the arc. From the curve for $H(r)$ such as Fig. 4, the total energy received by the part of the probe within the core, for a probe passing through the arc axis, was found by integrating $H(r)$ from $r=0$ to $r=$ radius of the core.

With a noninductive circuit, the total power input sometimes actually decreased, as in Fig. 4, when the probe was in the arc, despite the energy abstracted by the probe, because of the large decrease in arc current resulting from the rise in arc voltage. When a heavy inductance was included in the circuit, then the measured arc power rose when the probe entered the arc. From experimental volt-ampere characteristics, it was

possible always to calculate the reduction in the arc power input caused by the decrease in arc current; this added to the actual measured effect on arc power by the probe, should give the change in the rate of energy input to the arc caused by the presence of the probe. The increase in arc watts due to the presence of the probe, calculated in this way for a number of tests, agreed well with the integral of $H(r)$ over the arc core.

From the energy standpoint, then, the effect of a probe upon a high pressure arc is to produce artificially an added surface, much larger than the probe wire itself, through which energy flows from the arc. The increased losses from the arc require additional energy input, and hence a higher arc voltage, in order to maintain the arc.

**Methods of conveyance of energy to probe. Radiation**

Energy may be conveyed to the probe by three ways: radiation, thermal conduction, and recombination upon the probe of dissociated particles (both atoms and positive ions and electrons). The radiant energy received is probably negligible: Holm and Lotz[7] from measurements of the total radiation from the positive column of a long carbon arc with large a.c. currents flowing, give the fraction of total energy loss appearing as radiation as 5 percent at 30 amperes. Extrapolation of their curve to below 10 amp. would carry the radiation loss to zero. This factor can thus be neglected.

**Thermal conduction**

The appearance of the dark space around the probe suggests that the gas at the outer boundary is at the temperature of the positive column, while the temperature of the probe is always quite low. Under this assumption, the heat flow to the probe may be calculated from the conduction equation

$$k(\partial T/\partial r)2\pi r = H_K, \qquad (6)$$

where $k$ is the thermal conductivity, $T$ the temperature in °$K$ at any point and $H_K$ the energy conducted per cm per sec. Now the temperature has such wide limits it will not be correct to take $k$ as a constant. Neglecting variation of specific heat and mean free path with temperature, simple kinetic theory makes the thermal conductivity proportional to $T^{\frac{1}{2}}$. In order to get an idea of the magnitude of the transport by thermal conduction, it will be assumed for the present $k = k_0 T^{\frac{1}{2}}$. Eq. (6) may be integrated then, with the boundary conditions that $T = T_0$ = temperature of probe for $r = r_0$ = probe radius and $T = T_R$ = temperature of arc core for $r = R$ = radius of dark space, with the result

$$H_K = (T_R^{\frac{3}{2}} - T_0^{\frac{3}{2}})((4\pi k_0)/(3 \log R/r_0)). \qquad (7)$$

The temperature rise of the tungsten coil in passing through the arc, gotten from the total change in resistance, was not over 200°; thus, roughly $T_0 = 500$°K. The temperature of the arc may be taken as 6000°K.[8] Putting in Eq. (7) these values, together with $2R = 0.13$, $2r_0 = 0.0297$, $k_0 = 1.45 \times 10^{-5}$ watt-sec. per cm² per degree from the value for air at room temperature, $H_K$ comes out 18.5 watts per cm.

Since the gas in the dark space is largely atomic the value of $k_0$ used should be modified: the smaller specific heats of the atoms and the increased specific heat of the remaining molecules at high temperatures would have opposite effects, however. Through the Sutherland correction for variation of mean free path with temperature, $k_0$ should be increased. A rough estimate of the net effect of all these factors raises the energy transported by thermal conduction to 20 to 25 watts per cm at the arc axis—about one-half the total input to the probe.

**Recombination**

In these heating experiments the probe was insulated so that the only electrical heat input came from direct recombination of positive ions and electrons on the surface. From direct measurements, the current of positive ions, and of electrons, was less than 1 ma per cm, so the heat of recombination amounted to not over 0.015 watts—entirely negligible compared with the total of 50.

[7] Holm and Lotz, Wis. Veroff. a.d. Siemens-Konzern **13** (2), 87 (1934).

[8] The temperature of the gas in the positive column has been measured in a variety of ways in the past few years: Ornstein, Physik Zeits. **32**, 517 (1931); Ramsauer, E. u. M. **51**, 189 (1933); v. Engel and Steenbeck, Wis. Veroff. a.d. Siemens Konzern **10** (2), 155 (1931); Suits, Phys. Rev. **47**, 335 (1935). Only Ornstein had experimental conditions like those in this paper (pure carbon electrodes, 2 to 12 amp.), so his value of 6000°K has been adopted.

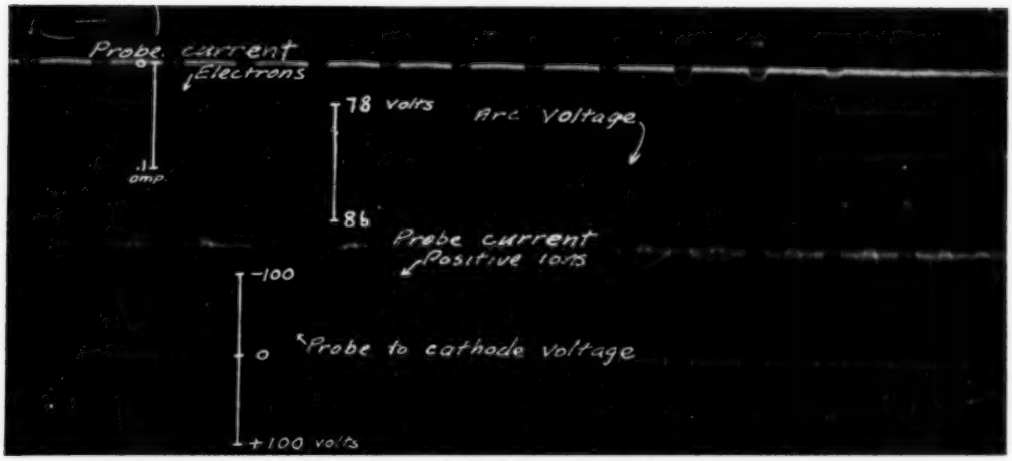


FIG. 5. Probe 0.51 cm from cathode of 6-amp., 1.14 cm long, arc. Probe moved through arc during exposure of film.

At the high temperature of the arc, complete dissociation of $O_2$ and about 80 percent dissociation of $N_2$ may be expected.[9, 10] It is likely no recombination of atoms occurs within the dark space.[11] Atoms diffuse, then, from the boundary of the dark space to the probe wire, where they recombine, giving up the heat of dissociation to the probe. From the previous rough calculations, it seems that roughly half, or a little over, of the total energy input to the probe must come from this source. A solution of the diffusion problem for the four-component gas in the dark space is impossible for the present state of diffusion theory. It is entirely plausible, however, that recombining atoms should contribute so largely to loss of energy from the arc to the probe.

**Temperature distribution in the arc**

From the measurement of the rate of heat flow to the probe and the assumed temperature at the arc axis of 6000°K, it is possible, with some uncertainty, to calculate the temperature distribution in the arc. If the diameter of the dark space remains constant, if the effective thermal conductivity does not change, if the ratio of the heat carried by thermal conduction to the total heat delivered to the probe is the same everywhere, then the temperature at any radius may be found, for by Eq. (7) $(T^4-T_0^4) \propto H(r)$. It seems likely these conditions may be met within the arc core, where the temperature is high; it is observed that the dark space diameter is constant throughout the core. Outside the core, the temperature may be very different. Such calculations may indicate the trend of the temperature, however; and in Fig. 4, $T(r)$ found in this way is plotted. The temperature does not fall much within the dark space around the arc core.

## III. Probe Current Voltage Characteristics

The effect of the probe on the arc from an energy standpoint having been considered, this section discusses the direct electrical consequences of the introduction of a probe, and the modifications which must result in the interpretation of the probe current voltage characteristic. The use of the continuous wire probe described above offered the great advantage of enabling one to measure quickly the current collected by a probe at a known position in the arc for a whole series of probe voltages. The probe potential, applied between the probe and the cathode, was derived from a d.c. battery in series with a 15-cycle a.c. generator. The magnitude of the voltages was adjusted so that during one cycle the probe current would vary from a large positive ion current to a large electron current. The currents and voltages are recorded by an oscillograph. Positive ion currents to the

[9] Lewis and v. Elbe, J. Am. Chem. Soc. **57**, 612 (1935) and literature there cited.
[10] Mulliken, Phys. Rev. **46**, 144 (1934).
[11] Kassel, *Kinetics of Homogeneous Gas Reactions* (Chemical Catalog Co.), p. 131.

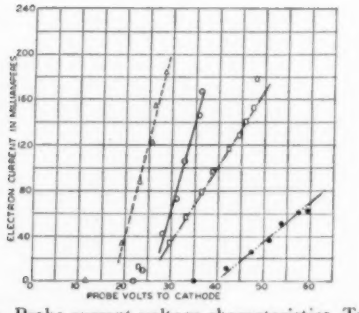


FIG. 6a. Probe current voltage characteristics. Triangle, probe 0.13 cm from cathode, arc 6 amp.; open circle, probe 0.38 cm from cathode, arc 8.7 amp.; square, probe 0.38 cm from cathode, arc 5.9 amp.; closed circle, probe 0.38 cm from cathode, arc 3.2 amp.

probe were measured by means of a two-stage vacuum tube amplifier, the saturation of one tube of which protected the oscillograph element from damage by the large electron currents. The electron currents were measured by another less sensitive element.

A typical oscillogram obtained is shown in Fig. 5. The top trace shows the probe current; when the probe was collecting positive ions, the sensitivity of the element was so low no deflection shows. The next trace gives the arc voltage, which decreased as the probe moved slowly from the center to the outside of the arc. The third trace also gives the probe current, but on an arbitrary scale, as it is actually the output current of the vacuum tube amplifier which is shown. Saturation of the amplifier resulted in a constant deflection when large electron currents were collected, but when positive ions were collected, the deflection was almost directly proportional to the positive ion current. The bottom trace gives the potential of the probe with respect to the cathode.

Current voltage records were attempted with the probe at several positions in the arc, for currents from 3 to 12 amp., and for three arc lengths. Because of the motion of the arc when the probe was introduced near the anode, described before, it was not possible to get a complete record with the probe near the arc axis for these positions. Some results are shown in Figs. 6a, b.

**Theoretical difficulties at high pressures**

Some of the reasons why the methods of analysis of probe current voltage characteristics applicable for low pressures break down at high pressures may be pointed out. In the first place, the potential drop over a length of the arc equal to the dark space thickness amounts to several volts; so, to speak of the "potential of the probe to space" has no meaning unless some particular point is specified. Because of the changes brought about by the probe, the potential distribution when the probe is in the arc is not at all like that in the undisturbed arc.

Within the dark space, it seems likely no ions are being produced, and none are lost except at the probe surface. Consequently, the current collected by the probe depends on the motion of the ions through the dark space from their point of origin in the arc. Changes in the probe potential, and in the absorption of ions by the probe, have a direct effect on the ion distribution throughout, and around, the dark space. In a low pressure discharge, the mean free paths of the ions are so long, the collection of ions by the probe has little effect on the discharge outside the space charge sheath around the probe.

At low pressures, it is assumed that the point of zero field marks the space charge boundary, and that all the potential applied to the probe is taken up within the space charge sheath. Practically it makes little difference exactly where the sheath boundary is located, or whether the field there is precisely zero, for it is assumed the random motion of the ions is responsible for carrying them up to and across the sheath boundary. To speak of the simple hypothetical case of a sharp boundary, with zero field, and current limited by space charge is sufficiently exact. In probe measurements at high pressures, however, where all ions which arrive at the probe must travel through the dark space, weak fields may have a large influence on the current collected. There may be *no* point

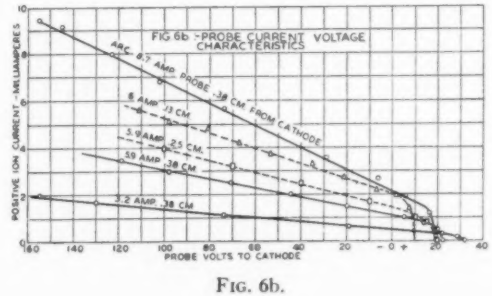
FIG 6b - PROBE CURRENT VOLTAGE CHARACTERISTICS
ARC 6.7 AMP. PROBE .38 CM FROM CATHODE
8 AMP .13 CM
5.9 AMP .25 CM
5.9 AMP .38 CM
3.2 AMP .38 CM
POSITIVE ION CURRENT - MILLIAMPERES
PROBE VOLTS TO CATHODE

FIG. 6b.

of zero field where one may say the space charge sheath terminates. In high pressure discharges, one may still divide the region about the probe into two parts, in one of which the ions move under the influence of strong electric fields and in the other, the ions are carried by weak fields and diffusion, with the boundary between the two defined in some arbitrary fashion. The first may be termed the space charge sheath; for the calculation of the current flowing through it, it will make little difference exactly where the boundary is located or what the field there is. The second may be called the weak field or diffusion region; the field at, and the location of, the boundary will be extremely important in determining the current which flows through the dark space up to the sheath boundary. In other words, at low pressures the potential applied to the probe has no effect on the current density at the sheath boundary for it is only the random motion of the ions which bring them up to the boundary; at high pressures, the influence of the potential applied to the probe extends far beyond what one would ordinarily think of as the sheath boundary, because weak fields and diffusion carry ions up to that boundary.

For precise determination of the current, then, it would be necessary to consider the whole of the dark space, and even beyond, as one region, and calculate the motion of the ions under diffusion and electrical forces. Even the approximation of breaking the region up into a strong field, or space charge, part and a weak field part still leaves the problem too complicated for solution: cylindrical symmetry does not occur because the ion density and fields are not constant around the probe; one must use diffusion and mobility constants which are functions of position through the variation of the temperature and field. A further complication is that the dark space boundary is not an equipotential surface. Though one could set up the differential equations describing the relations between the ion density, current and probe potential, their solution would be extremely difficult if not impossible.

The contrast between the regime to which the Langmuir theory applies and the high pressure discharge will be brought out more clearly by considering the results of some orienting calculations which have been made. Under the assumption that diffusion alone governs the motion of ions through the dark space, it has been found that diffusion velocities over most of the dark space are so much smaller than the velocities of the electrons and ions under even moderate fields, such as exist in the positive column, that the effect of electrical fields are predominant. Accordingly, it is incorrect to assume that the dark space boundary is an equipotential surface; the motion of ions across the boundary and in the outer part of the dark space will, in most cases, be determined largely by the fields there. Further confirmation may be adduced from the data for large negative probe potentials, which show positive ion currents many times the calculated diffusion currents. In some cases, however, particularly when the probe receives about equal numbers of positive ions and electrons, the diffusion of electrons must be important.

If the energy received from the electric field is neglected, rough calculations show that for high electron drift velocities through the dark space, the electron temperature at the probe surface must be almost the temperature possessed outside the dark space, while for low electron velocities, virtual thermal equilibrium with the gas will always exist. If the energy received from the electric field is considered, it is much more difficult to estimate the electron temperature near the probe. An electron, starting from rest in a uniform field, traverses a distance of about 100 mean free paths in the direction of the field before acquiring 90 percent of its terminal energy —a distance equivalent roughly to the dark space thickness. Consequently, if the field varies much within the dark space, the electron temperature may lag behind considerably. The electron temperature will not necessarily be the same at all points the same distance from the probe, depending as it does both upon the field, the time spent in the dark space, and the gas temperature. The temperature of the electrons at the probe surface, or at the boundary of any region of strongly attracting forces about the probe, may be higher, or lower, than their temperature outside the dark space, depending upon the path followed by the electrons in reaching the probe. Since the electron temperature is not a constant, the Boltzmann equation has no applicability. The positive ions in the dark space may be expected

to be in thermal equilibrium with the gas, except in very strong fields, or space charge regions, near the probe.

Other calculations, while not exact, are of sufficient accuracy for one to draw the following conclusions: all space charge sheaths, or strong field regions, about the probe are small in extent compared to the dimensions of the dark space. Recombination of ions within the dark space is negligible under most conditions, but the possibility exists that sometimes recombination may occur near the probe; in which case, the effect is merely to increase the probe diameter slightly.

Summarizing, the usual concepts applicable to the explanation of probe characteristics at low pressures have no force at high pressures, because the ions reaching the probe must travel through the dark space from the arc. Since their motion through the dark space is influenced by the fields present there, the effect of the change in voltage applied to the probe is not confined to a narrow space charge sheath about the probe, but is felt throughout the dark space. For the same reason, the current density at the sheath boundary is not constant but depends upon the probe voltage.

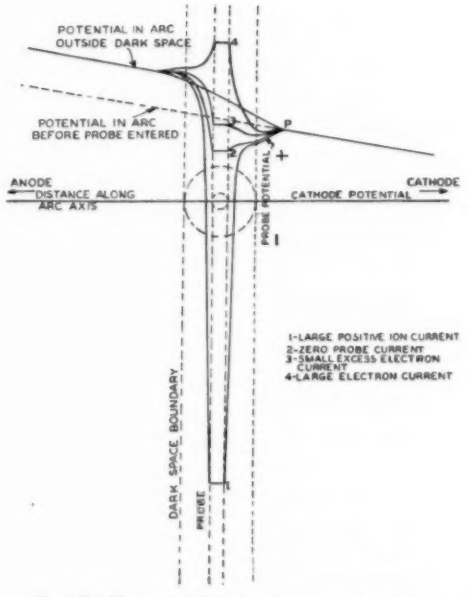


FIG. 7a. Potential distribution around probe.

**Qualitative explanation of probe characteristic**

In the light of the ideas developed above, it is possible to explain the general shape of the probe characteristic. Since no ions are generated or lost within the dark space, except at the probe, there can be no potential maxima or minima within the dark space. When the probe has a large negative potential with respect to all surrounding space, it can collect only positive ions. As all electrons which reach the probe are turned back, the potential distribution within the dark space must so adjust itself that the field opposes the motion of electrons toward the probe. In Fig. 7a, the potential distribution over a section through the arc axis is shown. The drawing is not to scale, but is exaggerated in order to portray more clearly the fields. With large negative potential on the probe, there is *no* electron current to the probe; hence the field is negative all the way from the probe to the dark space boundary. As the electrons advancing from the cathode cannot halt abruptly, a negative space charge develops at the cathode side of the boundary which diverts the current around the probe. In Fig. 7b is shown the space charge distribution and lines of current flow around the probe for a negative probe potential. The space charges shown are the *net* charges and do not indicate the presence of ions of one sign alone. The gas in the dark space is cooler than in the arc, so the mobilities of the positive and negative carriers are lower there than in the arc core. Under the same field, ions move slowly in the dark space; hence there will be an accumulation of positive ions on the anode side of the dark space, and electrons on the cathode side, until most of the carriers are turned around the dark space. The space charges push away from the axis the electrons on the cathode side, and pull them together again on the anode side, and conversely for the positive ions. The resulting lines of flow are as shown. With sufficiently large potential on the probe, the field along the center line might be large enough to move the ions in to the probe as fast as they come up to the boundary, and hence prevent the development of the space charges, but apparently this condition was not attained experimentally. With a large negative voltage, the current of positive ions collected was much larger than field free diffusion would give, so

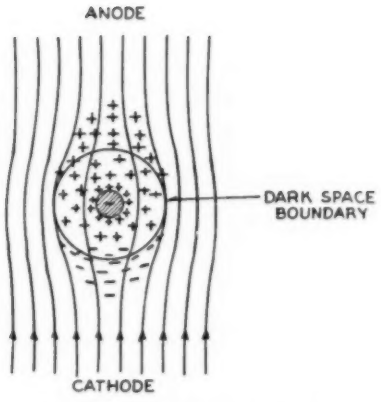


FIG. 7b. Space charges and lines of current flow around probe. Section perpendicular to probe.

actually accelerating fields must have carried positive ions to the probe from all sides.

The figure shows conditions for several probe potentials. Suppose the potential is reduced from the high negative value. Since in a space charge sheath, a reduction in voltage across the sheath causes a reduction in current, larger than the change in the sheath dimensions, a decrease in current to the probe must result. This can come about only through a change in the electric field all the way from the probe to the dark space boundary. No pronounced effect outside the boundary can occur for it is observed that changing the probe potential scarcely affects the disturbance caused by the probe.

As the probe is made more positive with respect to the cathode, finally a point is reached where the net current to the probe becomes zero; then the probe receives equal numbers of electrons and positive ions. As the electrons move so much more rapidly than the positive ions, the zero current condition will be attained when the probe receives a few electrons at the point nearest the cathode, but only positive ions over the rest of the periphery. The zero current point corresponds to a probe potential a little negative with respect to the arc at the point *P*. A slight negative field occurs from the probe all the way to *P*, but electrons are able to diffuse against this field in sufficient numbers to balance the positive ions attracted to all other sides of the probe.

For higher probe potentials, the electron current increases quite rapidly; even with zero field on the cathode side, diffusion will carry electrons to the probe far in excess of the positive ions arriving elsewhere. With still higher probe potentials, the electron current increases rapidly, and a region of electron space charge develops about the probe. It is possible for the probe potential to be considerably above all the surrounding space, and still the current to the probe to be limited by the reduced mobility in the cold dark space to a value less than the drift current to it would be if a dark space did not form.

Fig. 6 shows a considerably larger total probe current, and a faster increase of current with voltage, the larger the arc current. Some increase should occur merely from the longer length of probe immersed in the larger arcs and some should be caused by the slight increase of ion density with current, but these two do not seem quite adequate to explain the large difference noted. The current collected was also the larger the closer the probe approached the cathode. Because of the decreased section of the arc near the electrodes, the ion density probably is actually higher there: in addition, the dark space around a probe near the cathode was smaller than in the body of the arc, so both the fields and concentration gradients in the dark space would be higher.

**Potential distribution in the arc**

From the points of zero current for the probe in different positions, some idea of the potential distribution in the arc may be secured. The average values of the voltage between probe and cathode for zero current, for a few conditions, are given in Table II.

For zero current, the probe potential is probably 1 or 2 volts negative with respect to the dark space boundary nearest the cathode. The boundary itself must be negative with respect to adjacent parts of the arc, which remain undisturbed by the probe,—sufficiently negative to produce fields of the same magnitude as the longitudinal fields in order to redistribute the current flow around the probe. Possibly the boundary is 4 to 6 volts negative with respect to the same point in an undisturbed arc. The actual potential of an undisturbed arc at a point corresponding to the probe axis, measured from the cathode, will be the sum of these two po-

tentials, plus the potential for zero current and the voltage drop in the undisturbed arc over a distance equal to half the dark space diameter. In round numbers, for a probe at the center of a 6-amp. arc, something like 8 volts must be added to the figures in Table II in order to give the space potential. More must be added near the cathode, where the field is higher; for the same reason, the addition must be greater the smaller the current. The probable space potential distribution for different currents is shown in Fig. 8. It should be realized that this is merely a rough approximation, representative only in magnitude. The cathode fall seems to be a little over 10 volts, and the anode fall of the order of 20 volts.

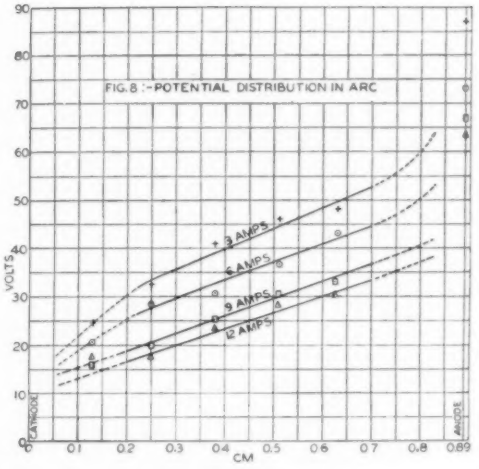


FIG. 8.

### Ion density and distribution in the arc core

Quite apart from any probe measurements, it is possible to get a rough estimate of the ion density in the positive column of the arc from observed current density and the gradient, which was obtained from volt-ampere characteristics for different length arcs. For a gas temperature of 6000° and a field of 33 volts per cm, for a 6-amp. arc, the equivalent value of $E/p$ is 1 volt per cm per mm pressure. By the Compton theory of terminal velocities,[12] the energy of electrons making only elastic collisions in $N_2$ would be 4.24 volts, and the corresponding drift velocity, using the Langevin mobility formula[12] comes out $4.88\times10^5$ cm per sec. Townsend[13] has measured the energy of electrons in $N_2$ for $E/p=1$, but at room temperature, and found 0.778 volt (6000°) for the terminal energy, and $8.5\times10^5$ for the drift velocity. In the present case, the high gas temperature will probably make the terminal energy larger, and hence the drift velocity smaller, than Townsend's values. If one uses a velocity $8.5\times10^5$, then a value of electron density will be found which is too low, but of the correct order of magnitude. Taking the current density as 20, the electron density comes out $1.48\times10^{14}$ per cm³. If one uses the value of velocity calculated above, then the density would be almost twice as large. Since no large space charges are present, the positive ion density in the positive column must be about the same. As the gradient has been found to vary only 25 percent for a change in current by a factor of 4, while the current density remained substantially constant, the ion density must change not over 25 percent in the same range.

TABLE II. *Potential from probe to cathode for various arc currents.*

| DISTANCE OF THE PROBE AXIS FROM CATHODE | 3 AMP. | 6 AMP. | 9 AMP. | 12 AMP. |
|---|---|---|---|---|
| 0.13 cm | 14 volts | 11.5 volts | 7.5 volts | 9 volts |
| .25 | 22.7 | 20 | 12 | 10 |
| .38 | 32 | 22.5 | 18 | 17 |
| .51 | 37 | 28.5 | 23 | 21 |
| .63 | 39 | 35.5 | 25.5 | 23 |

From the total current measured by a revolving probe, with constant voltage applied, the current collected per unit length of the probe at different radii from the arc axis may be found, just as the exactly similar energy input to the probe was gotten previously. If $i(x)$ represents the total current for the straight probe at a distance $x$ from the arc axis, and $i(r)$, the current per unit length for a point $r$ from the axis, then

$$i(r)=-\frac{1}{\pi}\int_r^\infty i'(x)\frac{dx}{(x^2-r^2)^{\frac{1}{2}}}. \qquad (8)$$

From this equation $i(r)$ was calculated from measured $i(x)$. Since positive ion current varies more slowly with probe potential than does

[12] Compton and Langmuir, Rev. Mod. Phys. **2**, 220 (1930).

[13] Townsend, J. Frank. Inst. **200**, 586 (1925); Phil. Mag. **42**, 883 (1921).

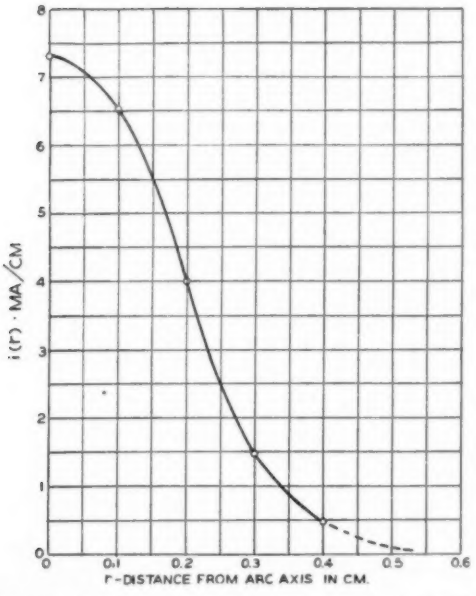


FIG. 9. Positive ion current collected per cm length of probe.

electron current, the consequence of different radii in the same transverse plane of the arc being at different potentials has less effect on the positive ion results. Fig. 9 represents $i(r)$ for a 0.025 cm diameter probe, passing 0.51 cm from the cathode of a 5.85 amp., 1.15 cm long arc, with the probe 130 volts negative to the cathode. The curve gives some indication of the radial distribution of ion density in the arc, but $i(r)$ is not necessarily directly proportional to the ion density: the current collected must also depend on the temperature distribution around the probe, which in turn changes with $r$. The curve does show, however, that the ion density falls to a low value outside the intense central core of the arc ($r=0.3$ cm).

## IV. Critique of Other Investigations

Although the errors into which other investigators have fallen will be obvious from the above results, perhaps a brief mention of some specific points may be worthwhile in view of the wide acceptance in the literature of their work.

From the point of zero probe current, the electron current to the probe rises rapidly with increase in probe to cathode voltage. The rate of increase of current bears no obvious relation to the electron temperature in the positive column, for in order to reach the probe the electrons must travel from where they are produced a long distance through a gas with varying temperature to a probe whose immediate surroundings are at a low temperature compared to the arc. In this part of the characteristic, it is the change in drift velocity of the electrons to the probe which is responsible primarily for the change in current, so whatever the temperature of the electrons finally arriving at the probe, their temperature is not constant throughout the dark space. Furthermore, a change in slope of the current voltage characteristic at a few volts positive with respect to the point of zero current cannot arbitrarily be called the space potential for an undisturbed arc. The interpretation of results which Nottingham[1] used led him to space potentials which are certainly much too low near the cathode—giving a cathode fall of only 5 volts for the carbon arc—and probably too high near the anode.

Bramhall[2] observed the increase in arc voltage caused by passage of the probe, but he failed completely to realize the significance of the disturbance caused, making the same errors that Nottingham did in interpretation of data. Some inconsistencies into which he was led may be pointed out: for instance, he gives the volt equivalent of the electron drift velocity as 0.64, and of the random velocity as 2.7; from these, the random electron current should be about twice the drift current. In other parts of his paper, however, from his interpretations, he gives the random current density as from 1 to 5 amp. per cm$^2$, and the drift current density 70 to 310 amp. per cm$^2$. Again, in his attempt to determine the recombination coefficient from the decrease of probe current after extinction of an arc, Bramhall also falls into serious errors, though finally arriving at reasonable results, through his misinterpretation of the probe characteristic, and through neglect of the production of ions. Here, this internal inconsistency may be pointed out: using Bramhall's figures, and graphically integrating his probe current curve, one finds that in the period after arc extinction in which ions were supposed to disappear only by volume recombination, the total

number of ions collected by the probe was over 200 times the total number existing in the whole arc initially. The probe measurements of previous investigators of high pressure arcs must be considered as of little value.

## V. General Discussion

From experiments on a carbon arc at atmospheric pressure, this paper has brought out the restrictions in the use of probes for investigating high pressure discharges. In a discharge at low pressures, the gas temperature is not much above room temperature and the discharge substantially fills the containing vessel. At high pressures (above a few millimeters) the positive column of the discharge contracts to a definite section, independent of the dimensions of the vessel, if these are larger than the natural section of the discharge. The contraction of the positive column is accompanied by, or more likely, is *caused* by an increase in the gas temperature to several thousand degrees. The positive column may be expected to take that section for which the losses are a minimum. Now if by any means the section of the arc is changed from the minimum, without any change in current, the energy necessary to maintain the discharge increases. As the energy in a self-maintained discharge is supplied only from the electrical power source, a change in section necessitates an increase gradient in the positive column, and a larger arc voltage.

If a solid probe of finite size is placed in the arc, then the arc voltage must increase. As the temperature of the probe, if it remains a solid, is only a fraction of the gas temperature in the arc (around 6000°K at atmospheric pressure), there will not be a sudden transition of temperature, but a region around the probe in which the gas temperature falls from the several thousand degrees of the arc to the few hundred degrees of the probe. Within the transition region, which appears as a dark space around the probe, probably very few ions are produced, so the effect of the probe on the arc cross section extends over a distance several times the probe dimensions, with consequent greater increase in the voltage required for the arc. Put in other words, from an energy standpoint, the introduction of a probe cools the arc and increases the energy input necessary for maintenance of the arc; the effect of the probe extends far beyond the probe surface because of the lowering of the gas temperature around the probe. From an electrical standpoint, the presence of a region of lowered gas temperature impedes the flow of ions and develops space charges which divert most of the current around the dark space.

The interpretation of probe current voltage characteristics which has been developed for the use of probes in low pressure discharges, does not apply at high pressures. The ions or electrons which reach the probe must travel a long distance through the dark space from the point of their generation in the arc. The current which the probe collects depends not only upon the strong fields, or space charge sheaths which develop about the probe, but also upon the weak fields and concentration gradients which move the ions through the dark space. Since it is likely no ions are lost within the dark space except at the probe, when the net probe current is zero, the probe potential must be negative with respect to the part of the dark space boundary nearest the cathode. From this condition, the distribution of potential in an undisturbed arc may be estimated. An exact mathematical formulation of the probe current voltage relations appears difficult, if not impossible, so that the use of probes in high pressure discharges probably can never bring such exact information about the nature of the discharge as it can at low pressures. Through a study of the thermal as well as electrical characteristics of probes, together with observations of the general properties of the arc, perhaps some knowledge of high pressure discharges can be gained.

The writer is indebted to Professors H. D. Smyth and G. P. Harnwell for criticizing this paper, and to Dr. Joseph Slepian for helpful discussion throughout the course of the experiments.

# Polymorphism of Rochelle Salt

HANS VON R. JAFFE, *Wesleyan University, Middletown, Connecticut*

(Received November 16, 1936)

A careful analysis of the properties of Rochelle salt leads to the conclusion that this crystal belongs to the *monoclinic hemimorphic* symmetry class between the so-called Curie points (+23.7°C and −18°C), whereas it is orthorhombic hemihedric at other temperatures. The Curie points are to be regarded as crystallographic inversion points like the high-low inversion points in quartz and other crystals. Dielectric anomalies as observed for Rochelle salt must be expected near inversions from a pyroelectric to a nonpyroelectric crystal glass. Other properties of Rochelle salt discussed in the light of the new classification are the electrooptic effect, the converse and the direct piezoelectric effect, and the specific heat. A comparison with symmetry conditions in ferromagnetic crystals is made.

## I. INTRODUCTION

THE anomalous dielectric behavior of Rochelle salt between −18°C and +23.7°C, and the discontinuities observed at these two points show a close analogy to ferromagnetism and its transition to paramagnetism at the Curie point.[1-3] These characteristic temperatures have therefore been called the lower and the upper Curie points of Rochelle salt.

It is the purpose of this paper to deduce from well-known physical properties that at these temperatures crystallographic inversions occur in Rochelle salt, and that it belongs to the *hemimorphic* class of the *monoclinic* system (sphenoidal class, $C_2$) *between* the Curie points, whereas there is no reason to question its *orthorhombic hemihedral* symmetry (rhombic-bisphenoidal class, V) at other temperatures.

## II. CRYSTALLOGRAPHIC MEASUREMENTS

These conclusions have hitherto not been drawn because Rochelle crystals, whether grown above or below the upper Curie point, *appear* to possess orthorhombic symmetry. This, the accepted classification, is confirmed, within the limits of experimental precision, by goniometric measurements[4] and x-ray analysis.[5, 6] Even the space group has been determined as $V^9$. All these measurements were carried out at room temperature, i.e., between the Curie points, though the crystals had probably been grown at higher temperatures in most cases.

## III. PHYSICAL PROPERTIES OF LOWER SYMMETRY

However, a variety of physical experiments have led to an interpretation[2d, 3, 7] of the electric behavior of Rochelle salt which, as will be shown in this paper, is in contradiction to orthorhombic hemihedric symmetry for temperatures between the Curie points. It is now agreed that in this range a Rochelle crystal consists of regions having a *spontaneous electric moment*, analogous to the Weiss regions in ferromagnetic metals. The electric moments are, however, always parallel to the crystallographic *a* axis. It depends on mechanical stresses or other accidental circumstances which of the two possible orientations the moment will have in any region in the crystal. Regions of opposite polarization are in general not balanced, thus giving rise to a polarity of the crystal as a whole.

Unipolar conductivity,[1c] asymmetry in the dielectric polarizibility[1b, 2c] and in the converse piezoelectric effect,[8] and also a pyroelectric effect[1c, 3] have indeed been measured. With the powder test for pyroelectricity, Mueller succeeded in making the single regions visible; their dimensions are of the order of 1 cm.

[1] (a) J. Valasek, Phys. Rev. **17**, 475 (1921); (b) **19**, 478 (1922); (c) **20**, 639 (1922).
[2] (a) P. Kobeko and I. Kurtschatov, Zeits. f. Physik **66**, 192 (1930); (b) B. Kurtschatov and I. Kurtschatov, Physik Zeits Sowjetunion **3**, 321 (1933); (c) I. Kurtschatov, Physik Zeits Sowjetunion **4**, 125 (1933); (d) **5**, 200 (1934).
[3] H. Mueller, Phys. Rev. **47**, 175 (1935).
[4] See P. Groth, *Physikalische Krystallographie* (Leipzig, 1905), p. 392.
[5] B. E. Warren and H. M. Krutter, Phys. Rev. **43**, 500 (1933).
[6] H. Staub, Helv. Phys. Acta **7**, 3 (1934).
[7] H. Staub, Naturwiss. **23**, 728 (1935).
[8] (a) I. Vigness, Phys. Rev., **46**, 255 (1934); (b) **48**, 198 (1935).

Smaller crystals are often a single region. The magnitude of the spontaneous polarization is best obtained from the polarization cycle with low frequency a.c. It has a flat maximum of about 600 e.s.u. $= 20 \times 10^{-8}$ coul./cm$^2$ near 0°C, and falls off to zero as either Curie point is approached.[3, 9]

No unipolarities or other signs of a spontaneous moment are present above the upper or below the lower Curie point.

## IV. Crystallographic Conclusion

The only correct crystallographic description of this behavior is the following. Between the Curie points the *a* axis is a polar axis; consequently the *b* and *c* axes are no longer axes of symmetry. With only one twofold axis of symmetry left the crystal belongs to the *hemimorphic* class of the *monoclinic* system. The apparent orthorhombic symmetry is a "pseudosymmetry."[10] Large specimens are twins; the *b* or the *c* axis can be regarded as twinning axis. The Curie points are *inversion points* to orthorhombic hemihedric symmetry.

The polymorphism of Rochelle salt is a typical case of *polysyngony*,[11] for which the high-low inversions of *quartz* and *cristobalite* are classical examples. The twinning of monoclinic Rochelle salt corresponds to the Dauphiné, or orientational, twinning shown by low quartz prepared by cooling from uniform high quartz.[12] For low-cristobalite, as for monoclinic Rochelle salt, the deviations of the geometrical forms from the higher symmetry are so small that they could not be detected by x-ray measurements.[13] Here, as for most other inversions of the polysyngonic type, it was the sudden disappearance of optical double refraction which revealed the inversion.

## V. Hypotheses of Other Authors

In one of his early papers *Valasek* (reference 1c, p. 660) points out that a pyroelectric effect in the orthorhombic-hemihedric class is forbidden by *Neumann's principle;* he therefore questions the unconditional validity of this fundamental principle of crystal physics. At the same time Valasek discusses the possibility that Rochelle salt belongs to the *orthorhombic-hemimorphic* class; he finds it impossible because for this class the piezoelectric constant $d_{14}$, which is very high in Rochelle salt, should vanish. We may add that the orthorhombic-hemimorphic class has a plane of symmetry, whereas the absence of such a plane in Rochelle crystals was known to *Pasteur* more than 80 years ago.[14] Nevertheless, the same question was recently discussed again by *Taschek and Osterberg*,[15] of course with the same result.

*Mueller* tries to overcome the dilemma by the following remark (ref. 3, p. 180): "The crystallographic symmetry of Rochelle salt does not permit an ordinary pyroelectric effect. Its apparent pyroelectricity is due to this[16] spontaneous polarization. The existence of this effect is therefore no violation of Neumann's principle."

We cannot agree with Mueller's differentiation of "apparent" and "ordinary" pyroelectricity. Unless a "false effect of the first kind," i.e., produced by nonuniform heating, pyroelectricity is always due to a spontaneous electric moment necessarily linked with an interior field. It has to be taken into account in the determination of the symmetry class, irrespective of the insight we may or may not have into the molecular origin of the polarization.

## VI. The Converse Piezoelectric Effect of the Interior Field

It is possible to deduce indirectly from experimental data that between the Curie points the *geometrical* form of Rochelle salt as well as the physical properties exhibits monoclinic symmetry only. Measurements on the converse piezoelectric effect[8] show that a reversal of the spontaneous polarization, as achieved by an electric field parallel to the *a* axis, is accompanied by a shearing deformation $y_z$ which amounts to about $16 \times 10^{-4}$ between 0°C and +10°C. This corre-

[9] C. B. Sawyer, and C. H. Tower, Phys. Rev. **35**, 269 (1930).

[10] Groth (reference 4), p. 271.

[11] For a definition of this term see T. F. W. Barth, Am. J. Sci., **27**, 273 (1934).

[12] R. B. Sosman, *The Properties of Silica* (New York 1927), p. 194.

[13] T. F. W. Barth, Am. J. Sci. **24**, 97 (1932).

[14] L. Pasteur. Ann. chim. phys. (3) **28**, 56 (1850).

[15] R. Taschek and H. Osterberg, Phys. Rev. **50**, 572 (1936).

[16] The quoted sentences are preceded by a theory of the electrical properties of Rochelle salt analogous to the Weiss theory of magnetism. See Section VII.

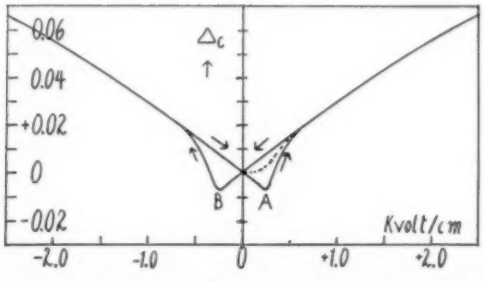


FIG. 1. Electrooptic effect for rays in the *c* direction; schematic, after *Mueller* (reference 3, Figs. 23 and 24). Temperature about +20°C. The ordinates give the increase in optic path length difference (in fractions of one wave-length per cm path) between the two linear light components. The abscissas are field strengths in the *a* direction. Dotted curve: virgin polarization.

sponds to a change in the angle between the *b* and *c* axes of $16\times10^{-4}$ radians = 5.5′. The departure of the angle from 90° must be the same for both orientations of the polarization; at the temperature quoted, therefore, the *b and c axes intersect* at an angle different from 90° by 5.5′/2 or *at 89° 57.3′*. Only measurements of high precision, using *un-twinned* material, could directly detect this slight deviation from orthorhombic symmetry.

## VII. Relation to Mueller's Theory

H. Mueller's theory of Rochelle salt is based on the assumption that, between the Curie points, its "molecules" assume an electric moment parallel to and dependent upon an interior electric field, which in turn is maintained by this polarization.

There is no contradiction to our crystallographic results if Rochelle salt is regarded as built up of *unit cells* which would be orthorhombic if isolated, but which, between the Curie points, become polarized and slightly deformed under the influence of neighboring unit cells. Mueller only overlooked the fact that, as a consequence of his own assumptions, the *entire crystal* is not orthorhombic but monoclinic.

Mueller's theory is in quantitative accord with his dielectric and electrooptic measurements just *above* the upper Curie point; it yields the correct order of magnitude for these effects between the Curie points. The present crystallographic treatment does not provide quantitative predictions, but it gives a more direct qualitative interpretation of the effects between the Curie points, and is entirely free of any molecular assumptions. In the following sections various effects will be studied from both points of view.

## VIII. Dielectric Polarization

In Mueller's theory, the dielectric hysteresis loop observed for Rochelle salt between the Curie points is a complete analog to the ferromagnetic hysteresis loop. The spontaneous polarization corresponds to remanent magnetism.

From the crystallographic point of view, this polarization is the pyroelectric moment present in all crystals of certain symmetry classes. Its reversal by the action of an electric field or of a mechanical shearing stress is a *reversal* of the *polar axis* of the crystal. The nearness of the transition points accounts for this effect in Rochelle salt. It has a parallel in the peculiar transformation under a shearing stress observed in calcite.[17] Both processes are internal movements which end in a state that is identical with the original state except for orientation in space. For both calcite and Rochelle salt the configuration midway between the stable states is of higher symmetry than the latter. As the temperature of Rochelle salt approaches the transition point, the stable states come nearer and nearer to the higher symmetry and the energy required to effect the reversal approaches zero. This means that the susceptibility for the *a* direction and the corresponding piezoelectric constant $d_{14}$ approach infinity at the Curie points, as is indeed indicated by experiments.[3, 18]

## IX. Electrooptic Effect

The symmetry of the orthorhombic hemihedric class does not permit a linear electrooptic effect of an electric field in the *a* direction for rays traveling along one of the crystallographic axes. The effects observed in these directions by *Pockels*[19] and by *Mueller*[3] have therefore been interpreted as *quadratic*, or *Kerr effects*. Indeed, they have the same sign for opposite directions of the field (Fig. 1); however the observed variation with the intensity of the field is *linear*

[17] Groth (reference 4), pp. 245–250; Tutton, *Crystallography* (London, 1911), pp. 449–451.
[18] O. Norgorden, Phys. Rev. **49**, 820 (1936).
[19] F. Pockels, Göttinger Abhandl. **39**, 161 (1894).

below the upper Curie point, with an approach to saturation from 2.5 kv/cm upwards. Mueller's explanation is that the exterior field $E$ produces only a relatively small addition $\Delta F$ to the spontaneous interior field $F_0$. The Kerr effect is proportional to $(F_0+\Delta F)^2 \approx F_0^2+2F_0\Delta F$. $\Delta F$ is in first approximation proportional to $E$. As the effect of $F_0^2$ is already included in the natural birefringence, the variation of the birefringence with the applied field is indeed linear.

The crystallographic interpretation is simply this: what is observed is really a *linear electro-optic effect*, which is no longer impossible for the direction studied if the crystal is regarded as monoclinic hemimorphic. Owing to the reversal of the polar axis when the field is sufficient to overcome the coercive force (points $A$, $B$, Fig. 1), the effect is the same for both directions of the field, but there is no discontinuity at zero field.

## X. Electrostriction and Piezoelectric Effect

As *optic refractivity* and *strain* are represented by tensors of the same kind, the same symmetry relations as for the *Kerr effect* must hold for the *quadratic electrostriction*.

From the point of view of Mueller's theory, Rochelle salt would therefore be an orthorhombic hemihedric crystal in which, owing to the spontaneous polarization, the quadratic electrostriction, like the Kerr effect, depends linearly on the applied field if the temperature is between the Curie points. *Five* coefficients are needed to describe in an orthorhombic crystal all possible effects of such a combination of a spontaneous polarization along one of the axes and an applied field in an arbitrary direction.[20]

These five coefficients correspond exactly to the *five piezoelectric constants* which the *monoclinic hemimorphic* class has in addition to the three constants present for the orthorhombic hemihedric class.[21]

Before enumerating these we must adopt a convention concerning the crystal axes. It is usual to call the polar axis in a hemimorphic crystal the $c$ axis. However, it seems expedient to retain the designation commonly employed with Rochelle salt, even when it becomes monoclinic hemimorphic. The axis of Rochelle salt generally known as $a$ axis shall retain this name *although* it is a *polar* axis. Where a rectangular coordinate system is required, the $X$ axis shall coincide with $a$, and the $Y$ axis with $b$. The $Z$ axis will then form an angle of a few minutes with the $c$ axis (see Section VI). The system of piezoelectric constants is now obtained from that of Voigt[22] by exchanging the index 1 with 3, and 4 with 6, and rearranging the constants in the usual order. We thus have

$$\begin{matrix} d_{11} & d_{12} & d_{13} & d_{14} & 0 & 0 \\ 0 & 0 & 0 & 0 & d_{25} & d_{26} \\ 0 & 0 & 0 & 0 & d_{35} & d_{36}. \end{matrix}$$

An experimental search for the new constants would not decide in favor of either theory, as both Mueller's and the crystallographic point of view require their presence. As far as we know no attempt to find these constants has yet been made. It is true that Taschek and Osterberg[15] looked for a set of five new piezoelectric constants which might possibly take the place of the well-known constants $d_{14}$, $d_{25}$, $d_{36}$; but their search was, erroneously, for constants connected with a polarity of the $c$ axis and not the $a$ axis; their result has therefore no bearing on our problem.[22a]

## XI. Specific Heat

At the upper Curie point of Rochelle salt an anomaly in the specific heat is observed, just as at the Curie points of ferromagnetic metals.[23] This effect has been regarded as one of the strongest arguments for the existence of a spontaneous polarization.[7]

From our crystallographic point of view we note that an anomaly of similar shape is observed at polysyngonic inversion points which are *not*

[20] On the quadratic electrostriction in crystals see F. Pockels, in *Encyclopädie der Mathem. Wiss.* (Leipzig, 1906) vol. V/2, p. 360.

[21] The electrostrictive effect derived from Mueller's theory is the *converse* piezoelectric effect for monoclinic-hemim. symmetry; however the system of coefficients is the same for direct and converse effect.

[22] W. Voigt, *Lehrbuch der Kristallphysik* (Leipzig, 1910) (or second edition, 1928), p. 829.

[22a] *Note added in proof.* Since the completion of this paper H. Körner, Zeits. f. Physik **103**, 170 (1936), has published measurements which show the absence of other constants than $d_{14}$, $d_{25}$, $d_{36}$ within his limits of error. However, these observations were made at temperatures so little below the upper Curie point that only very small values for the other constants could be expected from our theory.

[23] A. Rusterholz, Helv. Phys. Acta **8**, 39 (1935).

linked with the disappearance of a spontaneous electric moment, as for quartz.[24] One is therefore not justified in assuming that the anomalous specific heat of Rochelle salt is entirely due to the process of depolarization. Indeed, the observed discontinuous decrease in the specific heat at the transition point is more than 10 times greater than the value calculated from the electrical theory with Mueller's data for spontaneous polarization and interior field (reference 3, pp. 189, 191). Only from a detailed knowledge of the molecular rearrangement involved would a calculation of the specific heat be possible.

## XII. Relation to Transitions in Other Crystals

A first step towards a *molecular theory* of Rochelle salt has been taken by R. H. Fowler.[25] His theory connects the anomalies in Rochelle salt, especially the lower Curie point, with the large group of recently discovered oscillation-rotation transitions.

Without in any way questioning this connection, or the analogy to ferromagnetism, we have here emphasized the relation of the Rochelle anomalies to a group of transitions which have long been recognized as crystallographic inversions, whereas little is known about their molecular dynamics. The similarity of the anomalous specific heat for these different groups of transitions leads to the assumption that they all can be explained by the same molecular fact, namely the breakdown of a *cooperative state* (in the terminology of Fowler).

We have to mention an early attempt of *Perrier* to correlate the high-low inversion in quartz with the ferromagnetic Curie points.[26] However, Perrier, with his associates, did not succeed in finding the sharp maximum in the dielectric constant which he had predicted.[27] It was shown above (Section VIII) that such an infinity point in the dielectric constant is to be expected at a transition from a pyroelectric to a nonpyroelectric crystal class. Quartz however is not truly pyroelectric on either side of its inversion point.

In recent literature there is, however, one new example for an infinity point of a dielectric constant: the transition of HBr at $-183°$C.[28] In the light of the present discussion it can be concluded that in this case a transition from a pyroelectric to a nonpyroelectric crystal class occurs.

## XIII. Symmetry of Ferromagnetic Crystals

It is possible to extend the crystallographic argument of this paper to the ferromagnetic crystals themselves and to postulate that, e.g., an iron single crystal is a pseudocubic crystal; and that the real crystal individuals are the Weiss regions, which have, in absence of an applied magnetic field, a spontaneous polarization in the direction of one of the cube edges and are therefore *tetragonal paramorphic*, $C_4^h$.[29] Owing to magnetostriction, the geometrical forms will also be of this lower symmetry.

This point of view seems correct, but hardly fertile, because: (1) the moment of spontaneous magnetization can easily be rotated away from the axis of easiest magnetization; (2) the molecular *magnetic* moments are only slightly coupled with the forces which determine the configuration of the crystal, of which the most important are the *electrostatic* forces. This is entirely different for the case of spontaneous *electric* polarization in Rochelle salt.

The writer wishes to thank Professor W. G. Cady for his most valuable help in the preparation of this paper.

[24] Sosman (reference 12), p. 334f.
[25] R. H. Fowler, Proc. Roy. Soc. **A149**, 1; **151**, 1 (1935).
[26] A. Perrier, Arch. sci. phys. nat. (Geneva) (4) **41**, 492 (1916).
[27] S. Gagnebin, Arch. sci. phys. nat. (Geneva) (5) **6**, 161 (1924).
[28] C. P. Smyth and C. S. Hitchcock, J. Am. Chem. Soc. **55**, 1830 (1933).
[29] In this classification it is taken into account that the magnetic polarization is an *axial* vector.

# LETTERS TO THE EDITOR

*Prompt publication of brief reports of important discoveries in physics may be secured by addressing them to this department. Closing dates for this department are, for the first issue of the month, the eighteenth of the preceding month, for the second issue, the third of the month. The Board of Editors does not hold itself responsible for the opinions expressed by the correspondents.*

**Communications should not in general exceed 600 words in length.**

## Pressure Broadening in Bands of Dipole Molecules

Recent measurements of the widths of lines of absorption bands of a number of different molecules in the photographic infrared indicate that the HCN band lines are relatively quite broad.[1] There must then be particularly large van der Waals forces perturbing the absorbing HCN molecules, with resulting magnification of the details of the pressure broadening due to such perturbations. On one of these details, the possibility of the variation of the line-broadening with the rotational state of the molecule, some rather rough and inconclusive observations have been made.[1-3] What variation, if any, is to be expected theoretically?

It has been shown[4, 5] that pressure effects other than those due to permanent polarity of the molecules are quite independent of the rotational quantum number. But the major portion of the relatively large line widths of HCN ($\nu_{\frac{1}{2}}=1.5$ cm$^{-1}$ for a pressure of 1 atmosphere) may well be due to dipole interactions,[6] for the dipole moment $\mu$ of HCN is large, $2.5-2.6\times10^{-18}$ e.s.u., and energy expressions for dipole-dipole interactions depend strongly on $\mu$. From such perturbations slight variations of pressure effects with the rotational state of the absorbing molecule are to be expected.

The forces between dipole molecules are in general due to a complicated superposition of three effects: the static induction effect of Debye, London's dispersion effect, and the effect of alignment of the dipoles. For dipoles of ordinary strengths ($\mu\sim10^{-18}$ e.s.u.) the dispersion effect is predominant. But a simple computation shows that, if $\mu$ approaches $2\times10^{-18}$ e.s.u., the effect of alignment becomes comparable with the dispersion effect, and indeed outweighs the latter for molecules with even greater dipole moments. It is therefore not surprising that the dipole moment should be a determining factor in the pressure broadening of HCN. In a qualitative discussion, and this is all that we wish to offer in the present note, we shall treat the effect of alignment as though it were the only one present. Accordingly, the molecules will be idealized as *rigid*, unpolarizable dipoles.

The following points are known about the interaction of such dipoles:[7]

(1) The forces are weak unless the interacting dipoles are in rotational states whose quantum numbers are nearly equal. ($|K_1-K_2|<2$ or 3.)

(2) The lowest rotational state is influenced more strongly by molecules in low states than any other; its energy perturbations are predominantly downward, i.e., its energy will usually be lowered by interactions.

Let us now consider an absorption line originating in a certain rotational level $K_1''$ of the lowest vibrational state of the molecule, and terminating in the level $K_1'$ of a higher vibrational state. Suppose at present that $K_1''$ is not the lowest level. It will be perturbed most strongly by molecules in neighboring rotational states because of statement (1). The broadening effect will, however, be approximately proportional to the chance that a perturber be in a neighboring state, and this probability is greatest if $K_1''$ corresponds to the maximum of the Maxwell distribution of rotational velocities. The conclusion is, therefore, that the lines arising from the most densely populated states should be most strongly broadened. This argument cannot be applied with equal force to the level $K_1'$ whose broadening also impresses itself on the line width. For the dipole moment will be different in the excited vibrational state than in the normal state and the selectivity of the interactions reflected in statement (1) is then less pronounced. The effect in question, by which lines originating in states favored by the thermal distribution (the most intense lines) would show stronger broadening, is therefore merely in excess of a general broadening of all lines and should not be pronounced, yet probably measurable.

Statement (2) leads to an interesting consequence regarding the line originating in the lowest state. This line may be broader than the neighboring lines because of the greater strength of the perturbations on the lowest state, although the fact that at ordinary temperatures there are few perturbers in nearby states might counteract this tendency. It should, however, manifest itself increasingly as the temperature of the absorbing gas is lowered.

At sufficiently low temperature the effect of alignment here considered should produce an asymmetry to the blue, if not a measurable shift, in the line originating in the lowest level because, as pointed out, this level has greater "flexibility" downward than upward.

W. W. WATSON
H. MARGENAU

Sloane Physics Laboratory,
Yale University,
New Haven, Connecticut,
December 11, 1936.

[1] G. Herzberg, J. W. T. Spinks and W. W. Watson, Phys. Rev. **50**, 1186 (L) (1936).
[2] G. Herzberg and J. W. T. Spinks, Proc. Roy. Soc. **A147**, 434 (1934).
[3] S. D. Cornell and W. W. Watson, Phys. Rev. **50**, 279 (1936).
[4] H. Margenau, Phys. Rev. **49**, 596 (1936).
[5] W. W. Watson and G. F. Hull, Jr., Phys. Rev. **49**, 592 (1936).
[6] W. W. Watson, J. Phys. Chem. Jan. (1937).
[7] See, for instance, F. London, Zeits. f. Physik **63**, 245 (1930).

## The Gamma-Radiation from Lithium Bombarded with Protons

The recoil electrons ejected from the glass wall of a cloud chamber by the radiation from lithium bombarded by protons were studied by Crane, Delsasso, Fowler and Lauritsen,[1] and were interpreted as indicating a complex spectrum extending up to 16 Mev. Measurements on pairs ejected from a thin lead sheet were later reported by Delsasso, Fowler and Lauritsen.[2] These were grouped in a band or line at about 17 Mev, and it was therefore concluded that there was little, if any, radiation below about 17 Mev. In a more recent report[3] these authors confirm this distribution of pairs. Hafstad, Heydenburg and Tuve[4] have reported finding recoil electrons which give some indication of radiation at 8 and possibly 11 Mev.

We have made further measurements on this radiation, using an entirely different experimental arrangement.[5] A metallic lithium target was placed in a well inside the cloud chamber and surrounded by a small carbon cylinder having a wall about 2.5 mm thick, as sketched in Fig. 1. Recoil negative electrons and electron pairs were ejected from this thin wall by the gamma-radiation. Nearly all the tracks appearing in the cloud chamber clearly originated in the carbon. The stopping power of the carbon was about 1 Mev for the single electrons and 2 Mev for the pairs. Fig. 2 shows plots of the negative electrons and pairs observed. The distribution of pairs is in agreement with the observations of Delsasso, Fowler and Lauritsen on pairs, and could easily be attributed to a single gamma-ray line at about 17.5 Mev.[6] The distribution of Compton electrons, on the other hand, is consistent, at least as to general over-all shape, with the distribution previously found.[1] The present negative electron distribution indicates that by far the strongest components of the radiation are at about 14.5, 11 and 8.5 Mev, with only a small group at 17.5 Mev. The plot below 8 Mev should not be considered seriously because of the possibility that it may contain some beta-rays from $Li^8$, formed by deuteron contamination in the ion beam.

The reaction (1) postulated to account for the complex spectrum up to 16 Mev

$$\begin{aligned} &Li^7+H^1\rightarrow He^{4*}+He^4; \\ &He^{4*}\rightarrow He^4+\gamma \end{aligned} \qquad (1)$$

may still account for the spectrum, but perhaps with the exception of the 17.5 Mev component. It is not so easy to account for radiation as high as 17.5 Mev in this way, because that would leave almost no kinetic energy for the separation of the two alpha-particles. On the other hand, reaction (2), which has been discussed by several authors[4]

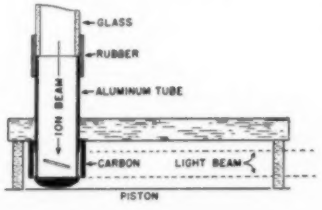


FIG. 1.

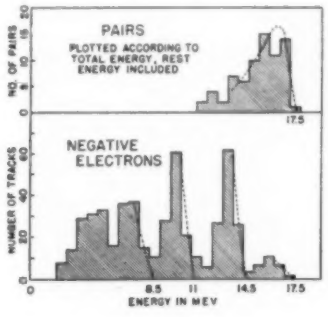


FIG. 2.

to account for the single 17.5 Mev component would not so readily

$$\begin{aligned} &Li^7+H^1\rightarrow Be^{8*}; \\ &Be^{8*}\rightarrow Be^8+\gamma \end{aligned} \qquad (2)$$

explain the presence of radiation of considerably lower energy, because the excited $Be^8$ nucleus would disintegrate into two alpha-particles too quickly to emit radiation of low energy. A plausible solution of the present problem may be to assume that the reaction occurs both ways, the capture reaction accounting for the highest line and the excited alpha-particle accounting for all the radiation of lower energy.

The striking feature of the plots in Fig. 2 is that the radiation indicated by the highest energy group of Compton electrons seems to give rise to far more pairs (by a factor of 10 at least) than it should, in comparison to the number of pairs produced by the radiation indicated by the lower groups of Compton electrons, especially the group at about 14.5 Mev. In fact, the pairs seem largely to correspond to the small group of Compton electrons at about 17.5 Mev. We have attempted to reconcile the two plots by considering the possible ways in which pairs of low energy can be systematically lost, such as by the stopping and scattering of the members of pairs in the material in which they are produced. These effects, however, are small and do not vary sharply with energy. The ratio of the pair and Klein-Nishina absorption coefficients also does not vary rapidly with energy in this range. Therefore, while the possibility of an explanation on the basis of the above effects should not be given up, we incline at present toward the belief that the contradiction between the pair and Compton electron distributions is real and must be explained in some other way. In the letter which follows a suggestion is offered which may be of help in formulating the problem.

E. R. GAERTTNER
H. R. CRANE

University of Michigan,
Ann Arbor, Michigan,
December 10, 1936.

[1] Crane, Delsasso, Fowler and Lauritsen, Phys. Rev. **48**, 125 (1935).
[2] Delsasso, Fowler and Lauritsen, Phys. Rev. **50**, 389 (1936).
[3] Pasadena Meeting, Am. Phys. Society, Dec. 18–19 (1936).
[4] Hafstad, Heydenburg and Tuve, Phys. Rev. **50**, 504 (1936).
[5] Chicago Meeting, Am. Phys. Society, Nov. 27–28 (1936).
[6] It is important to remember that the spread toward lower energies in the pair distribution should be twice that in the Compton electron groups because the carbon is effectively twice as thick for pairs as for single electrons.

### Is the Momentum a Sufficient Description of a Photon or an Electron?

The apparent contradiction between the results given by the pairs and the negative electrons in the case of the $Li+H^1$ radiation has been pointed out in the preceding letter. If this cannot be explained by means of our present knowledge of absorption coefficients, etc., the only alternative seems to be to discuss the possibility that the photons responsible for the 17.5 Mev group differ, in some way besides in their quantum energy, from those responsible for the lower groups of electrons, and in such a way as to affect radically the ratio of the pair and Klein-Nishina absorption coefficients. In searching for a possible reason for such a difference, we see that the matter of frequency can hardly be important, since its relative change is small, especially in going from the 17.5 Mev to the 14.5 or even to the 11 Mev line. The only thing which can be radically different for the various lines is the time of emission of the photon; in other words the length of the photon wave train. This might easily differ by a factor of 100 or more, even between the 17.5 and the 14.5 Mev lines.

According to the half-width for the proton energy,[1] the time involved in the radiation of the 17.5 Mev photon is of the order of $10^{-20}$ second. This means that the photon wave train must be extremely short (less than $10^{-9}$ cm) and also is not very long compared to its wave-length. Since the time for radiation by the excited alpha-particle is not restricted by the proton energy half-width, it might easily be 100 times as long. This would be equally true if the lower lines were attributed to transitions from lower levels in $Be^8$. Thus the 17.5 Mev line may be radically different from all the other lines in two ways: the extreme shortness of the wave train, and the fact that the wave train is not many wave-lengths long. It is noticed that the length of the wave train of the 17.5 Mev photon is in a region in which it may be small compared to the spatial extent of the wave function of a bound electron. Here we might look for an anomalous decrease in cross section for interaction with the bound electrons (Klein-Nishina absorption) although the approximations used in present theory do not provide for it.

If the interpretation of the present experimental results should prove to have something to do with the length of the photon wave train, it would amount to the introduction of an additional variable in the description of the *individual* photon, and would mean that photons of a given quantum energy cannot, as at present, be treated as identical regardless of the type of experiment. This view would tend to draw the wave and particle conceptions of the photon closer together, by describing the photon as a wave *packet* having *experimentally determinable* limits in space, in contrast to the present practice of describing it in some cases as an infinite wave and in other cases as an ideally small corpuscle.

The idea that the length of the photon wave train might have a real meaning in relation to experiment should be considered in regard to the interpretation of some cosmic-ray phenomena, which at present seem to demand either some such new variable or the introduction of new particles. The same argument applies to the electron wave packet, with the interesting difference that, because of dispersion, the wave packet would grow in length during its flight through space. Thus an electron which has traveled through space for a long time without interaction with matter might have a different cross section, for some processes, from one which has recently interacted with matter. There is already some evidence suggesting that electrons produced in showers have in general a different cross section for interaction with matter from those electrons occurring singly.

H. R. Crane

University of Michigan,
Ann Arbor, Michigan,
December 14, 1936.

[1] Hafstad, Heydenburg and Tuve, Phys. Rev. **50**, 504 (1936).

---

### Quantum Theory of the Second Virial Coefficient

In a recent article* on the Equation of State at Low Temperatures, the writer developed rigorous quantum formulae for the second virial coefficient for gases obeying the various statistics, the one for the Einstein-Bose statistics, for example, being, in the absence of any discrete state,

$$B=-\frac{N\pi^{\frac{1}{2}}\lambda^3}{2}+2\sum_{\text{even } l}(l+\tfrac{1}{2})B_l \qquad (1)$$

with the same notation as in the paper mentioned.

There were further developed from these formulae other (approximate) ones for the virial coefficient in terms of the phase shift of the wave functions involved. Subsequent calculation, using a rectangular potential well, with both the rigorous formula (1) and the approximate one in terms of the phases, throws light on the nature of this approximation. For this case, the rigorous formula at low temperatures, apart from the degeneracy term, will be of the form,

$$B=\frac{a}{T}+b+cT+dT^2+\cdots$$

whereas the approximate one will be given by

$$B=\frac{a'}{T}+b'+c'T+d'T^2+\cdots$$

where $a=a'$, the other coefficients differing by amounts depending on the constants of the rectangular well. Thus, for sufficiently low temperatures, when the first term becomes the most important, the rigorous and approximate calculations agree more and more closely. However, as it would seem difficult to establish *quantitative* criteria for the degree of approximation in the formulae involving the phases of an arbitrary interaction, it would appear to be much safer (although much more onerous), in comparing theory with experiment, to work with the rigorous formula (1).

I am indebted to Professor E. Wigner for his criticism of the formulae given in terms of the phases.

Leon Gropper

Washington Square College,
New York University,
December 12, 1936.

* L. Gropper, Phys. Rev. **50**, 963 (1936).

**Experiments on the Magnetic Properties of the Neutron**

Certain experiments have been made to detect an alignment or polarization of neutrons, due to their magnetic moment, on passing through strongly magnetized materials. If the neutron has a magnetic moment of possibly $-2$ nuclear magnetons, it might be expected that while the magnetic forces are small, the long range of the atomic magnetic fields might give rise to an appreciable magnetic scattering for slow neutrons.[1, 2] If so, a change in the scattering of a neutron beam might be produced by a change in the orientation of the neutron moments.

In the first type of experiment, the scattering of a beam of thermal neutrons, on passing successively through two sheets of iron magnetized to saturation, was investigated. In one set of experiments the neutron beam passed normally through the two plates. In a second set the beam passed normally through the first plate, and at 70° to the normal through the second plate. In a third set the neutrons passed through both plates at an angle of 65° to the normal. In the first two cases, on reversal of the magnetization of the first plate, no changes in neutron transmission larger than the probable error (0.5 percent $\pm$1.5 percent) were observed. Table I shows the results for the third case in which readings were also taken with no field in the first plate. Under these conditions, the effect, it if exists, can scarcely be larger than 2 percent.

In the second type of experiment, as shown in Fig. 1, the neutrons were first passed through a sheet of iron magnetized to saturation (polarized at approximately 45° to the normal in one arrangement, and 30° in a second arrangement, and then scattered from the pole face of a second magnet (about 3000 gauss), which should serve as an "analyzer" if the scattering cross section depends on parallel or anti-parallel orientation of the neutron with respect to the field). Table II shows the results for 3 runs at 45° incidence and 2 runs at 30° incidence averaged together

TABLE I.

| First Plate Field | Parallel to Second Plate | Anti-parallel to Second Plate | Zero |
|---|---|---|---|
| Total No. Counts | 30,200 | 30,100 | 29,300 |
| No./Minute | 186.70 $\pm$ 1.07 | 185.28 $\pm$ 1.07 | 183.33 $\pm$ 1.07 |
| Differences | | 1.42 $\pm$ 1.53 | 3.37 $\pm$ 1.53 |
| Background with Cd (averaged) | 23.0 | | |

TABLE II.

| Polarizer Field Direction | Parallel to Analyzer Field | Anti-parallel to Analyzer Field | Zero Field, i.e., Unpolarized |
|---|---|---|---|
| Total No. Counts | 12,700 | 11,500 | 15,600 |
| No./Minute | 50.81 $\pm$ 0.48 | 49.40 $\pm$ 0.44 | 48.80 $\pm$ 0.40 |
| Differences | | 1.41 $\pm$ 0.66 | 2.01 $\pm$ 0.65 |
| Background with Cd (averaged) | 22.4 | | |

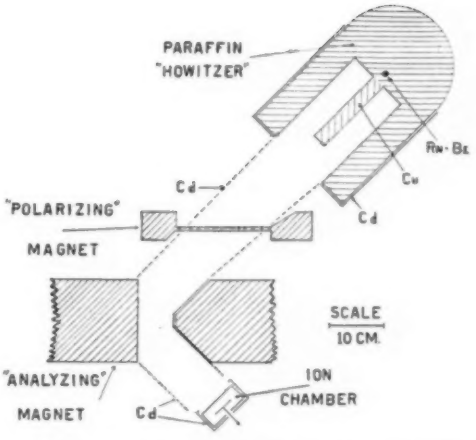


FIG. 1. Arrangement of apparatus for the second type of scattering experiment.

to increase the precision as they showed approximately the same trend. Runs were also taken with the polarizer field current zero, i.e., random orientation.

The difference 2.01$\pm$0.65 per minute between the unpolarized and the parallel case, and the difference of 1.41 $\pm$0.66 per minute between the parallel and anti-parallel cases, are not considered to prove conclusively the existence of an effect. However, the consistency of the various runs is very good, and from a purely statistical standpoint, the probability that these results do not indicate a real effect should be small. The smaller difference, if real, between the parallel and anti-parallel cases, compared to the unpolarized case, may be reasonable if we consider that in the anti-parallel case, a considerable fraction of the neutrons after leaving the polarizing plate may lose their space quantization and reorient themselves parallel to the field of the large magnet. Hence there may be little difference between the two cases. The observed results in any given case would depend on the field configuration. It is, however, difficult to understand the direction of the changes, i.e., why the number per minute in the parallel case is larger than in the anti-parallel or in the unpolarized case. Tests have shown no appreciable effects due to the stray magnetic fields on the detection chamber.

The number of thermal neutrons per minute is only about 0.55 of the total count per minute, due to the background of faster neutrons, and hence these changes represent approximately 7.5$\pm$2.5 percent and 5$\pm$2.5 percent of the thermal neutron count. The nuclear cross section (scattering plus capture) is so large compared to the observable magnetic interaction cross section that detection of such effects is clearly difficult, but the indications are that further experiments are desirable.

J. R. DUNNING
P. N. POWERS
H. G. BEYER

Pupin Physics Laboratories,
Columbia University, New York City.
December 17, 1936.

[1] Bloch, Phys. Rev. **50**, 259 (1936).
[2] Schwinger, Unpublished.

### The Intermediate Nucleus and Atomic Disintegration in Steps

In 1928 the writer[1] considered that the first step in a nuclear reaction is the synthesis of an intermediate nucleus which is unstable or excited on account of its high content of energy, and in 1933 Harkins, Gans and Newson[2] formulated all nuclear reactions of neutrons on this basis even though current opinion (Gamow, Feather, Chadwick, Rutherford, etc.) at that time was that part of these reactions occur by "noncapture." As a first step in the more definite proof of the formation of an intermediate nucleus, Harkins and Gans[3] developed the mechanics of noncapture disintegrations, and showed that only "capture" disintegrations occur. These were designated in 1926 by Harkins and Shadduck[4] by the term "synthesis and disintegration" of the atom, which assumed that the primary step is a synthesis, and only the secondary step, a disintegration of the atom.

Thus Harkins and Gans[3] formulated nuclear reactions as follows (Fig. 1).

$$A+B\rightarrow AB^*\rightarrow C+D.$$

That is the first step in the collision between the projectile $P$ and the target atom $T$, to synthesize an excited intermediate atom $I^*$

$$T+P\rightarrow I^*$$

and the second step is the disintegration:

$$I^*\rightarrow C^*+D,$$

where $C$ may or may not be excited.

The purpose of this letter is to express in more detail the point of view expressed in an address by the writer[5] presented Jan. 1, 1936. The theory expressed above was opposed by all nuclear quantum theorists until very recently, but was given support by Bohr in a lecture presented in February, 1936.

The purpose of this letter is to outline in more detail the postulates of the theory.

1. The fundamental postulate is that the intermediate nucleus has an actual existence, and that the duration of its life *is not given* by the value of $R/v$, as assumed by all nuclear quantum theorists prior to 1936, since they assumed the nonexistence of the intermediate nucleus.

Certain supplementary postulates are listed below, but these are not all essential to the theory.

2. The life period of any definite intermediate nucleus is independent of the components from which it has been formed provided it is in a definite excited state, but the state of excitation depends upon both the kinetic and mass energies of these components.

3. The life period depends upon the particular excited state of $I^*$, and on the energy of this state, and upon the nature and upon the energy states of its possible products.

4. When a definite intermediate nucleus is formed by the union of two definite nuclei, the life period should decrease in general with increase in the kinetic energy of the projectile.

5. The total number of primary nuclear disintegrations which occur is equal to the number of intermediate nuclei synthesized minus the number of excited intermediate nuclei which are able to return to a stable state by $\gamma$-ray emission alone.

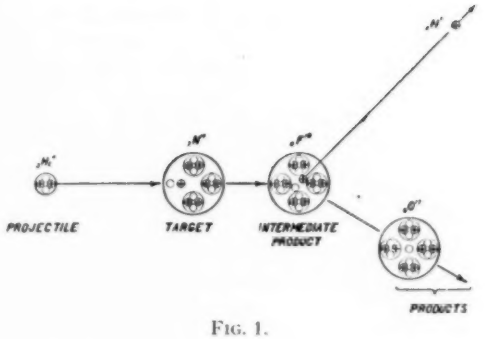


FIG. 1.

6. The types of disintegration which occur and their corresponding partial widths of level depend upon the state of the intermediate nucleus, particularly upon its energy, and the angular momentum, and upon the energy levels of the possible products.

7. The disintegration of the intermediate product $I^*$ may occur in several steps, and on the whole is more apt to do so as the energy of excitation increases.

8. The intermediate nucleus may disintegrate into its original components.

Direct evidence for this theory should be secured most easily in reactions in which 3 instead of 2 heavy particles are formed. Thus the reaction studied by Oliphant, Kinsey and Rutherford, and by Bonner and Brubaker may be formulated

$$_3Li^7+{}_1H^2\rightarrow{}_4Be^{9*}$$
$$_4Be^{9*}\rightarrow{}_4Be^{8*}+{}_0n^1$$
$$_4Be^{8*}\rightarrow 2{}_2He^4.$$

Even better are the reactions studied by Dee and Gilbert and others which may be formulated:

$$_5B^{11}+{}_{-1}H^1\rightarrow{}_6C^{12*}$$
$$_5B^{10}+{}_1H^2\rightarrow{}_6C^{12*}.$$

Then this may disintegrate:

$$_6C^{12*}\rightarrow{}_5B^{11}+{}_1{}^{-1}H^1$$

or a series of reactions may occur.

$$_6C^{12*}\rightarrow{}_4Be^{8*}+{}_2He^4$$
$$_4Be^{8*}\rightarrow 2{}_2He^4.$$

The life of $_4Be^{8*}$ in one of its states has been estimated from the energy of the state as $10^{-8}$ second by Bethe (private communication) on the basis of the energy of the state which now seems most probable. From what is known of the width of nuclear energy levels the writer has calculated that the half-life of the intermediate nucleus is most commonly in the range from $10^{-12}$ second to $10^{-19}$ second.

Where the writer in 1926 assumed the formation of an intermediate fluorine 18 from nitrogen and helium, the work of Haxel indicates that at $\alpha$ energies of above 4.5 Mev protons are given by the disintegration of the fluorine: at 5.5 Mev a maximum number of protons appears, and above 6 Mev the number of protons decreases since the

fluorine now disintegrates more and more into a neutron and fluorine 17, which then emits a positive electron. The final product in either case is oxygen 16.

W. D. HARKINS

Cornell University,
Ithaca, New York,
December 7, 1936.

[1] W. D. Harkins, Chem. Rev. **5**, 374 (1928).
[2] W. D. Harkins, D. M. Gans and H. Newson. Phys. Rev. **44**, 530, 533, 534, 537 (1933).
[3] W. D. Harkins and D. M. Gans, Phys. Rev. **46**, 397 (1934); Nature **133**, 794 (May, 1934).
[4] W. D. Harkins, Nat. Acad. Sci. **19**, pp. 307–318, March (1933).
[5] W. D. Harkins, Science **83**, 533 (1936). Address presented before Section C of the American Association for the Advancement of Science, and the St. Louis Section of the American Chemical Society, St. Louis, January 1, 1936.

## The Rotation-Vibration Spectrum of $C_2H_6$ and the Question of Internal Rotation

The problem of the order of magnitude of the potential restricting the relative rotation of the $CH_3$ groups about the symmetry axis in $C_2H_6$, once considered settled, has been revived by the statistical-mechanical calculations of several authors, the most recent being those of Kemp and Pitzer.[1] The latter authors find that by assuming a potential of about 3000 cal. restricting the internal rotation, it is possible to reconcile the equilibrium and calorimetric measurements of the $H_2+C_2H_4=C_2H_6$ reaction and to reproduce the experimentally determined entropy and specific heat of $C_2H_6$. The theoretical value of the restricting potential calculated by Eyring[2] is, on the other hand, only 350 cal.

We have made a dynamical study of a model of $C_2H_6$ in which vibration, over-all rotation and internal rotation subject to an arbitrary restricting potential may occur simultaneously, and have investigated how the rotation-vibration spectrum of $C_2H_6$ in the fundamental region will change in the transition from free to completely restricted internal rotation. In a comparison of theory and experiment the sole source of positive evidence concerning the extent of the freedom of the internal rotation is the rotational structure of certain perpendicular-type infrared bands in the fundamental region. From the observed structure of the bands a lower limit of 2000 cal. (700 $cm^{-1}$) is estimated for the potential restricting internal rotation. This result is in agreement with the conclusion of Kemp and Pitzer.[1]

It is found that there are two types of degenerate normal vibrations in $C_2H_6$, one of which is active, and one inactive in the infrared, regardless of the magnitude of the potential restricting internal rotation. The point group $D_3$, which assigned by Teller and Topley[3] to $C_2H_6$ and according to which they concluded that all degenerate vibrations would be active in the infrared, does not sufficiently describe the symmetry of the normal vibrations. The full symmetry properties of the vibrations are obtained by using the group $D_{3h}$ since the potential energy is invariant under a reflection in a plane perpendicular to the threefold symmetry axis regardless of the relative orientation of the $CH_3$ groups about the axis. (The transformation corresponding to this operation involves the internal angle.)

Barring *accidental* degeneracy of degenerate normal vibrations of different types (active and inactive), the same rotational structure of the infrared bands is predicted for all magnitudes of the potential restricting internal rotation. Consequently, the theory of the rotational spacings of the perpendicular-type infrared bands, inclusive of the effect of rotation-vibration coupling, is similar to the theory applied by Johnston and Dennison[4] to symmetrical top molecules without internal rotation. Table I gives the observed values of the line spacings of the perpendicular-type bands and the values we have calculated. However, as a result of the approximate accidental degeneracy between degenerate vibrations of different types with frequencies in the 1480 and 3000 $cm^{-1}$ regions, the internal rotation if it were free would be quasi-active and the simple rotational structure with the spacings calculated in Table I would not be observed. A perturbation calculation gives 2000 cal. as a limit to the potential restricting the internal rotation below which the rotational structure of the bands would be quite different from that observed.

TABLE I. *Rotational spacing in $cm^{-1}$ of perpendicular-type infrared bands of $C_2H_6$.*

| $\nu$ | $\Delta\nu$ obs. | $\Delta\nu$ calc. |
|---|---|---|
| 827 | 2.6 | 2.63 |
| 1480 | 4.9 | 5.60 |
| 3000 | 3.3 | 2.98 |

TABLE II. *Observed and calculated fundamental frequencies in $cm^{-1}$.*

| | Obs. | | Calc. | | Obs. | | Calc. |
|---|---|---|---|---|---|---|---|
| $\nu_1$ | 993 | R | (993) | $\nu_6$ | 827 | I. R. | 840 |
| $\nu_2$ | 1460 | R | 1570 | $\nu_7$ | 1480 | I. R. | 1480 |
| $\nu_3$ | (liq.) 2927* | R | 2910 | $\nu_8$ | 3000 | I. R. | 3020 |
| $\nu_4$ | 1380 | I. R. | (1380) | $\nu_9$ | — | | 1005 |
| $\nu_5$ | 2926** | I. R. | (2900) | $\nu_{10}$ | — | | 1515 |
| | | | | $\nu_{11}$ | — | | 3025 |

* $\nu_3 = 2927$ $cm^{-1}$ is the mean of the two Raman frequencies 2899 $cm^{-1}$ and 2955 $cm^{-1}$.
** $\nu_5 = 2926$ $cm^{-1}$ is the mean of the two infrared frequencies 2896 $cm^{-1}$ and 2955 $cm^{-1}$.

A three-constant valence-force type of potential function was chosen with which to calculate a set of frequencies and normal coordinates to be used in the perturbation calculation above. Table II gives the observed and calculated fundamental frequencies, which on the whole agree well considering the simplicity of the potential function used. The estimate of the lower limit to the restricting potential is not very dependent upon the accuracy of the normal coordinate treatment.

J. B. HOWARD

Mallinckrodt Chemical Laboratory,
Harvard University,
Cambridge, Massachusetts,
December 9, 1936.

[1] Kemp and Pitzer, J. Chem. Phys. **4**, 749 (1936).
[2] Eyring, J. Am. Chem. Soc. **54**, 3191 (1932).
[3] Teller and Topley, J. Chem. Soc. p. 885, July (1935).
[4] Johnston and Dennison, Phys. Rev. **48**, 868 (1935).

### The Elastic Scattering of Neutrons by Protons

Since the publication of our paper on the collision of neutron and proton,[1] ideas concerning the depth and size of the neutron-proton "hole" have become more clarified. Also, some experimental data[2] have been published on the angular distribution of the scattering. Accordingly, we have recomputed the elastic scattering formulae, using the value recently used for the binding energy of the deuteron.[3] We use the potential of the form given in Eq. (1) of our paper, with $x_1=0$, $r_0=0.3$; $D_t=71$ for the triplet state and $l=0$, $D_s=32$ for the singlet state (making the singlet state a virtual one). The corresponding $D$'s for $l=1$ have a reversed sign since we have chosen a combination of Majorana and Heisenberg operators.[4] The results are given in the accompanying figures. All units are in the nuclear system: unit energy ($W$) being 0.506 Mev in the c.g. system or 1.012 Mev absolute neutron energy and unit cross section being $0.8\times10^{-24}$ cm$^2$. These assumptions correspond to a deuteron energy of 4.35 and a limiting cross section $Q_0=53$.

Fig. 1 shows the phase defects, calculated as described in reference 1, as functions of neutron velocity. It is to be noted that $\delta_1$ is not negligible at $W=20$ (i.e., 20 Mev). The statement of Bethe and Bacher,[5] that neutrons of energy less than about 20 Mev (i.e., $W=20$) would show no appreciable deviation from the spherically symmetrical angular scattering of slow neutrons, is untrue (cf. Fig. 4).

Fig. 2 shows the total elastic cross section as a function of neutron velocity. The experimental value[6] of 2.1 at $W=4$ checks satisfactorily. The slow neutron cross section ($W\to0$) is taken as 53 from Amaldi and Fermi.[7]

Fig. 3 shows the calculated distribution in angle of the scattered *neutrons*, considering the center of gravity of the system to be at rest. The vertical scale has been adjusted to make the curves correspond at $\theta=0$. There is already considerable dependence on angle for neutron energies as low as 10 Mev ($W=10$).

Fig. 4 shows the computed number of recoil *protons* per

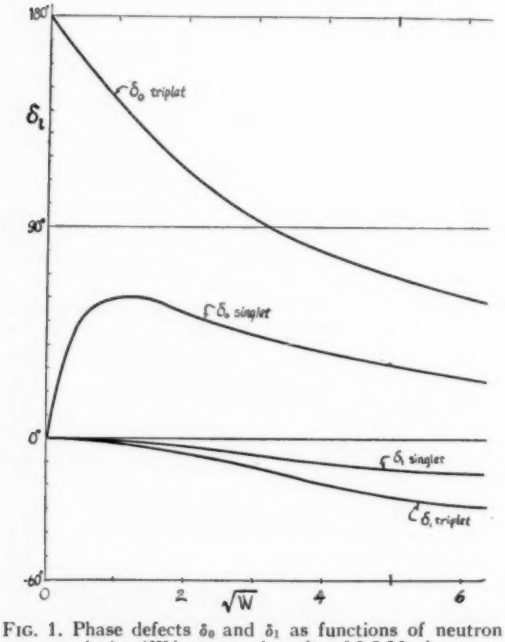


FIG. 1. Phase defects $\delta_0$ and $\delta_1$ as functions of neutron velocity ($W$ is energy, in units of 0.5 Mev).

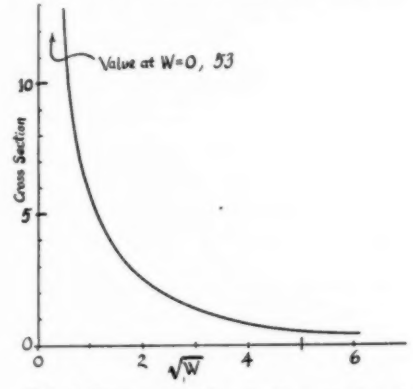


FIG. 2. Cross section for elastic scattering.

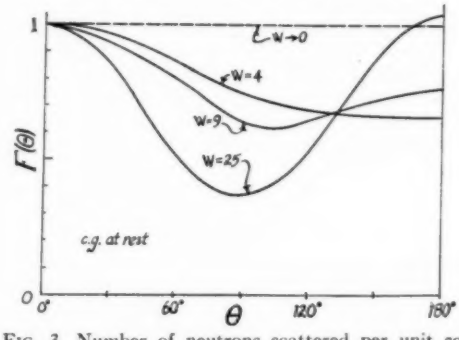


FIG. 3. Number of neutrons scattered per unit solid angle, at an angle $\theta$ with respect to the center of gravity of the system.

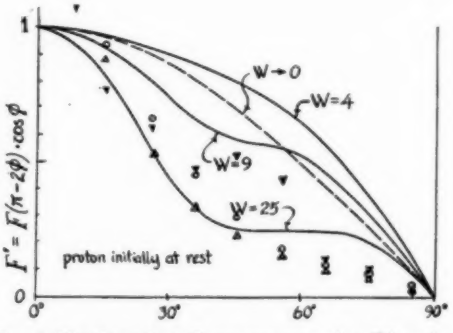


FIG. 4. Number of recoil protons per unit solid angle, at an angle $\varphi$ with respect to the initial position of the proton. The points marked by open circles and triangles are those given by Harkins, *et al.*, the darkened triangles those of Kurie,[8] with ordinates adjusted to our arbitrary scale.

unit solid angle. The available experimental data[2, 6] have been put on this plot, with a vertical adjustment of scale. The majority of the neutrons used in these experiments were between $W=0$ and $W=20$. If the neutron energies and abundances could be known, the precise shape of the theoretical curve could be obtained, and would be intermediate between the curves for $W=0$ and $W=20$.

In conclusion, it is seen that the calculations, based on present nuclear theory, and the experiments, are by no means in disagreement.

J. B. Fisk,
Philip M. Morse,

Society of Fellows,
Harvard University,
Massachusetts Institute of Technology,
Cambridge, Massachusetts,
December 14, 1936.

[1] Morse, Fisk and Schiff, Phys. Rev. **50**, 748 (1936).
[2] Harkins, Kamen, Newson and Gans, Phys. Rev. **50**, 980 (1936).
[3] Breit and Condon, Phys. Rev. **49**, 904 (1936).
[4] Breit and Feenberg, Phys. Rev. **50**, 850 (1936); Cassen and Condon, Phys. Rev. **50**, 857 (1936).
[5] Bethe and Bacher, Rev. Mod. Phys. **8**, 82 (1936). Cf. pp. 120, 121.
[6] Dunning, Pegram, Fink and Mitchell, Phys. Rev. **48**, 265 (1935).
[7] Amaldi and Fermi, Phys. Rev. **50**, 899 (1936).
[8] Kurie, Phys. Rev. **44**, 463 (1933).

## The Self-Consistent Field and Bohr's Nuclear Model

Some time ago, Bohr[1] proposed a semiclassical model of the nucleus and showed in what respect the mechanical properties of a nucleus differ essentially from those of an atom. He pointed out that owing to the great number of almost equivalent nuclear constituents an excitation energy given to the nucleus will rapidly be divided up among numerous particles. We want to indicate here shortly how such a picture is connected with the Hartree-Fock model of one-particle orbits, applied so successfully to atomic electrons. As Bethe[2] has shown, even in a Hartree model the spectral density of terms becomes very high for somewhat larger excitation energies. (The theory of the Fock field is slightly more complex since the one-particle eigenfunctions need not be all members of one orthogonal set. There is, however, still a linear transformation free in the Fock determinant and one can use this freedom to represent in a good approximation at least several eigenfunctions, say all of a certain spectral interval, by means of functions belonging to the same orthogonal set.) If we introduce the difference between the true and the self-consistent Hamiltonian as a perturbation of the self-consistent model[3] the perturbation energy will be very much larger than the average spacing of the levels. Therefore linear combinations of a large number of successive levels have to be taken as zero-order approximation of the perturbed eigenfunctions and this fact appears just as the quantum mechanical analog of Bohr's energy division among many particles.

There are on the other hand certain empirical features, usually referred to as "shell formation" in nuclei[4] which are difficult to explain by such a model, whereas their existence will follow immediately from any model of the Hartree-Fock type. In the field covered by the spontaneously radioactive nuclei those effects have been computed[5] from the known disintegration energies and it has been shown that the discontinuities in binding energy amount to several millions of volts and that they are much more pronounced for even than for odd nuclei. If we started originally with a self-consistent model of the nucleus, its characteristic features will be wiped out by the effect of the calculation just described, unless the spacing of the levels is sufficiently large, in which case some specific properties of the self-consistent model can partially subside. Now the spacing of levels is largest for the lowest levels. Furthermore, if strong forces between like particles exist—as seems now generally admitted—a closer binding between pairs will result, in which case the ground term of even nuclei, corresponding to all particles being bound in pairs with anti-parallel spins, will be considerably lower than the first excited state. The empirical facts known from the fine structure of $\alpha$-particles and from the $\gamma$-rays emitted by naturally radioactive substances support this conclusion. They show that odd nuclei usually have many excited states rather close to the ground state, whereas even nuclei have not. In the light of the above considerations this affords a qualitative explanation of the fact that even nuclei show the mentioned strong "shell" effects. A quantitative account seems however rather difficult due to the complexity of the model. The above considerations may also be considered as a qualitative justification for Bethe's[2] method of computing the term density.

W. M. Elsasser

Norman Bridge Laboratory of Physics,
California Institute of Technology,
December 1, 1936.

[1] N. Bohr, Nature **137**, 344 (1936).
[2] H. A. Bethe, Phys. Rev. **50**, 332 (1936).
[3] C. Møller and M. S. Plesset, Phys. Rev. **46**, 618 (1934).
[4] See ch. 4, in Bethe and Bacher's article, Rev. Mod. Phys. **8**, 82 (1936).
[5] W. M. Elsasser, J. de phys. **6**, 473 (1935).

## Current Difference in $\gamma$-Ray Ionization Measurements

New experiments have been conducted with the uniform field ionization chamber used by Bowen[1] and the writer[2] to see if this apparatus gave a difference between the number of positive ions collected per second and the number of negative ions collected per second. Clay and Van Tijn[3] and Broxon and Meredith[4] have reported finding that the number of negative ions collected per second was larger than the number of positive ions collected per second for the same collecting field and pressure of air.

The procedure used in the new experiments is that given by Bowen with precautions added to secure unbiased results. After the pressure had been adjusted to some given value, a positive collecting voltage was applied for thirty minutes and then a series of ten collection times recorded. A set of ten readings was taken on collection time for negative ions after the field battery had been reversed for thirty minutes. For about one hour the potential plates were grounded, and the potential on the electrometer string was reversed for the remaining readings. Again the negative field voltage was applied for half an hour and ten readings made; thirty minutes of positive voltage and a series of ten readings completed the run. Data were taken for air pressures of 51.8 and 71.7 atmos. with low intensity $\gamma$-radiation and 51.8 atmos. with high intensity radiation; the collecting fields were from 22.5 to 1655 volts/cm.

From the observations with low ion density the largest observed difference between the average collecting time for positive ions and that for negative ions was 0.7 percent of the mean collecting time; the probable error in each average was less than 0.4 percent. Half of the averages showed the positive current larger than the negative, thirty-three percent showed the opposite effect, and in all cases the difference between averages was less than the mean deviation of individual collecting time readings.

The ion density used by Broxon and Meredith was of the same order of magnitude as the low ion density here used: i.e., about ten to twenty times the residual ionization. Clay and Van Tijn have used an ion density of about 3000 times the residual ionization, and it was thought that this great factor might produce some difference between positive and negative collecting times. Again, however, when an ion density comparable with that of Clay and Van Tijn was used the differences between average times were all within 0.3 percent and showed no general preference.

It is a pleasure to acknowledge the courtesies of the California Institute of Technology in allowing me to perform these experiments with their facilities.

EVERETT F. COX

Colgate University,
Hamilton, New York,
December 1, 1936.

[1] I. S. Bowen, Phys. Rev. **41**, 24 (1932).
[2] E. F. Cox, Phys. Rev. **45**, 503 (1934).
[3] J. Clay and M. A. Van Tijn, Physica II **8**, 825 (1935). Clay and Van Tijn state by correspondence that the words *positive* and *negative* are to be interchanged on pages 827 and 828.
[4] J. W. Broxon and G. T. Meredith, Phys. Rev. **49**, 415 (1936).

## Correction to The Photoelectric Effect of the Deuteron

Two of us[1] published formulas and graphs for the collision cross section of a photon with a deuteron. Miss Katharine Way of the University of North Carolina has been comparing the calculations with some of her own and she has found arithmetical mistakes in the graphs. These mistakes were made in the calculations which involved the Majorana interaction. The calculations have been repeated and checked. The corrected graphs are reproduced below. They are numbered in the same way as in the paper.[1] Instead of Fig. 3b one should use the following values of $10^{27}\sigma$ (accurate to approximately 1 percent):

TABLE I. *Values of* $10^{27}\sigma$ (*Majorana*).

| $E$ | $a=1\times10^{-13}$ cm | $a=2\times10^{-13}$ cm | $a=3\times10^{-13}$ cm | $a=4\times10^{-13}$ cm |
|---|---|---|---|---|
| 0.275 Mev | 0.45 | 0.57 | 0.72 | 0.92 |
| 0.55 | 0.92 | 1.17 | 1.47 | 1.86 |
| 1.1 | 1.51 | 1.90 | 2.39 | 2.97 |
| 2.2 | 1.78 | 2.26 | 2.82 | 3.41 |
| 3.3 | 1.68 | 2.12 | 2.60 | 3.14 |
| 4.4 | 1.50 | 1.89 | 2.31 | 2.78 |
| 6.6 | 1.16 | 1.45 | 1.78 | 2.17 |
| 8.8 | 0.92 | 1.14 | 1.38 | 1.72 |

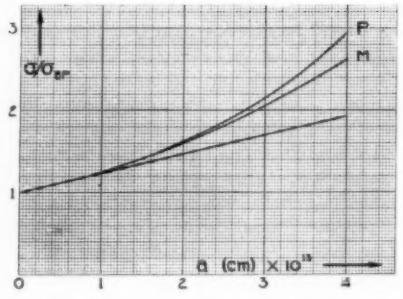


Corrected FIG. 1. Dependence of cross section on range and type of interaction law at the photoelectric threshold, $E=0$. Ratio $\sigma/\sigma_{BP}$ is plotted against $a$ in $10^{-13}$ cm. $P$ refers to ordinary, $M$ to Majorana interaction.

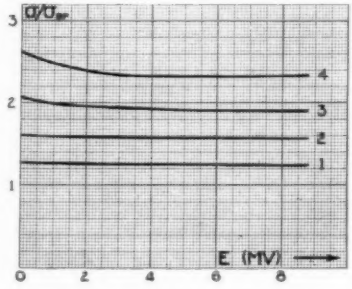


Corrected FIG. 2b. (Majorana interaction.) Dependence of cross section on range and type of interaction law for energies up to $E=8.8$ Mev. Ratio $\sigma/\sigma_{BP}$ is plotted against $E$ in Mev. Curves are labeled by values of $a$ in $10^{-13}$ cm.

In Fig. 4 the curve $M$ should be replaced by a straight horizontal line corresponding to $\sigma(h\nu=8.8\ \text{Mev})/\sigma(h\nu=4.4\ \text{Mev})=0.64$. It is seen that the photoelectric effect of the deuteron in the region $h\nu=0\rightarrow10$ Mev is not very suitable for distinguishing between exchange and non-exchange interactions, the collision cross sections being nearly the same in the two cases. The determination of the radius of the deuteron from experimental material on the photoelectric cross section is simpler, taking into account the above corrections, because nearly the same values for the radius are obtained whether one uses Wigner, Heisenberg or Majorana forces.

G. BREIT
J. R. STEHN

University of Wisconsin,
Madison, Wisconsin,

E. U. CONDON

Princeton University,
Princeton, New Jersey,
December 11, 1936.

[1] G. Breit and E. U. Condon, Phys. Rev. **49**, 904 (1936).

# Proceedings of the American Physical Society

## Minutes of the Chicago Meeting, November 27–28, 1936

THE 209th regular meeting of the American Physical Society was held in Chicago, Illinois, at the University of Chicago on Friday and Saturday, November 27 and 28, 1936. The presiding officers were F. K. Richtmyer, President of the Society, H. M. Randall, Vice President, Julian E. Mack and Ralph A. Sawyer. The attendance at the meeting was about three hundred.

On Friday evening in the International House the Society held a joint dinner with the Chicago Physics Club. President Richtmyer introduced Professor A. H. Compton, President of the Chicago Physics Club, who presided. Professor Compton called upon Professor John T. Tate, Chairman of the American Institute of Physics Incorporated, to extend congratulations to Professor Carl D. Anderson upon the award to him of the Nobel Prize. Professor Anderson who was present responded briefly. After this Dr. K. K. Darrow spoke on "Spinning Atoms and Spinning Electrons." There were one hundred and ninety-five guests present.

**Meeting of the Council.** At the meeting of the Council held on Friday, November 27, 1936, the deaths of two members were reported. (William D. Lansing and Tokutaro Sawai.) Six candidates were elected to fellowship, thirteen candidates were transferred from membership to fellowship, and twenty-eight candidates were elected to membership. *Elected to fellowship:* H. Beutler, Eli F. Burton, M. F. Crawford, Donald D. Foster, R. H. Fowler, and Sterling B. Hendricks. *Transferred from membership to fellowship:* Norris E. Bradbury, Paul H. Dike, Wendell H. Furry, Lachlan Gilchrist, H. Grayson-Smith, Frederick V. Hunt, Hubert M. James, Henry Victor Neher, John L. Rose, George H. Shortley, L. B. Slichter, Robert N. Varney and John P. Vinti. *Elected to membership:* Robert J. Adams, David L. Arenberg, Richard F. Baker, A. Clarke Beiler, Raymond M. Bell, Cornelis Bol, Dean P. Crawford, Warner Eustis, James J. Fleming, Gorton R. Fonda, Robert Hofstadter, Clifford Holley, Toyohiko Kagawa, C. D. Keen, Rolf Landshoff, Stewart W. Matson, B. S. Maximoff, Donald S. Miller, Kenneth W. Miller, John S. O'Conor, Roland Schaffert, Samuel Silver, Paul W. Thompson, George Valley, Carel W. van der Merwe, H. von Halban, Kenneth L. Warren, and Richard E. Watson.

The regular scientific program of the Society consisted of forty-one contributed papers of which numbers 17, 23, 27 and 29 were read by title. The abstracts of these papers are given in the following pages. An *Author Index* will be found at the end.

W. L. Severinghaus, *Secretary*

## Abstracts

**1. A Million Volt Cyclotron.** P. Gerald Kruger and G. K. Green, *University of Illinois.*—During the past fifteen months a cyclotron capable of producing 2.5$\mu$ amp. of deuterons at $10^6$ ev energy, has been assembled and put into operation. Slides showing various features of the apparatus will be shown. The deuteron beam has been brought out of the vacuum chamber to a point about three feet from the edge of the magnet poles. This removes one of the formerly objectionable features of the cyclotron and makes it possible to study nuclear disintegrations without the intense fields of the cyclotron affecting the detecting apparatus. Examination of the shape of the beam current with an oscilloscope shows from 10 to 20 percent 360-cycle ripple, which corresponds to the rectified current supplied to the oscillators. The high frequency potential applied to the accelerating electrodes has been measured with an oscilloscope and found to be about 32 kilovolts. Various adjustments and their effect on the deuteron beam will be discussed.

**2. A Radiofrequency Source and Transmission Line for the Cyclotron.** G. K. Green and P. Gerald Kruger, *University of Illinois.*—Two commercial oscillator tubes have been connected in a tuned-plate tuned-grid circuit coupled to the cyclotron vacuum chamber with a matched-impedance transmission line. This system has better frequency stability than the direct coupled TNT circuit and is not thrown out of oscillation when bursts of gas occur in the vacuum chamber. In addition the radiofrequency source may be placed at any distance from the magnet.

The radiofrequency energy delivered to the electrode resonant circuit is over 60 percent of the direct current energy input. The transmission line, condensers, and other parts of the circuit have been constructed in this laboratory and will be described. Accelerating electrode insulators which will withstand the intense high frequency fields and mechanical strain have been developed. A pair of these insulators has been in operation since March 1936, with no trouble from overheating or glass puncture.

**3. An Electrostatic Generator for the Production of Positrons.** G. B. COLLINS, R. SCHAGER AND A. L. VITTER, *University of Notre Dame.*—An electrostatic generator of the type described by Tuve, Hafstad and Dahl has been erected in a room 40×40×40 ft. The sphere is 12 feet in diameter and was constructed at a comparatively small cost by nailing copper sheets on a spherical wooden form. The slightly irregular surface which resulted apparently does not greatly increase the corona loss since a potential of about 2 Mev is obtained with a charging current of only $10^{-4}$ amp. An accelerating tube 9 inches in diameter and 24 feet long has been set up for the purpose of accelerating electrons. A system of protective rings has been devised which has a small corona loss and protects the glass tube against puncture. The apparatus is to be used for the production of positrons.

**4. Construction of a Voltage Multiplying Circuit to Yield 700 kv.** SAMUEL K. ALLISON, GRAHAM T. HATCH AND LESTER S. SKAGGS, *University of Chicago.*—A voltage multiplying circuit of the type first used by Cockcroft and Walton in nuclear disintegration experiments has been constructed with the hope of reaching positive or negative potentials of 600–800 kv. The design of the vacuum tube rectifiers has some novel features. The filament assemblies are pushed into place or pulled out through conduit tubes which are closed at their outer ends with vacuum tight removable plates. This makes possible rapid replacement of burnt out filaments. The sign of the high voltage produced can be changed by reinsertion of the filament assemblies into the set of conduit tubes which have previously acted as electron collectors. The problem of insulating the sources of heating current for the filaments has been solved by heating each filament from the output of a small direct current generator. These generators are mounted on a vertical insulating drive shaft; their output is stabilized by small storage batteries acting as floats. Preliminary trials with 60-cycle current have produced 600 kv (tested with a gap between 75 cm spheres) and reveal no serious obstacle to operation at voltages 100 to 150 kv higher. It is intended ultimately to operate the circuit with the laboratory supply of 540-cycle current.

**5. The Development and Performance of an Electrostatic Generator Operating under High Air Pressure.** R. G. HERB, D. B. PARKINSON AND D. W. KERST, *University of Wisconsin.*—A belt type electrostatic generator has been developed which operates in a steel tank, 5½ feet in diameter and 20 feet long, under an air pressure of 100 lbs./in.$^2$. The generator is provided with a high potential electrode system of a new design which serves both to give a high breakdown potential and to furnish a satisfactory potential distribution along the charging belts and the accelerating tube. The maximum potential of the generator is about 2500 kv and the highest steady potential at which reliable data have been obtained is 2160 kv. An evacuated tube for acceleration of ions has been developed which withstands the highest generator potential. The apparatus has been successfully used in experiments on atomic disintegration.

**6. High Potential Apparatus for Nuclear Studies.** H. R. CRANE, *University of Michigan.*—A 1,000,000-volt transformer and vacuum tube apparatus for nuclear disintegration work has recently been completed at the University of Michigan. The transformer consists of five 200,000-volt sections, in a cascade circuit. The tube is made of five heavy Pyrex glass sections 24 inches long and 16 inches in diameter, with hollow steel electrodes 6 inches in diameter. Each accelerating gap in the tube is connected across one of the sections of the transformer to insure uniform potential distribution. A focused ion beam of 250 microamperes is obtained at the target. Cloud chambers are operated in synchronism with this apparatus by means of a common contact system, in such a way that both the ion source and the transformers are energized for only about ½ second, during which the chamber expansion takes place. Details of the construction and operation of this apparatus will be given at the meeting.

**7. Focusing Criteria for Electrons in Superimposed Electric and Magnetic Fields.** A. E. SHAW, *University of Chicago.*—The precision of most deflection measurements of $e/m$ for electrons is limited by the uncertainties due to contact potential difference in the accelerating field. In the present paper, experiments are described which have as their purpose the investigation of supplementary criteria which eliminate these uncertainties from the method of superimposed electric and magnetic fields. The equation for $e/m$ employed in this work is

$$e/m = 4E/(H^2\rho^2),$$

where $E$ represents the electric field intensity; $H$, the magnetic field intensity; and $\rho$, the radius of curvature of the path. Although the velocity does not appear explicitly in this equation, provision must be made by focusing to adjust the velocity for any given ratio of intensities of electric and magnetic fields. This adjustment can be carried out by a series of observations to give the appropriate values of $E$ and $H$ to an accuracy of 1 : 10,000. A provisional value of $e/m$ agrees approximately with the average of five recent results based on four different methods. A final value will be given as soon as a redetermination can be made of the geometrical constants of the apparatus.

**8. An Improved Method for the Measurements of High Energy Gamma-Rays.** E. R. GAERTTNER AND H. R. CRANE, *University of Michigan.*—Measurements of the quantum

energies of gamma-rays arising from artificial disintegration processes have heretofore been made by placing a cloud chamber near the source and observing Compton electrons and electron pairs ejected from the walls of the chamber or from a thin sheet of material placed within the chamber. If only those electrons which are known to come from a small depth of absorber are counted, the method becomes slow and confusion is introduced by scattered radiation. The present authors have constructed a target in a small thimble inside a cloud chamber, which is bombarded by an ion beam for an instant at the time of expansion. With almost no exception, the tracks appearing in the chamber originate in the thin wall of the thimble. In preliminary experiments with lithium bombarded with protons, using 0.7 mm brass wall, many electron pairs and single negative electrons having the entire available energy, 17 Mev were observed. Similar measurements are now being made with a thimble having a thin carbon wall.

**9. The Bombardment of Gold with Deuterons.** J. M. CORK AND R. L. THORNTON, *University of Michigan.*—The products of disintegration formed by bombarding gold with high energy deuterons (6 to 7 Mev) have been studied. The deuterons were produced in a new magnetic resonance accelerator. Chemical separations show the radioactivity to be associated with a gold isotope and an iridium isotope. Observations with the cloud chamber show the gold to emit negative electrons and the iridium to emit both positives and negatives. The corresponding reactions are probably as follows:

(a) $_{79}Au^{197}+{}_1H^2\rightarrow{}_{79}Au^{198}+{}_1H^1\rightarrow{}_{80}Hg^{198}+{}_1H^1+{}_{-1}e^0$,

(b) $_{79}Au^{197}+{}_1H^2\rightarrow{}_{77}Ir^{196}+{}_1H^1+{}_2He^4$,
$_{77}Ir^{196}\rightarrow{}_{78}Pt^{196}+{}_{-1}e^0$ and $_{76}OS^{194}+{}_{+1}e^0$.

Estimations of the half-life periods and of the beta-energies are made.

**10. The Disintegration of Beryllium by Protons.** JAMES S. ALLEN, *University of Chicago.*—In order to study the disintegration of Be by low velocity protons a three-section tube was designed. The proton source was of the low-voltage arc type and produced total ion currents of the order of 40 microamperes. The usable proton currents ranged from one to six microamperes. The energy of the protons was measured both by means of a magnetic field and by spark-gap readings of the voltage. The disintegration products were recorded by an ionization chamber 2.5 mm deep and a linear amplifier using Dunning's circuit. The yield curve for a thick target of Be was determined for voltages from 45 to 125 kv and the ratio of the number of alpha-particles and deuterons ejected from the target was found for various proton energies. The ratio was very close to unity. The ranges of both groups of particles were found to be 7.1 mm. From the energy considerations the mass of $Be^8$ was found to be 8.0074. The experimental value of the effective area for collision was found to be of the same magnitude as that predicted by Gamow's theory for the penetration of a potential barrier by protons.

**11. Alpha-Particle Yield from Protons on Lithium.** L. J. HAWORTH AND L. D. P. KING, *University of Wisconsin.*—The yield of eight centimeter alpha-particles produced when metallic lithium is bombarded with protons was obtained as a function of proton energies from 20 to 200 kilovolts. Observations were made on both massive and thin (3 kilovolts absorption at 120 kilovolts) films. To avoid effects of surface impurities new lithium was evaporated after each five minutes of bombardment. Comparison of the thick and thin film data indicates that the $V^4$ absorption law is probably not valid at these low energies.

**12. Gamma-Ray Yield from Light Elements due to Proton Bombardment.** R. G. HERB, D. W. KERST AND J. L. MCKIBBEN, *University of Wisconsin.*—With the high potential electrostatic generator recently developed at this laboratory a survey of a number of elements has been made in a search for gamma-ray emission due to proton bombardment. Six of the elements examined gave gamma-rays of sufficient intensity to permit accurate measurement. These six elements are Li, Be, B, F, Na and Al. Their gamma-ray yield was studied as a function of proton energy, or generator voltage, starting with the minimum potential at which the yield was easily measurable. In the region of fairly low potentials the yield curves from the six elements studied gave evidence for resonance excitation of the gamma-rays and certain indications of fine structure. At high potentials each of the six elements gave a gamma-ray intensity which increased nearly exponentially with voltage up to the maximum voltage obtainable from the generator (approximately 2 Mv). The other elements which were bombarded are C, O, Si, Cl, K, Ca, V, Ni, Cu, Zn, Mo, Pt, Pb. Gamma-rays from these elements were weak, and from some of them the gamma-ray intensity was not above the x-ray background of the generator.

**13. An Energy Distribution Analysis of Primary Cosmic Rays.** ARTHUR H. COMPTON, *University of Chicago.*—An energy distribution analysis, following the method suggested by Zanstra, is given, with the use of new latitude effect data collected on the Pacific Ocean in collaboration with R. N. Turner, of the *R.M.S. Aorangi.* The method depends upon Störmer's theory which relates the minimum energy of the vertical rays to the magnetic latitude, and the close experimental approximation that the intensity of the vertical cosmic rays is proportional to that of the total radiation coming from all directions. Below 9 Bev (Bev = $10^9$ electron volts) the effect of the earth's atmosphere becomes evident in limiting the rays that are received to a higher energy than the minimum admitted by the magnetic barrier. The form of the curve for lower energies suggests two components, one with a limiting energy imposed by the atmosphere of about 8 Bev, and the other of about 3 Bev, though the data are inconclusive. Between 9 and 19 Bev the energy spectrum appears continuous and indicates an electrical particle origin of a large part, very possibly the whole, of the cosmic-ray ionization.

**14. High Altitude Test of a Radio-Equipped Cosmic-Ray Meter.** C. D. KEEN, *University of Chicago.*—A high altitude cosmic-ray meter, of the type proposed by Benade,[1] has been built and flown. The ionization current of an unshielded argon-filled chamber moves the mirror of a Dershem electrometer. When the reflected light beam falls on a photoelectric cell, the electrometer is discharged and the radio signal is modulated. A pressure device also modulates the signal when certain altitudes are reached. A small quantity of radioactive material introducing a small fixed ionization makes possible convenient measurement of cosmic-ray ionization through a large ratio. On April 14, 1936, a balloon flight was made from Shreveport, Louisiana. The instrument and batteries weighed 41 pounds, and were raised by three 8-foot balloons to an altitude of 52,000 feet. During the rapid ascent the swaying of the gondola affected the electrometer mirror, and the cosmic-ray signals were irregular. More satisfactory data were obtained on the slower descent. At 78 mm of mercury an intensity of 288 $I$ was measured. This preliminary curve is somewhat steeper than that obtained by Millikan and Bowen[2] at about the same latitude.

[1] J. M. Benade and R. L. Doan, Phys. Rev. **47**, 198 (1935).
[2] I. S. Bowen and R. A. Millikan, Phys. Rev. **43**, 695 (1933).

**15. Heights of Reflection of Radio Waves in the Ionosphere.** F. H. MURRAY AND J. BARTON HOAG, *University of Chicago.*—A general method has been developed whereby, from the virtual height-frequency curves, it is possible to calculate an upper limit to the height of reflection of a radio wave of a particular frequency in the ionosphere. It is shown that a discontinuity in a virtual height-frequency curve is a necessary but not a sufficient condition for the existence of two distinct layers. The application of the method to a particular day and place, over the frequency range from 2.5 to 4.4 megacycles, has yielded several interesting results. For example, at certain times and for certain frequencies, the highest altitudes to which the waves can travel are very much lower than the virtual heights, indicating that the group velocity over extended regions in the ionosphere is much less than the velocity of light. It was also found that, during the morning hours and for the range of frequencies studied, the upper limits of the true heights in the $F_2$ region decreased whereas the virtual heights increased.

**16. Electron Beam Oscillators.** J. BARTON HOAG AND GEORGE E. FLODIN, *University of Chicago.*—In order to produce ultra-short radio waves at comparatively high power levels with the usual tubes and circuits it is necessary to employ large structures to dissipate the heat and simultaneously to use small structures to reduce the capacities and shorten the transit time of the electrons. With the object of alleviating these contradictory conditions, we have developed a type of oscillator using an electron beam. The beam passes through several electrodes whose relative potentials are varied periodically by feed-back from parts of the beam more distant from the electron gun. In one form, the electrons are deflected by periodic reversals of the potentials on condenser plates;[1] in another, they are alternately converged and diverged by an electron lens. The feed-back may be accomplished by coupling with electrodes at the end of the beam or by charges induced on electrodes through which the electrons are passing (the latter was suggested by A. and O. Heil). Under certain operating conditions, we have observed a wave with more than two hundred harmonics.

[1] C. M. Shanks, M.A. Thesis, University of Chicago, 1935.

**17. The Preferred Orientation Produced in Pure Iron-Nickel Alloys by Cold-Rolling.** D. MCLACHLAN, JR., AND WHEELER P. DAVEY, *Pennsylvania State College, State College, Pa.*—Ribbons whose total impurities did not exceed 40 parts per million were cold-rolled in a single direction at a speed of about 6 inches per minute. Underneath a surface skin one mil thick the degree of orientation depends only upon the percent total reduction. It is independent of the reduction per pass and of the nickel content up to 22 percent nickel. By using a quantitative concept for a unit-pole, the degree of preferment of orientation is expressed in terms of pole density on a sphere of reference. Three assumptions are made as to the mechanism of rolling. These enable orientations to be expressed by two parameters instead of three. A simple probability function has been found for the chance that a crystal fragment will have a given orientation. Pole densities from this probability function agree with those found by experiment. The theoretical equation requires a knowledge from experiment of only the ratio of two numbers which express the maximum deviation of orientation from the optimum along each of two coordinates used in plotting the results.

**18. A New Method of Determining the Relative Location of Points Within a Body by X-ray Photography.** A. D. HUMMELL, *Eastern Kentucky State Teachers College,* AND O. F. HUME, *Richmond, Ky.*—Two pairs of scales are mounted in parallel planes with a known distance between them in such a way that the images of these scales and the points in question will appear on the same radiograph. To determine the three-dimensional location of a point with respect to an arbitrary zero, two radiographs are necessary and differ only in a small lateral displacement of the source of x-rays. The actual relative position of the points in question and the scales must be the same for these two radiographs. The image of the point whose position is desired is found in each radiograph and perpendiculars drawn to each of the scale shadows. The intersections with the latter are noted in terms of the units into which the scale images are divided. From these readings the spatial coordinates are determined. The distance between two points may then be found. The method is useful in determining the pelvic measurements of a pregnant woman, in locating foreign particles in the human body, and its simplicity should make it applicable in industry.

**19. The Atomic Vibrations of Zinc Crystals at Liquid Air Temperature.** G. E. M. JAUNCEY AND W. A. BRUCE, *Washington University, St. Louis, Mo.*—The coherent part of the diffuse scattering of x-rays from a crystal is proportional to $(1-e^{-2M})$. Zener has shown from theory that for a hexagonal crystal like zinc $M$ should be of the form

$(a\cos^2\psi+b\sin^2\psi)\cdot(\sin^2\frac{1}{2}\phi)/\lambda^2$, where $\psi$ is the angle between the $c$ axis of the crystal and the line bisecting the angle between the forward direction of the scattered rays and the backward direction of the primary rays. The quantities $a$ and $b$ are functions of the temperature and $\phi$ is the angle of scattering. In a previous paper[1] we have reported that, for zinc crystals at room temperature (298°K) and for $\phi=30°$, $a=2.34A^2$ and $b=0.68A^2$. These correspond to root mean square displacements of 0.172A and 0.093A, respectively. Using primary rays with the same spectral distribution as in the previous paper, we have now obtained a curve of $S$ against $\psi$ for the crystals at liquid air temperature (100°K) and for $\phi=30°$. From this curve we obtain $a=0.84A^2$ and $b=0.23A^2$. These correspond to root mean square displacements due to thermal vibration of 0.103A and 0.054A, respectively, parallel and perpendicular to the $c$ axis of zinc.

[1] Jauncey and Bruce, Phys. Rev. **50**, 413 (1936).

**20. Dependence of Diffuse Scattering of X-Rays from Quartz Upon the Crystal Orientation II.** E. S. Foster, Jr., G. E. M. Jauncey and W. A. Bruce, *Washington University, St. Louis, Mo.*—The coherent part of x-rays diffusely scattered from a crystal has been shown by theory to be proportional to $(1-\epsilon^{-2M})$, where $M$, the Debye-Waller temperature factor, is a measure of the mean square displacement of the atoms. The structure of quartz as determined by x-ray analysis has been found very complicated. A number of rules have been established concerning the symmetry of the diffuse scattering from an $X$-cut crystal. Whereas, in the case of zinc, $M$ is a simple function of $\psi$, the orientation angle, for quartz the relation is very complicated. At a scattering angle of $\varphi=25°$ we have shown the following relations:

$$S(A,\psi)\neq S(B,\psi),$$
$$S(A,\psi)=S(B,-\psi),$$
$$S(A,\psi)\neq S(A,-\psi),$$
and
$$S(A,\psi+\pi)=S(A,\psi),$$

where $S(A,\psi)$ is defined as the diffuse scattering coefficient for a scattering angle $\varphi$ when the side $A$ of an $X$-cut crystal is towards the primary x-rays and $\psi$ is the angle between the $c$ axis and the bisector of the angle between the forward direction of the scattered rays and the backward direction of the primary rays.

**21. The Structure of Molten Salts.**[1] E. P. Miller and K. Lark-Horovitz, *Purdue University.*—Different methods have been worked out for the evaluation of the distribution function as determined by the x-ray scattering curve $Si(s)$ and given by the formula

$$G(r)=(1/2\pi^2r)\int_0^\infty Si(s)\sin(sr)ds.$$

As the most satisfactory method the punched card method has been found which allows a completely automatic analysis to be carried out in a few hours.[2] The results have been applied to the determination of the number of atoms around any atom in molten KCl and LiCl. In the first case both atoms can be treated as identical. In the second case Li can be neglected as compared with Cl. The results as given below indicate that for the next neighbors the coordination as found in the solid is maintained for the liquid but that the distribution of the second next neighbors is already disturbed.

| Substance | Solid | | Liquid | |
|---|---|---|---|---|
| | Number | $d$ | Number | $d$ |
| KCl | 6 | 3.14 | 5.8 | 3.14 |
| (K=Cl) | 12 | 4.44 | 8.3 | 4.3 |
| LiCl | 12 | 3.64 | 9.8 | 3.8 |
| (Li≪Cl) | 6 | 5.14 | (5.0?) | 5.15 |

[1] Phys. Rev. **49**, 418 (1936).
[2] Complete sin ($sr$) tables and punched cards for the method worked out from these can be obtained from this laboratory

**22. The Faraday Effect in the X-Ray Region.** H. T. Clark and K. Lark-Horovitz, *Purdue University.*—Co $K\alpha$ x-rays produced in a tube with steel body (as magnetic shield) have been polarized by reflection from the 220 plane of Ni and were passed through iron foils of varying thicknesses and in different magnetic fields. This monochromatic radiation was then "analyzed" by scattering from crystalline tungsten and the analyzed radiation was recorded photographically on a cylindrical film coaxial with the tungsten scatterer. Records of the radiation scattered after passing the iron foil with and without magnetic field were obtained side by side on the same film. A rotation of one degree could have been detected. With completely monochromatic radiation (carefully shielding any stray radiation from the continuous background), no effect was found. This agrees with expectations from theory since for x-rays in the $K$ region virtual transitions from the $K$ shell to the partially filled $d$ levels (ferro-magnetism!) are forbidden, and therefore for this region iron must be treated like a nonferromagnetic substance, and the Faraday effect calculated from the ordinary dispersion formula: $\varphi\sim10^{-50}$.

**23. Crystallization of Polymorphous Substances from the Vapor Phase II.** S. E. Madigan and K. Lark-Horovitz, *Purdue University.*—A method has been developed for the quantitative determination of the constitution of polymorphous mixtures by using monochromatic x-rays and intensity comparisons of coincident lines. This was applied to the investigation of the deposition of ZnS from the vapor phase. It has been found that the amount deposited in the cubic or hexagonal form depends on pressure and temperature conditions. The results show that at high speed of evaporation and in the presence of inert gases the unstable form is always deposited regardless of what support is used: Ostwald's rule of stages. If the evaporation and deposition is conducted at slow rate in a high vacuum, most of the nuclei seem to form at the interface gas-solid as indicated by the prevalence of the hexagonal form on CdS, and ZnO as compared with the deposit of Cu and Zn cubic. Experiments with single crystals of zinc blende split in high vacuum immediately before deposition show that the crystal growth starts from different centers distributed at random over the surface.

**24. Orientation of Liquid Crystals by Heat Conduction.** D. O. HOLLAND AND G. W. STEWART, *University of Iowa.*—One of the authors has previously reported upon an apparently new phenomenon, i.e., a definite effect upon the orientation of liquid crystalline para-azoxyanisol presumably by heat conduction. Former results have now been checked by the density of photographs of the x-ray halo with various vertical alterations in temperature gradients. With a higher temperature at the bottom the convection currents caused a distribution favoring an orientation with "swarm" axes vertical. As the temperature gradient was varied until in the opposite sense the halo first became circumferentially uniform and then indicative of a similar orientation with "swarm" axes horizontal. These results favor the conclusion that the orientation is produced by heat conduction. Perhaps the orientation is caused by the scattering of elastic waves, but this is not certain.

**25. Influence of Temperature of Uranin Solution on the Fluorescence Decay Time.*** WINSTON CRAM,† *University of J. Pilsudski at Warsaw.*—The values of the fluorescence decay time for 8 different uranin solutions were measured when the temperature of the solution was varied from 0°C to 70°C, with the Szymanowski[1] version of the Gaviola fluorometer. It was found that for weak concentrations ($1\times10^{-4}$ g/cm³) in water and ethyl alcohol solutions the fluorescence decay time decreased 25 percent with increase of temperature from 0°C to 30°C. A further increase of temperature, however, caused no further observable change in the decay time. Increase in the concentration of uranin tended to weaken this observed temperature effect. At a concentration of $6\times10^{-3}$ g/cm³ the effect was not observable, within the limits of experimental error (less than 3 percent). The use of more viscous solutions showed that the increase in viscosity also decreased the observed temperature effect. In agreement with Gaviola, no temperature effect was observed for glycerin solutions of any concentration. The temperature effect for all solutions was unchanged when the polarization system for observing the fluorescent light was rotated through 90°. The observed results are not in agreement with the equation of Franck and Wawiłów.[2]

* The more detailed report of this work will be published soon in the Zeits. f. Physik.
† Now at University of Wisconsin.
[1] Szymanowski, Zeits. f. Physik **95**, 466 (1935).
[2] Franck and Wawiłów, Zeits. f. Physik **69**, 100 (1931).

**26. X-Ray Fluorescence Yields.** R. J. STEPHENSON, *University of Chicago.*—The x-ray fluorescence yield for the $K$ shell, that is, the ratio of the number of fluorescence quanta emitted from the $K$ shell of an assemblage of atoms to the number of quanta absorbed in the $K$ shell, has been measured for several elements whose atomic numbers lie between nickel and tin. An ionization method similar to that of Professor Compton's[1] was used. The ionization chamber contained argon under pressure. The ionization current was measured by means of an FP 54 vacuum amplifier. A rotating sector disk was used to reduce the intensity of the incident x-ray beam to a value comparable with that of the excited fluorescence beam. The results show an increase of fluorescence yield with atomic number and give a good agreement with the relativistic quantum-mechanical calculations of Massey and Burhop.[2] The fluorescence yield for the $L_{III}$ shell has been measured for lead, thorium and uranium. In this case the incident radiation used was of such a frequency that photoelectrons from the $L_{III}$ shell were ejected but not those from shells requiring greater energy. An increase in the fluorescence yield with atomic number was found.

[1] Compton, Phil. Mag. VIII, 961 (1929).
[2] Massey and Burhop, Proc. Roy. Soc. **A153**, 661 (1936).

**27. The Zeeman Effect of Tellurium.** J. B. GREEN AND R. A. LORING, *Ohio State University and University of Louisville.*—The Zeeman effect of tellurium has been studied at field strengths of about 36,000 gauss, by using an interrupted arc between powdered tellurium packed in a hollow brass electrode and a copper disk, such as was used in the study of the Zeeman effect of arsenic.[1] About 100 lines have been measured including 4 arc lines, about 20 lines of Te III and one line of Te IV (λ3585), according to the assignments given by L. and E. Bloch.[2] The spectrum of Te II was especially well excited, and the measurements lead to definitive assignment of $j$ and $g$ values in a large number of cases. We are at present engaged in an attempted classification of the spectrum of Te II based on this work.

[1] Green and Barrows, Phys. Rev. **47**, 131 (1935).
[2] L. and E. Bloch, Ann. de Phys. **13**, 233 (1930).

**28. Two New Band Systems of Diatomic Antimony.** G. M. ALMY AND H. A. SCHULTZ, *University of Illinois.*—The spectrum of diatomic antimony has been obtained by heating antimony in an atmosphere of nitrogen in a graphite tube furnace. In addition to the two ultraviolet systems photographed by Naudé, two new systems have been photographed, in absorption at temperatures of 1350–1600°C and in thermal emission at 1550–1750°C. One system extends from 4500 to 6000A and the other from 6000 to 7500A. Both of the systems involve the ground state. The three upper states which have been analyzed show a surprising similarity in vibrational constants. The analysis into two visible systems is supported by the isotope effect. The distributions of intensity are similar to those found for $P_2$ and for $As_2$, having subsidiary Franck-Condon parabolas. In each system bands are observed approximately to $v'=10$ and $v''=10$. The constants for the three states are:

| State | $T_e$(cm$^{-1}$) | | $\omega_e$(cm$^{-1}$) | $x_e\omega_e$(cm$^{-1}$) |
|---|---|---|---|---|
| $X$ | 0 | $(A\leftrightarrow X)$ | 269.7 ±.5 | 0.60 ±.14 |
| | | $(B\leftrightarrow X)$ | 270.0 ±.2 | 0.60 ±.04 |
| $A$ | 14,991.5 | | 217.0 ±.4 | 0.45 ±.08 |
| $B$ | 19,067.9 | | 218.1 ±.4 | 0.52 ±.12 |

Rough extrapolation gives 3.7 volts for the heat of dissociation of the ground state; this value is almost certainly too high.

**29. The Optically Active $CD_4$ Fundamental Bands.** H. H. NIELSEN, *Ohio State University,* AND A. H. NIELSEN, *University of Tennessee.*—The two active fundamental vibration-rotation bands $\nu_3$ and $\nu_4$ in the spectrum of $CD_4$

have been located and their rotational structure studied under high resolving power. The centers of these bands have been determined respectively to be $\nu_3 = 2259.0$ cm$^{-1}$, in good agreement with the value 2258.0 cm$^{-1}$ obtained by MacWood and Urey[1] from Raman spectra, and $\nu_4 = 996$ cm$^{-1}$. The average spacing between rotational lines in $\nu_3$ is about 4.43 cm$^{-1}$. While the rotational lines of $\nu_4$ show a multiplet structure similar to that in the corresponding short frequency bands in the spectra of other tetrahedral molecules it is nevertheless possible, especially on the positive side of the band, to determine what may be called an average spacing between lines. This spacing takes the value 3.2 cm$^{-1}$. It is possible to compute the value of the moment of inertia from the relation $\Sigma\Delta\nu = 3h/8\pi^2 A$ developed by Johnston and Dennison.[2] The value obtained for $A$ is $1.091 \times 10^{-39}$ gm-cm$^2$, or very nearly twice that for ordinary methane. The combination bands $\nu_1+\nu_4$ and $\nu_3+\nu_4$ have not been located, probably because they would lie in the region of the 3.16$\mu$ atmospheric water vapor band.

[1] G. E. MacWood and H. C. Urey, J. Chem. Phys. **4**, 402 (1936).
[2] M. Johnston and D. M. Dennison, Phys. Rev. **48**, 868 (1936).

**30. Constants of $^3\Pi$ States of AlH, OH$^+$, BH.** C. N. Challacombe and G. M. Almy, *University of Illinois.*—The methods of Budo[1] and Gilbert[2] for applying the theory of $^3\Pi$ states between case *a* and case *b*, developed originally by Hill and Van Vleck, and Van Vleck, have been used to determine the molecular constants $B$, $D$, $\lambda$ or $A/B$, for the $^3\Pi$ states of AlH, OH$^+$ and BH. By Gilbert's method, for AlH, $\lambda = 6.02$; for OH$^+$, (0, 0), $\lambda = -6.35$; for BH, $\lambda = 0.47$. The determination of $\lambda$ is greatly facilitated by drawing a set of graphs of $W/B$ *versus* $\lambda$, each graph showing three levels having the same value of $K$($K$-multiplet). If the constant $B$ for any $^3\Pi$ state is approximately known, a value of $\lambda$ is easily read off each graph by fitting the observed $K$-multiplet separations divided by $B$ to the plotted separations. In practice good agreement is found among the values of $\lambda$ obtained from graphs for $K = 2,3,4,5$ for each molecule, and the values of $\lambda$ obtained graphically agreed well in each case with that determined by the much more laborious analytical method. The graphs also aid in analysis of certain bands, as they show clearly the confusing behavior of the $K$-multiplets to be expected at low $K$, for values of $\lambda$ between $+2$ and $+7$, as is found, for example, in the AlH $^3\Sigma \rightarrow {}^3\Pi$ band.

[1] A. Budo, Zeits. f. Physik **96**, 219 (1935).
[2] Cecil Gilbert, Phys. Rev. **48**, 619 (1936).

**31. Field Current Emission from Metals into Gases at High Pressures.** J. B. Adams, J. C. Hubbard and R. T. K. Murray, *Johns Hopkins University.*—By making use of the well-known property that the breakdown gradient of a gas increases with the pressure, sufficient fields have been obtained at the surface of a metal cathode immersed in a gas at high pressures to give field currents of magnitude greater than the background currents due to residual ionization. The apparatus consisted of spherical electrodes placed in a steel chamber into which nitrogen was introduced at pressures up to 110 atmospheres. Steady potentials up to 25 kv were applied to the cathode and the resulting field calculated from the distance between the spheres as measured through a glass window. Curves of log current against reciprocal field were linear in accord with the Fowler-Nordheim equation; the curves were independent of pressure. At a pressure of 110 atmospheres a maximum gradient of 1600 kv/cm was reached without breakdown, the field current at this gradient being of the order of $10^{-8}$ amp. It should be pointed out that in employing high pressures for maintaining high potential gradients between electrodes the degree of insulation is limited not only by the currents due to residual ionization but also by field current emission from the cathode.

**32. Contact Potential between Filaments in Vacuum by Kelvin Method.** A. T. Waterman, *Yale University*, and J. G. Potter, *Armour Institute of Technology.*—Two parallel filaments constitute a condenser whose capacity is varied by vibrating one of the filaments under tension, in order to detect any unbalanced contact potential difference. An alternating current of properly adjusted frequency through this filament, in the presence of an applied magnetic field, causes it to vibrate with a satisfactory amplitude while heating it to any desired temperature above 420°K. The other filament is connected to an audio-frequency amplifier, the circuits being similar to those employed by Zisman[1] in measuring contact potentials between plates in air. Measurement consists in adjusting a measured potential applied to the electrical mid-point of the vibrating filament until the amplifier indicates that the contact potential is completely balanced out. With proper adjustment, disturbance from the applied a.c. is eliminated. The filaments are electrically shielded from external disturbance, appreciable contact P.D. between shield and filaments being compensated. To reduce the tension on the filaments while outgassing and to restore it for vibration, a system of glass levers, bearings, cams and iron armatures, encased in glass, are operated by magnets from outside the tube. Although not to be regarded as final, measurements made to date, employing two tungsten filaments, indicate an increase with temperature in the work function of tungsten of approximately $6 \times 10^{-5}$ volts per degree centigrade.

[1] Zisman, R. S. I. **3**, 367 (1932).

**33. Four Forms of the Copper Arc in Air.** A. S. Fry, *Northwestern University.* (*Introduced by W. S. Huxford.*)—Four distinct and reproducible forms of the copper arc in air at atmospheric pressure have been identified. The following table indicates the main features of each arc form:

| Electrode | Potential* (volts) | Gradient (volts/cm) | Fall near Cathode (volts) | Fall near Anode (volts) |
|---|---|---|---|---|
| 1. Clean Cu | 46 | 52 | 11 | 10 |
| 2. Cold CuO | 41 | 25–31 | 10.5 | 7 |
| 3. Hot CuO | 37 | 25 | 14 | 7 |
| 4. Hot $Cu_2O$ | 34 | 25 | 14.5 | 4 |

* Voltage across 6 ampere arc, electrode separation, 3 mm.

That the controlling gas in the first arc is nitrogen is confirmed by gradient measurements carried out in a pure nitrogen atmosphere. The gradient in arcs (3) and (4) is determined by the presence of copper vapor furnished by thermal decomposition of the oxides. Space potentials were measured by means of a Langmuir probe consisting of a tungsten wire 0.07 mm in diameter. Although the field near the center of the arc column is uniform, a continuously increasing gradient occurs within the space extending from 1 mm to ½ mm from the electrode surfaces. The decrease in anode fall from 10 to 4 volts is accompanied by an increase in potential at the cathode. The lowering of the anode fall is due to several effects which combine to cause a decrease in electron concentration in the anode sheath. The changes in cathode fall are most easily explained on the basis of the field theory of electron emission.

**34. Density of Excited Levels in Heavy Nuclei.** S. GOUDSMIT, *University of Michigan*.—Bethe's calculation of the level spacing of excited nuclei does not explain why some heavy nuclei do not possess resonance levels for slow neutrons. Another method of calculating, closely related to Bethe's, seems to throw some light on this problem. The possible energies for the individual particles are calculated again statistically. Over a certain range these energies may be taken as approximately equidistant with a spacing $\epsilon$. If the excitation of the total nucleus is $Q=n\epsilon$ the level spacing of nondegenerate levels in the neighborhood of $Q$ is given by $\epsilon/\Sigma_\nu p_s(\nu)p_t(n-\nu)$. In this expression $s$ and $t$ are the numbers of neutrons and protons available for the excitation and the symbol $p_s(\nu)$ means "the partition of the integer $\nu$ into parts none of which exceeds $s$." If both $s$ and $t$ are larger than $n$, the result comes out to be identical with that of Bethe. The spacing will be much wider, however, if this condition is not fulfilled. This could happen if nuclei contain shells differing considerably in energy. If the stability of the normal nucleus causes the first excitation energies of the individual particles to be larger than the assumed distance $\epsilon$, the level spacing for the total excitation will also be increased greatly.

**35. On the Matrix Element in the Fermi Theory of β-Decay.** L. W. NORDHEIM, *Purdue University*.—How the many body constitutions of the nuclei have to be taken into account in the theory of β-decay is discussed. It is found to be necessary to make the theory completely symmetrical in all the heavy particles (protons and neutrons). A definite prescription can then be given for computing the matrix element in terms of nuclear eigenfunctions of proper symmetry which differs slightly from what one would expect from elementary considerations. The magnitude of the matrix element will be of the order unity (as hitherto generally assumed for allowed transitions) only if there is just one surplus neutron which goes over into a proton (and *vice versa*) and if the initial and final states of the nucleus contain the same configurations, or corresponding ones if a spin dependent transformation operator is chosen. With the coupling schemes proposed at present the latter case seems to be indicated for light nuclei. If the numbers of neutrons and protons differ by more than one, the matrix element will be smaller, which explains the difference in lifetime for light and heavy β-emitters.

**36. On the Non-Association of Photoconductivity with Optical Absorption in Non-Conducting Crystals.** CLARENCE ZENER, *Washington University, St. Louis, Mo.*—While all the electrical and magnetic properties of a metal may be qualitatively understood by the use solely of Bloch wave functions, it is generally recognized that the strongly peaked absorption spectra of the alkali halides is due to excited atomic states. The perturbation method, which has heretofore been used exclusively, does not give definite information when the perturbations are as large as they are at the actual lattice spacing. Two new methods of approach are here used to study the electrical properties of insulators. Both methods start from the basic property of an insulator, the ability to support an electric field. The first method uses the variation principle to show that in the lowest excited state of an insulator, the negative electron in the excited band is bound to the positive hole in the lower band. The second method solves exactly an idealized model of an insulator crystal with one impurity atom. The excited Bloch energy bands, as viewed by the valence electrons of the impurity atom, have a dip in the region of the impurity ion. Both methods come to the conclusion that in insulators photoconductivity is not associated with the long wave-length edge of the first absorption band.

**37. Magnetic Deflection of HD Molecules.** I. ESTERMANN, O. C. SIMPSON, AND O. STERN, *Carnegie Institute of Technology*.—The magnetic deflection of molecular beams of HD (kindly furnished by Dr. Brickwedde) has been investigated by the same method previously used for $H_2$[1] and $D_2$.[2] The HD differs from $H_2$ and $D_2$ by the absence of molecules with zero moment. This makes the weakening by the magnetic field at the position of the undeflected beam very effective. This weakening is nearly independent of the magnetic moment of the deuteron and of the rotational magnetic moment, but very sensitive to the moment of the proton, much more than in the case of ordinary hydrogen. The influence of the distortion of the Maxwell-distribution has been eliminated by extrapolation to zero pressure. The accuracy of the value for the proton moment is now limited only by the accuracy of the field measurement.

[1] Frisch and Stern, Zeits. f. Physik **85**, 4 (1933); Estermann and Stern, Zeits. f. Physik **85**, 17 (1933).
[2] Estermann and Stern, Zeits. f. Physik **86**, 132 (1933); Phys. Rev. **45**, 761 (1934).

**38. A Stern-Gerlach Magnetic Field as a Velocity Analyzer for Atomic Beams.** ALEXANDER ELLETT AND VICTOR W. COHEN, *State University of Iowa*.—A detailed examination has been made of the deflection pattern of a beam of alkali atoms traversing an inhomogeneous magnetic field with view of determining the constancy of the gradient and the validity of the Maxwell distribution. The displacement of an atom after traversing the field will be

$$s \sim (1/mv^2)\mu(\partial H/\partial s).$$

Consequently if the gradient is constant, $st^2$ will be constant. If one assumes a Maxwell distribution, one can evaluate, through graphical integration of the deflection pattern, the distance which atoms of arbitrary velocity have been deflected. The results with the beam suitably defined show that $sv$ is constant to better than 1 percent. Conversely, if one assumes the gradient to be constant, one may use the formula of Stern[1]

$$I(s)=\frac{I_0}{2}\left[e^{-y}(y+1)\right]_{r_0(s+a)}^{r_0(s-a)}$$

to calculate the intensity distribution in the deflected beam. The results show excellent agreement in form for oven vapor pressures from 0.002 to 0.04 mm Hg and a marked deviation setting in at 0.13 mm.

[1] Stern, Zeits. f. Physik **41**, 563 (1927).

**39. Velocity Analysis of K Atoms Scattered by a MgO Crystal.** VICTOR W. COHEN AND ALEXANDER ELLETT, *State University of Iowa.*—A beam of neutral potassium atoms with approximately thermal velocities characteristic of the temperature of the source is directed toward a MgO crystal. The consequent scattering is adequately described by the cosine law; neither specular reflection nor any evidence of diffraction is observed. Those atoms scattered at right angles to the initial direction are passed through the magnetic analyzer described in the preceding paper. The results show that within the limits of error the velocity distribution is Maxwellian and characteristic of the temperature of the crystal. That is, the accommodation coefficient is almost unity. In the course of the experiment the source was maintained at a temperature of about 615°K, while the crystal temperature was varied from 440 to 800°K. The process is, therefore, probably one of adsorption and reevaporation, with the adsorbed atoms attaining thermal equilibrium with the crystal surface. The MgO crystals used in this work were furnished through the courtesy of the Norton Co. of Worcester, Mass.

**40. An Elementary Constant of Energy.** ARTHUR HAAS, *University of Notre Dame.*—The red-shift exhibited by extra-galactic nebulae can be described by the formula (1) $\Delta\nu/\nu=T/T^*$ where $\Delta\nu$ means the diminution of the frequency of a photon in a time $T$, whereas $T^*$ means a period of 1700 million years. Therefore (2) $1/T^*=1.8\times10^{-17}$ sec.$^{-1}$. The product of the elementary quantum of action ($h$) and $1/T^*$ represents a universal constant of the dimensions of energy. We find for this constant, which might be called the primordial energy-element, (3) $w=1.2\times10^{-43}$ erg. If we denote the energy of the photon ($h\nu$) by $\epsilon$, we may write Eq. (1) in the form (4) $\Delta\epsilon=wvT$. This means that every photon, independently of its wave-length, gives off a primordial energy element during each oscillation or in traveling one wave-length. There is in the universe, on the average, a quantity of radiant energy of about $3\times10^{15}$ ergs, referred to one gram of matter.[1] The loss in radiant energy which is the consequence of the continual output of primordial energy elements would, therefore, be $3\times10^{15}\times1.8\times10^{-17}$ or about 0.1 erg per gram and sec. On the other hand, the energy produced by the stars and star-systems amounts also to about 0.1 erg per gram and sec.[1] The energy which is given off in the form of primordial energy elements might, therefore, be compensated by the energy production of the stars.

[1] Cf. A. Haas, *Die kosmologischen Probleme der Physik* (Akademische Verlagsgesellschaft, Leipzig, 1934).

**41. Helium I Like Spectra.** HOWARD A. ROBINSON, *Ohio State University.*—Measurements of the $1s^2\,{}^1S_0-1snp\,{}^1P_1$ series of the spectra He I, Li II, Be III, B IV, C V, N VI and O VII carried out on the new 5 meter grazing incidence spectrograph in Professor Siegbahn's Laboratory in Uppsala, Sweden, allow of accurate evaluations of the several ground states of these spectra. The Hylleraas extrapolation formula, changed slightly to include new calculations for Li II made by Mr. H. A. S. Eriksson of Uppsala, show remarkable agreement with these results when spin and relativity corrections are made. A small discrepancy appears in the case of Li II. This discrepancy undoubtedly arises from the approximate method of calculation of the final corrections.

## AUTHOR INDEX TO ABSTRACTS OF CHICAGO MEETING

**Adams, J. B., J. C. Hubbard and R. T. K. Murray**—No. 31
**Allen, James S.**—No. 10
**Allison, Samuel K., Graham T. Hatch and Lester S. Skaggs**—No. 4
**Almy, G. M.**—see Challacombe
——— **and H. A. Schultz**—No. 28

**Bruce, W. A.**—see Foster
——— — see Jauncey

**Challacombe, C. N. and G. N. Almy**—No. 30
**Clark, H. T. and K. Lark-Horovitz**—No. 22
**Collins, G. B., R. Schager and A. L. Vitter**—No. 3
**Cohen, Victor W.**—see Ellett
——— **and Alexander Ellett**—No. 39
**Compton, Arthur H.**—No. 13
**Cork, J. M. and R. L. Thornton**—No. 9
**Cram, Winston**—No. 25
**Crane, H. R.**—see Gaerttner
——— — No. 6

**Davey, Wheeler P.**—see McLachlan

**Ellett, Alexander**—see Cohen
——— **and Victor W. Cohen**—No. 38
**Estermann, I., O. C. Simpson and O. Stern**—No. 37

**Flodin, George E.**—see Hoag
**Foster, E. S. Jr., G. E. M. Jauncey and W. A. Bruce**—No. 20
**Fry, A. S.**—No. 33

**Gaerttner, E. R. and H. R. Crane**—No. 8
**Goudsmit, S.**—No. 34
**Green, J. B. and R. A. Loring**—No. 27
**Green, G. K.**—See Kruger
———**and P. Gerald Kruger**—No. 2

**Haas, Arthur**—No. 40
**Hatch, Graham**—see Allison
**Haworth, L. J. and L. D. P. King**—No. 11
**Herb, R. G., H. B. Parkinson and D. W. Kerst**—No. 5
———, **D. W. Kerst and J. L. McKibben**—No. 12
**Hoag, J. Barton**—see Murray
——— **and George E. Flodin**—No. 16
**Holland, D. O. and G. W. Stewart**—No. 24
**Hubbard, J. C.**—see Adams
**Hume, O. F.**—see Hummell
**Hummell, A. D. and O. F. Hume**—No. 18

**Jauncey, G. E. M.**—see Foster
——— **and W. A. Bruce**—No. 19

**Keen, C. E.**—No. 14
**Kerst, D. W.**—see Herb
**King, L. D. P.**—see Haworth
**Kruger, P. Gerald**—see Green
——— **and G. K. Green**—No. 1

**Lark-Horovitz, K.**—see Clark
——— — see Madigan
——— — see Miller
**Loring, R. A.**—see Green

**McKibben, J. L.**—see Herb
**McLachlan, D., Jr., and Wheeler P. Davey**—No. 17

**Madigan, S. E. and K. Lark-Horovitz**—No. 23
**Miller, E. P. and K. Lark-Horovitz**—No. 21
**Murray, F. H. and J. Barton Hoag**—No. 15
**Murray, R. T. K.**—see Adams

**Nielsen, A. H.**—see Nielsen
**Nielsen, H. H. and A. H. Nielsen**—No. 29
**Nordheim, C. W.**—No. 35

**Parkinson, H. B.**—see Herb
**Potter, J. C.**—see Waterman

**Robinson, Howard A.**—No. 41

**Schager, R.**—see Collins
**Schultz, H. A.**—see Almy
**Shaw, A. W.**—No. 7
**Simpson, O. C.**—see Estermann
**Skaggs, Lester S.**—see Allison
**Stephenson, R. J.**—No. 26
**Stern, O.**—see Estermann
**Stewart, G. W.**—see Holland

**Thornton, R. L.**—see Cork

**Vitter, A. L.**—see Collins

**Waterman, A. T. and J. G. Potter**—No. 32

**Zener, Clarence**—No. 36

THE
PHYSICAL REVIEW
*A Journal of Experimental and Theoretical Physics Established by E. L. Nichols in 1893*
VOL. 51, NO. 2 JANUARY 15, 1937 SECOND SERIES

# Electric and Magnetic Focusing in Mass Spectroscopy

A. J. DEMPSTER
*University of Chicago, Chicago, Illinois*
(Received October 7, 1936)

The theory of a mass spectrograph is described. The instrument is arranged so that an electric field forms near the entrance to the magnetic field a real image of the entrance slit with rays of one velocity. The velocity dispersion produced by the electric field is counterbalanced by the velocity dispersion in the magnetic field.

IN mass spectrographs of high resolving power, great advantages are obtained by focusing a beam of charged atoms which not only diverges in direction but also contains particles with slightly different velocities. If focusing methods are not used, the selection of a sufficiently narrow bundle and a sufficiently restricted velocity range implies a very great loss of intensity.

In this paper the theory of one type of mass spectrograph is discussed in which an electric field forms a real image of the entrance slit with rays of one velocity near the entrance to a magnetic field, and in which the velocity dispersion produced by the electric field is counterbalanced by the velocity dispersion in the magnetic field.

## CHARGED PARTICLES IN A CYLINDRICAL CONDENSER

Let us consider a charged particle passing from the slit $S$ (Fig. 1) into an electric field at a distance $l'$ from $S$, and at a radial distance $y_1$ from the circular orbit $AB$ to which $SA$ is tangent at $A$. If the field is due to a potential $V$ applied to two cylinders of radius $r_1$ and $r_2$, its value at any radius $r$ is $c/r$ where $c=\log_e r_2/r_1$. Let $v_0$ be the velocity required for the circular orbit of radius $a$ ($v_0^2(m/a)=c(e/a)$; $v_0^2=(e/m)c$), and consider a particle with a velocity $v_1=v_0(1+\beta)$, making an angle $\alpha$ with $SA$ and entering the condenser at $y_1$ ($y_1=\alpha l'$). Here its energy $\frac{1}{2}mv^2$ is less than $\frac{1}{2}mv_1^2$ by the work done in moving the particle through a distance $y_1$ against the electric force. This potential energy is $y_1e(c/a)$ or $mv_0^2(y_1/a)$ so that $\frac{1}{2}mv^2=\frac{1}{2}mv_0^2(1+2\beta)-mv_0^2(y_1/a)$ or $v=v_0(1+\beta-(y_1/a))$.

The orbit has been calculated by R. Herzog[1] as a special case of a general theory in which electric and magnetic fields both act on the particle. The calculations may be considerably shortened if the equations of motion in polar coordinates $d^2r/dt^2-r(d\phi/dt)^2=-k^2/r$, where $k^2=(m/e)\times c=(m/e)\log_e r_2/r_1$ and $r^2d\phi/dt=A$ where $A$ is a constant for each orbit, are transformed into an equation between $1/r$ and $\phi$.[2] Setting $u=1/r$ we have $dr/dt=(-1/u^2)(du/d\phi)(d\phi/dt)=-A(du/d\phi)$ and $(d^2r/dt^2)=-A(d/dt)du/d\phi=-Au^2(d^2u/d\phi^2)$, so that the equation of motion is $(d^2u/d\phi^2)+u=(k^2/A^2)(1/u)$. We are interested in small devia-

[1] R. Herzog, Zeits. f. Physik **89**, 447–473 (1934).
[2] The author is indebted to Professor W. Bartky for pointing out the advantages of this transformation in this problem. The resulting equation was also used by Hughes and Rojansky (reference 3) for different initial conditions.

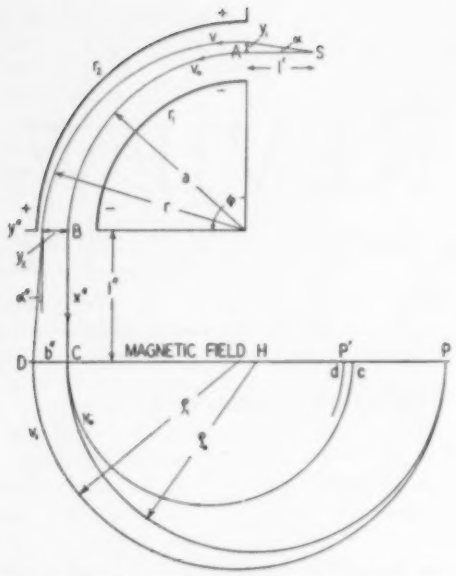


FIG. 1. Paths of ions in electric and magnetic fields.

tions from the circular orbit $u=1/a$ for which $A=ka=av_0$. For the general orbit discussed above $A=(a+y)^2\dot{\phi}=(a+y_1)v=av_0(1+\beta)$.

Setting $u=1/a(1+z)$, where $z$ is small, we have the following equation for $z$, $d^2z/d\phi^2=-2z-2\beta$, which gives $z=-\beta+P\cos\sqrt{2}\phi+Q\sin\sqrt{2}\phi$. One initial condition $\phi=0$, $u_0=1/a(1-(y_1/a))$ gives $P=-(y_1/a)+\beta$ and the other

$$\left.\frac{du}{d\phi}\right|_0=\frac{-1}{r^2}\frac{dr}{dt}\cdot\frac{dt}{d\phi}\Big|_0=\frac{-1}{A}\left.\frac{dr}{dt}\right|_0=-\frac{\alpha}{v_0}$$

gives $Q=-(\alpha/\sqrt{2})$, so that to a first approximation, the equation of the orbit in the electric field is $u=1/r=1/a\{1-\beta+(\beta-(y_1/a))\cos\sqrt{2}\phi-(\alpha/\sqrt{2})\sin\sqrt{2}\phi\}$. The special case discussed by Hughes and Rojansky[3] may be deduced by putting $y_1=0$, i.e. $l'=0$; then $r=a$ for $\phi=0$ and $\phi=\pi/\sqrt{2}$ showing that a divergent beam at $\phi=0$ is brought to a focus at $\phi=127°$.

We are interested in the more general case in which $l'\neq 0$ and in which the rays after being deviated through an angle $\phi$ leave the electric field and come to a focus at a distance $l''$. At the angle $\phi$,

$$r=a+y_2=a\{1+(\alpha/2)\sin\sqrt{2}\phi+\beta(1-\cos\phi)+(y_1/a)\cos\sqrt{2}\phi\}$$

and the angle $\alpha''$ with the tangent $BC$ to the circular orbit is given by $\alpha''=(1/a)dr/d\phi|_\phi=\alpha\cos\sqrt{2}\phi+\sqrt{2}(\beta-(y_1/a))\sin\sqrt{2}\phi$. In rectilinear coordinates, with the axis $x''$ in the direction $BC$ and the $y''$ coordinate at right angles, the equation of the path is $y''=y_2+\alpha''x''$. Putting $y_1=\alpha l'$, and substituting the values of $y_2$ and $\alpha''$ and collecting terms,

$$y''=\alpha\{l'\cos\sqrt{2}\phi+(\alpha/\sqrt{2})\sin\sqrt{2}\phi+x''(\cos\sqrt{2}\phi-\sqrt{2}(l'/a)\sin\sqrt{2}\phi)\}+\beta a\{1-\cos\sqrt{2}\phi+(x''/a)\sqrt{2}\sin\sqrt{2}\phi\}.$$

At a value of $x''=l''$ which makes the first bracket zero, the value of $y''$ is independent of the angle $\alpha$ at which the rays originally entered the condenser. A divergent bundle of one velocity is therefore brought to a focus at $l''$. The relation between $l'$ and $l''$ for which this occurs is:

$$(l'+l'')\cos\sqrt{2}\phi+(a/\sqrt{2})\sin\sqrt{2}\phi-(\sqrt{2}/a)l'l''\sin\sqrt{2}\phi=0$$

or $l'l''-(l'+l'')(a/\sqrt{2})\cot\sqrt{2}\phi-(a^2/2)=0$, as deduced by Herzog (Eq. (25)). This may be written $(l'-g)(l''-g)=f^2$, where $f=(a/\sqrt{2})\times(1/\sin\sqrt{2}\phi)$, $g=(a/\sqrt{2})\cot\sqrt{2}\phi$, in analogy with the formulae of geometrical optics.

The velocity dispersion is given by the second bracket in the above equation for the path after leaving the condenser. At $x''=l''$ let the value of $y''$ be $b''$. Then

$$b''=\beta a\{1-\cos\sqrt{2}\phi+(l''/a)\sqrt{2}\sin\sqrt{2}\phi\}=a\beta\{1+(l''-g)1/f\}=a\beta\{1+f/(l'-g)\}\quad\text{(Herzog, Eq. (34)).}$$

## Focusing Condition

For the paths of charged particles in a magnetic field analogous expressions may be deduced for the corresponding distances $l'$ and $l''$ (See Herzog, reference 1, p. 459). However in the mass spectrograph to which the present paper refers very simple relations hold, as the angle of deviation is 180°, and both $l'$ and $l''$ are zero. With these semicircular orbits two velocities $v_0$ and $v_1=v_0(1+\beta)$ will unite[4] at $P$ (Fig. 1) if they enter the field $H$ at two points $C$ and $D$ where $PC=2\rho_0=2mv_0/eH$ and $PD=2\rho_1=2mv_1/eH$ so that $DC=2\beta\rho_0$. If the velocity dispersion produced by the electric field is equal to $CD$, that

[3] A. L. Hughes and V. Rojansky, Phys. Rev. **34**, 284 (1929).

[4] A. J. Dempster, Phys. Rev. **20**, 638 (1922).

is if $2\rho_0 = a(1+f/(l'-g))$, the rays of different velocity will enter the magnetic field at the proper points to be united at $P$. In this way the velocity dispersion produced by the electric field is counterbalanced by the dispersion in the magnetic field, and a divergent beam entering at $S$ containing particles of slightly different velocities is brought to a focus at $P$. For example, if $a = 8.48$ cm, $\phi = 90°$, and $l' = 1$ cm, then $f = 7.55$ cm, $g = -4.57$ cm and $\rho_0$ must be 10 cm giving $l'' = 5.66$ cm.

This focusing condition can be filled exactly only by one radius of curvature $\rho_0$. If different ions of the same energy are used, the curvature in the electrostatic field will be the same for all, but in the magnetic field the paths will have different radii of curvature. For ions that do not follow the path for perfect focus, the image width $dc$ increases with their distance from $P$. A simple geometrical computation shows that $dc/DC = PP'/PC$. Thus with a diaphragm at $C$ of 2 mm opening the image width of an infinitely narrow slit would be increased to 0.1 mm at a distance of 1 cm from $P$. For the qualitative analysis of elements this widening of the image is not disturbing, and for exact comparisons of atomic weights by the method of doublets, the doublets may be always brought to the position of exact focus.

The observations made with an apparatus constructed on these principles will be described in a later paper.

---

JANUARY 15, 1937 PHYSICAL REVIEW VOLUME 51

# Electron and Negative Ion Mobilities in Oxygen, Air, Nitrous Oxide and Ammonia

RUSSELL A. NIELSEN AND NORRIS E. BRADBURY
*Department of Physics, Stanford University, California*

(Received November 13, 1936)

The electrical shutter method for measuring electron mobilities in gases has been extended to include experiments in oxygen, air, nitrous oxide and ammonia. The experimental data support the hypothesis that collisions of low energy electrons with molecules of these gases may be inelastic. Such collisions cause excitation of vibrational levels, electronic levels, or dissociation of the molecule. The results are compared with experiments reported elsewhere on negative ion formation in these gases. In general the onset of negative ion formation is accompanied by inelastic collisions which result in a marked increase in the electron drift velocity. Negative ion mobilities in these gases have been measured in the same apparatus by an adaptation of the Rutherford alternating current method. The ions were formed by electron attachment in an auxiliary field and their mobility determined at various ages. The probable character of the ions is discussed after comparing the experimental results with those predicted by the Langevin theory.

## A. ELECTRON MOBILITIES

AN electrical shutter method for measuring the drift velocities of electrons in gases has been described in previous communications.[1, 2] The results heretofore obtained have been restricted to gases in which the electrons remained free. By working at somewhat reduced pressures, however, it is possible to extend the method to take data in gases in which negative ions are formed by electron attachment. Under these circumstances there appears a negative ion background current upon which is superimposed the electron current to be measured. For gases in which the probability of electron attachment at a collision is of the order of $10^{-4}$ to $10^{-6}$, the background current can be reduced sufficiently to permit accurate measurement of the electron current maxima by restricting the pressure to values between 2 and 10 mm. In the present experiments the electrons were emitted from a photoelectric surface in the same apparatus employed in the measurements on hydrogen[1] using, however, the constant potential and varying frequency method of measurement.[2]

[1] N. E. Bradbury and R. A. Nielsen, Phys. Rev. **49**, 388 (1936).
[2] R. A. Nielsen, Phys. Rev. **50**, 950 (1936).

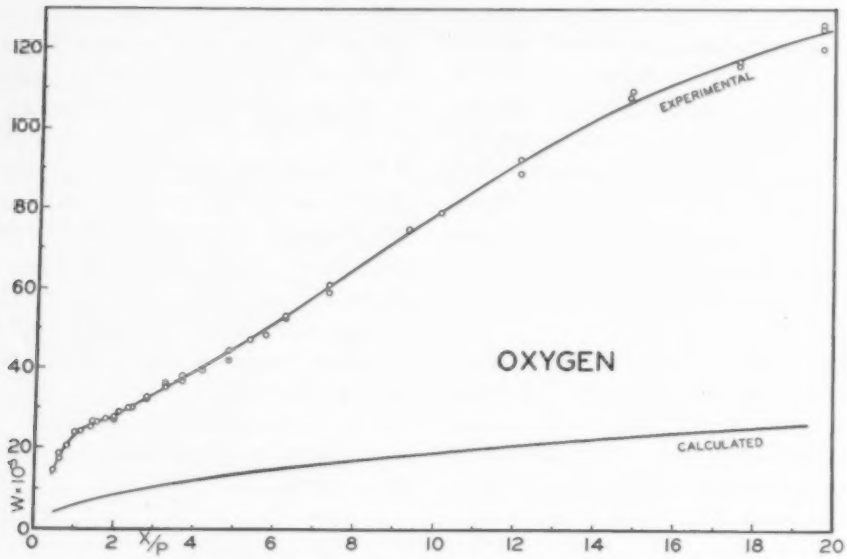


FIG. 1. Electron drift velocity in oxygen as a function of $X/p$.

**Oxygen**

Oxygen was obtained from a commercial tank of the gas and all condensable impurities were removed by passage through traps immersed in liquid nitrogen. The experimental data are reproduced in Fig. 1, together with a curve calculated on the basis of Brüche's[3] values for the collision cross section and Townsend and Bailey's[4] values for the mean energy of the electrons. It is seen that the experimental values are considerably greater than the theoretical and, as in the case of hydrogen and nitrogen, this may be ascribed to the presence of inelastic collisions. For values of $X/p<2$, where the average electron energy is less than one volt, these inelastic collisions occur in the excitation of vibrational levels. At an $X/p$ of about 2, a marked point of inflection is observed in the experimental curve. This is undoubtedly due to the increased possibility of excitation of the $^1\Sigma$ state of $O_2$ whose energy is 1.62 volts above the ground state. Electrons of this energy are available in consequence of their distribution about their mean energy of one volt. Support for this hypothesis is to be found in the experiments on negative ion formation in oxygen.[5] The probability of electron attachment at a collision in this gas, at first decreases with $X/p$ and then undergoes a rapid rise beginning at approximately an $X/p$ of 2. This rise as well as the increase in drift velocity at this point may be ascribed to the increase in number of low energy electrons following collisions in which the $^1\Sigma$ state is excited.

**Air**

Samples of air employed in these measurements were purified by passage through traps immersed in liquid air. The experimental results are shown in Fig. 2. It is of interest to note that Blanc's law[6] is obeyed for the drift velocity of electrons in air inasmuch as values calculated from the experimental drift velocities in nitrogen and oxygen agree closely with those found experimentally. This is, of course, true only in this instance because the mean energy as a function of $X/p$ as well as the distribution function of electron velocities, appear to be nearly the same for the two gases. The strong inflection at $X/p=2$ in oxygen may also be noticed in the curve for air.

**Nitrous oxide**

Nitrous oxide was obtained from a commercial cylinder of the gas stated to be of high purity.

[3] E. Brüche, Ergeb. d. exakt. Naturwiss. **8**, 185 (1929).
[4] J. S. Townsend and V. A. Bailey, Phil. Mag. **42**, 873 (1921).
[5] N. E. Bradbury, Phys. Rev. **44**, 883 (1933).
[6] L. B. Loeb, Phys. Rev. **32**, 81 (1928).

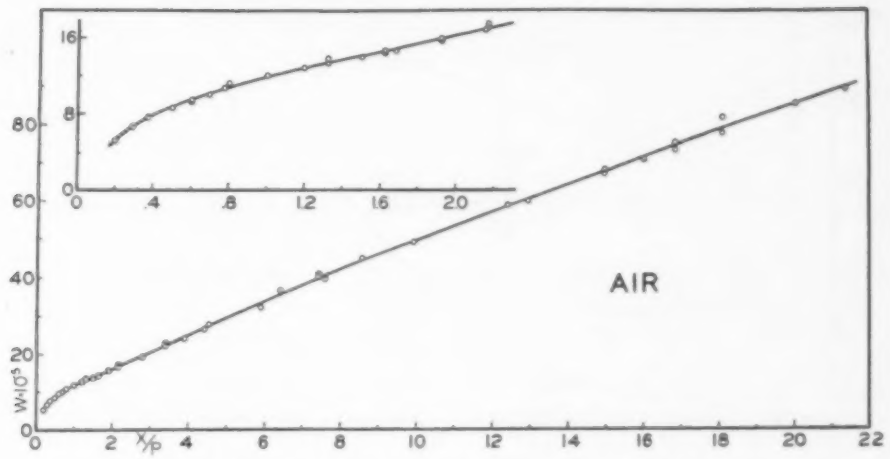


FIG. 2. Electron drift velocity in air as a function of $X/p$.

The gas was subjected to fractional distillation at reduced pressure at liquid-air temperatures, and the middle fractions only retained for use. The experimental data are presented in Fig. 3. While measurements have been made of the cross section of $N_2O$ as a function of electron energy,[7] the results do not extend to sufficiently low energies to permit the calculation of a theoretical curve. It is of interest to compare the curve of Fig. 3 with what is known of negative ion formation in this gas.[8] Negative ions are not formed in $N_2O$ by low energy electrons. At an $X/p$ of 2, however, negative ions begin to appear which are ascribed to the dissociation reaction

$$N_2O+e\rightarrow N_2+O^-.$$

It is thus not surprising to find evidence of the dissociation in the drift velocity curve where it takes the form of an increasingly rapid rise at an $X/p\sim 0.6$.

**Ammonia**

Ammonia was obtained from a commercial cylinder of the anhydrous gas. The gas was liquefied over metallic sodium and fractionated at low pressure with liquid air and solid $CO_2$. The experimental data are shown in Fig. 4. At $X/p\sim 8$, a rapid increase in drift velocity is observed. This is without doubt to be ascribed to the same process which causes the onset of negative ion formation[9] in this gas at approximately this same value of $X/p$. This process has been suggested to be one of dissociation of $NH_3$ by electron impact with the initial formation of $NH^-$. The behavior of the drift velocity at lower values of $X/p$ is remarkable for its linearity. Inasmuch as the variation of drift velocity with $X/p$ for constant cross section and in the absence of inelastic collisions, is as $(X/p)^{\frac{1}{2}}$, this must mean a cross section for collision in $NH_3$ which increases at least as rapidly as the inverse square root of the electron energy.

## B. Negative Ion Mobilities

In order to measure negative ion mobilities, the electrical connections to the experimental apparatus were changed so as to permit the use of

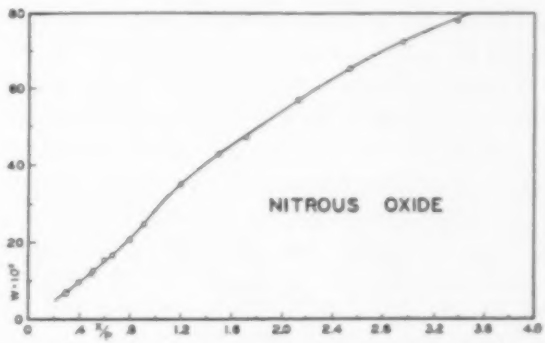


FIG. 3. Electron drift velocity in nitrous oxide as a function of $X/p$.

[7] V. A. Bailey and J. B. Rudd, Phil. Mag. **14**, 1033 (1932).

[8] N. E. Bradbury and H. E. Tatel, J. Chem. Phys. **2**, 835 (1934).

[9] N. E. Bradbury, J. Chem. Phys. **2**, 827 (1934).

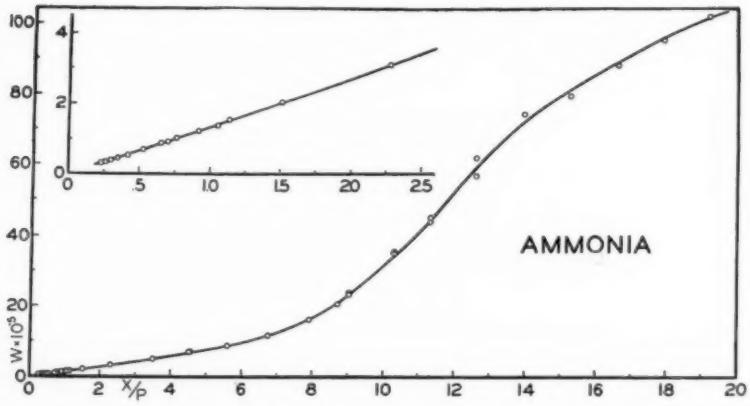


FIG. 4. Electron drift velocity in ammonia as a function of $X/p$.

the Franck and Pohl modification of the Rutherford alternating current method.[10] This was done in the following way: a steady auxiliary field was applied between the emitting surface and the lower grid which was of sufficient strength to insure the formation of negative ions in $NH_3$ and $N_2O$. Between alternate wires of this grid was maintained a high frequency alternating field, the magnitude of whose potential was sufficiently high to sweep from the current stream all electrons, but to permit the passage of negative ions. A square wave alternating potential was applied between this grid and the collecting electrode. This square wave was produced by commutation and had a variable frequency between 20 and 400 cycles/second. The second grid had no function, and was kept at a potential appropriate to its position in the field by connecting it to the surrounding guard ring. The wave form and frequency were determined by a cathode-ray oscillograph permanently connected to the apparatus.

The precautions to be observed in the use of this method have been pointed out by Loeb.[11] In particular, if the strength of the auxiliary field in which the ions are formed is not equal to that of the measuring field, interpenetration of fields will result, and the distance actually traveled by the ions in the measured time will not be the distance between the grid and the collector. Accordingly, the higher the ratio of auxiliary to main field, the shorter the effective distance, and therefore the greater the *apparent* mobility. For this reason, measurements of the mobility must be made as a function of the ratio $R=F_a/F_m$, where $F_a$ and $F_m$ refer to the auxiliary and the main field strength, respectively. The actual value of the mobility is then obtained by extrapolation to unity. It may be pointed out that in the experiments reported here, the distance between grid and collector was 80 mm and the grid spacing 1 mm. The use of such a relatively long distance tends to decrease the effect of field interpenetration on the measured value of the mobility.

The character of the experimental data obtained is shown in Fig. 5 in which the current is plotted as a function of frequency. Although the intercept of the current curve with the axis is not perfectly sharp, the extrapolation of the curve to the axis may be carried out with difficulty and is theoretically justified by the form of the current curve. The mobility may then be calculated from the expression $k=d^2/VT$, where $V$ is the potential carrying ions across the field, $d$ the distance through which the ions move, and $T$ the time of application of $V$. The mobility may then be reduced to standard conditions by the expression $k_{20°}=k(p/760)(293/T)$.

As, expected, the experimental values of $k$ are dependent upon the ratio $R$ of the field strengths on both sides of the grid. The values of the mobility obtained in oxygen as a function of $R$ are plotted in Fig. 6. The variation is seen to be

[10] Franck and Pohl, Ver. der Deut. Phys. Ges. **9**, 69 (1907).
[11] L. B. Loeb, J. Frank. Inst. **196**, 771 (1923).

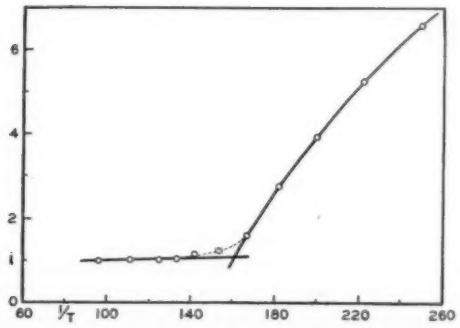


FIG. 5. Electrometer current as a function of the frequency of the square wave alternating potential.

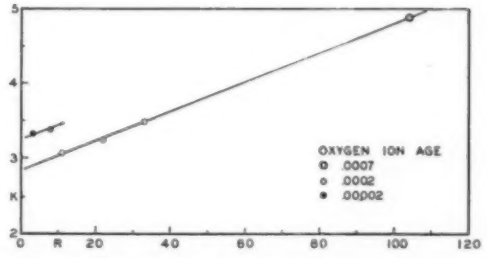


FIG. 6. Mobility of negative ions in oxygen as a function of the ratio of auxiliary to main field strength.

linear and may be extrapolated to $R=1$ to obtain the true value of the mobility. Actually, since the mobility of the ion may vary with its age, this procedure must be justified. In $O_2$, ions of the same age were measured with $R$ varying from 10 to 40. It will be noticed that these lie on a straight line which may be extrapolated to $R=1$ as well as to higher values. It will also be noticed that the point for $R=104$ lies on this line, although this ion is considerably older. Furthermore, points below $R=10$ which correspond to very short ion ages also lie upon a straight line whose slope is substantially the same as the first. From this data alone, however, it cannot be said that the actual variation of $k$ with $R$ is linear from $40<R<100$, for within this age range a decrease in mobility with age may occur. In these experiments, in general, an increase in $R$ may be associated with an increase in the age of the ion. If the mobility of the negative ion in oxygen remained approximately constant between the ages 0.0002 to 0.0007 second, corresponding to $20<R<104$, then the linear extrapolation to high $R$ is obviously justified. If, however, at the *oldest* age ($R=104$) the true mobility has decreased below that corresponding to $R\sim20$, the actual mobility *vs.* $R$ curve must be concave upwards. In the particular case of negative ions in air the ion of shortest age corresponds to the highest value of $R$. If the extrapolated curve deviated from linearity by being only very slightly concave upwards, one would be led to a value for the mobility of the negative ion in *air* which *increases* with age. Inasmuch as such a behavior is contrary to all previous experience, linear extrapolation in the reduction of data taken by this method seems justified.

**Oxygen**

The experimental results for the mobility of the negative ion in $O_2$ are presented in Fig. 7. The mobility is seen to be a function of ion age with a value of 3.3 cm²/volt sec. for the fastest ion, and to decrease with age to a value of 2.85 for the oldest ion measured. In order to provide a uniform age scale, which can be compared with other experiments, the actual ion ages in the gas at the pressure of the experiment have been recomputed to ages corresponding to atmospheric pressure and 20°C. The values for $k$ obtained in this experiment are much higher than those ordinarily given, and undoubtedly do not refer to the so-called "normal" mobility in this gas. However, ions with a mobility greater than the "normal" have been reported by one of the authors,[12] who found that in oxygen of high purity but at atmospheric pressure and ion ages of 0.05″, a transient mobility of 2.65 was observed which shortly decreased to 2.47 and lower. The older ion in the present experiments probably corresponds to an earlier phase of the 2.65 mobility ion previously reported. The meaning of these values with regard to the character of the ion will be considered separately

**Air**

The results for the mobility of the negative ion in air are presented in Fig. 7. Due to the low coefficient at attachment in this gas it was impossible to obtain sufficient ion currents under conditions which simultaneously gave short ion ages. Consequently the fastest ion observed had a mobility of 2.8 which appeared to decrease

[12] N. E. Bradbury, Phys. Rev. **40**, 508 (1932).

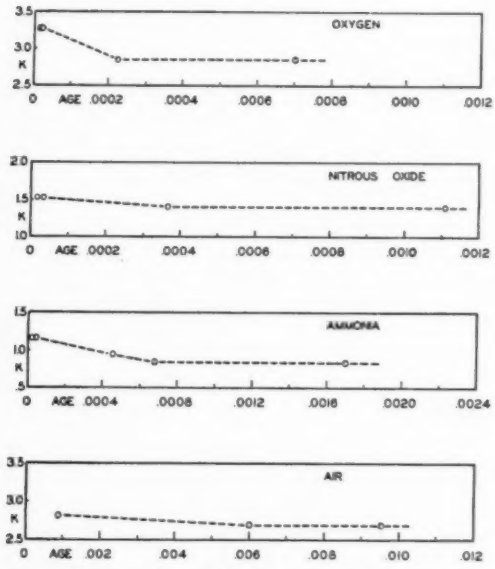


FIG. 7. Negative ion mobilities in oxygen, nitrous oxide, ammonia, and air, as a function of ion age, in seconds.

slowly with age up to 0.01″. This ion is probably of the same character as the ion of similar mobility and age in $O_2$ since it is known that nitrogen molecules do not attach electrons.

### Nitrous oxide

The mobility of negative ions in $N_2O$ are presented in Fig. 7. Since negative ions in this gas are apparently not formed by direct attachment, the ions measured were those formed in an auxiliary field with $X/p>2$. It is seen that the mobility decreases with age from a value of 1.5 to 1.4. This older value is almost exactly the same as that obtained by Loeb.[13]

### Ammonia

The mobility of negative ions in $NH_3$ decrease rapidly with age for short ages, dropping from a value of 1.15 to 0.85 in less than 0.001 second. The value for the older ion is in good agreement with that of 0.87 given by Loeb.[14]

## Discussion of Results

Various theories have been presented giving the dependence of ion mobility upon the physical constants of the ion and the gas through which it moves. The Langevin[15] theory assumes hard spherical ions of diameter $\sigma$, which experience an inverse 5th power law of attraction with neutral molecules resulting from dielectric forces. Hassé and Cook[16] have presented a theory which supposes an inverse 5th power law of attraction superimposed upon the dielectric forces together with an inverse 9th power law of repulsion. This latter equation does not require the use of an ion-molecule collision radius. However, since the coefficients of the inverse powers are not known with accuracy, and furthermore, since calculations by the two theories lead to substantially the same results, the Langevin theory will be used in this discussion. This theory has been used very successfully by Powell and Brata[17] to explain the mobility of positive alkali ions in the rare gases.

The Langevin theory gives the mobility to be of the form

$$k=\frac{A}{[\rho(D-1)]^{\frac{1}{2}}}\left(\frac{m+M}{M}\right)^{\frac{1}{2}},$$

where $M$ is the mass of the ion, $m$ the mass of the gas molecule, $\rho$ the gas density, and $D$ the dielectric constant of the gas, $A$ is a function of a quantity $\lambda$ where

$$\lambda^2=(8\pi p\sigma^4)/((D-1)e^2),$$

in which $p$ is the pressure, $\sigma$ the sum of the radii of ion and molecule, and $e$ the electronic charge. $A$ as a function of $\lambda$ may be obtained from a table given by Hassé.[18] The values of $\sigma$ used in these calculations will be those taken from viscosity measurements.

If values are substituted in the above equation corresponding to a *monomolecular* ion in $O_2$ using the value of $\sigma$ given by Jeans[19] of $3.6\times10^{-8}$ cm, one obtains a value of 3.46 for the mobility at 20°C. This corresponds remarkably well with the experimental value of 3.3 and serves to suggest the hypothesis that the *ion actually measured at these short times is* $O_2^-$. If, instead of the ion

[13] L. B. Loeb, Phil. Mag. **43**, 229 (1922).
[14] L. B. Loeb, Proc. Nat. Acad. Sci. **12**, 617 (1926).
[15] W. P. Langevin, Ann. chim. phys. **8**, 238 (1905).
[16] H. R. Hassé and W. R. Cook, Phil. Mag. **12**, 554 (1931).
[17] C. F. Powell and L. Brata, Proc. Roy. Soc. **A138**, 117 (1932).
[18] H. R. Hassé, Phil. Mag. **1**, 139 (1926).
[19] J. H. Jeans, *Dynamical Theory of Gases* (Cambridge University Press, London, 1925), p. 327.

$O_2^-$, the mass and approximate radius corresponding to a bimolecular oxygen ion is substituted, the value of 2.94 is obtained for the mobility. In this calculation, the value of $A$ is relatively insensitive to changes in $\sigma$ and the factor $((m+M)/M)^{\frac{1}{2}}$ plays the important role. The relative difference between this value and that calculated for a monomolecular ion is nearly the same difference as observed experimentally. Thus it is suggested from this data that within the first $2\times10^{-4}$ second, *the addition product to the initial monomolecular negative ion in $O_2$ is a molecule whose molecular weight is between 15 and 35.* This suggests either $H_2O$ or $O_2$. Subsequent ions have lower mobilities due either to the attachment of further molecules of impurity or the transfer of charge to some bulky impurity molecule inevitably present in the most stringently purified gas. Under such circumstances the factor $A$ plays an increasingly important role, and the mass factor a lesser one.

Similar calculations may be carried out for air. If an ion be assumed of the same mass and radius which leads to a value of 2.94 in $O_2$, a value of 2.88 is obtained for the mobility of such an ion in air. This is slightly lower than its mobility in $O_2$ and is in accord with the experimental results of 2.85 in $O_2$ compared to 2.8 in air. It is therefore suggested that the same ion was observed in both cases, and that the failure to observe a faster ion in air was due to the greater ion ages studied.

In $N_2O$ the original ion formed may be $O^-$. Assuming this to be so, the calculated value for the mobility is 2.73. This is much higher than the experimental value for the shortest ion ages measured, and therefore such an ion must lose its identity within $10^{-5}$ second. Using the molecular weight corresponding to the ion $(NO)_2^-$, a value for the mobility of 1.85 is obtained. It must be pointed out that the value of $\sigma$ for this ion is very uncertain; great reliance cannot therefore be placed upon the calculated value for the mobility. It may be said, however, that the ion at an age of $10^{-5}$ second apparently has a mass at least that of $(NO)_2$, and increases its mass and diameter but little thereafter.

It has been suggested that in the process of negative ion formation in $NH_3$ the initial process is the dissociation of the molecule with the formation of $NH^-$. Although values of $\sigma$ are not available for this molecule, the high value of the dielectric constant makes $A$ insensitive to variations in $\sigma$, and the mass factor plays the dominant role. If an approximate value of $5\times10^{-8}$ cm can be assigned to $\sigma$, one finds the mobility of an hypothetical $NH^-$ ion to be 1.25. This is not substantially higher than the fastest mobility observed. If one employs a mass corresponding to $(NH+NH_3)^-$ one calculates a mobility of 1.06 which is obtained experimentally at an age of approximately $2\times10^{-4}$ second. From the shape of the graph, a mobility of 1.25 for extremely short times seems probable. This ion apparently rapidly picks up an additional molecule and in less than 0.001″ reaches a stable value of 0.85 which is characteristic of ions in even impure ammonia.

---

JANUARY 15, 1937 PHYSICAL REVIEW VOLUME 51

# The Development and Performance of an Electrostatic Generator Operating Under High Air Pressure

R. G. Herb, D. B. Parkinson and D. W. Kerst
*University of Wisconsin, Madison, Wisconsin*

(Received October 22, 1936)

A belt type electrostatic generator has been developed which operates in a steel tank, 5½ feet in diameter and 20 feet long, under an air pressure of 100 lb./in.². The generator is provided with a high potential electrode system of a new design which serves both to give a high breakdown potential and to furnish a satisfactory potential distribution along the charging belts and the accelerating tube. The maximum potential of the generator is about 2500 kv and the highest steady potential at which reliable data have been obtained is 2160 kv. An evacuated tube for acceleration of ions has been developed which withstands the highest generator potential. The apparatus has been successfully used in experiments on atomic disintegration.

## Introduction

A FEW years ago an electrostatic generator of the Van de Graaff type was developed at this laboratory in which the apparatus was operated in a steel tank under high air pressure.[1] Because of the small size of the enclosing tank, the usable potential of this generator was limited to about 400 kv but its numerous advantages indicated the desirability of further development.

During the past year a second electrostatic generator has been constructed utilizing higher pressure and larger dimensions and has been successfully used in disintegration experiments. Although the generator is of the same type as the small generator referred to above, the increased dimensions of the new apparatus presented certain problems in the design of a satisfactory high potential electrode system; and for their solution a new type of electrode has been developed. This paper describes the development and performance of the large electrostatic generator, and because of the importance of the high potential electrode system for successful operation of the generator, considerable space is devoted to a description of its design.

## Design of Pressure Tank

From a consideration of the performance of electrostatic generators of the Van de Graaff type developed here and at other laboratories, it was expected that the peak voltage of the proposed generator would be approximately proportional to the diameter of the enclosing tank, assuming a fixed air pressure and sufficient tank length. From this consideration, a tank having a very large diameter would be desirable but for convenience in operation and low cost of construction, it was decided to install the generator in one of the regular research rooms available at this laboratory. To satisfy this condition the tank diameter was chosen to be $5\frac{1}{2}$ feet and, by making what seemed a reasonable assumption as to the lengths necessary for charging belts and the accelerating tube, the necessary tank length was determined to be 20 feet. The tank[2] was designed for a working pressure of 100 lb./in.$^2$, thus giving a total pressure almost twice as high as that used for the small generator referred to above.

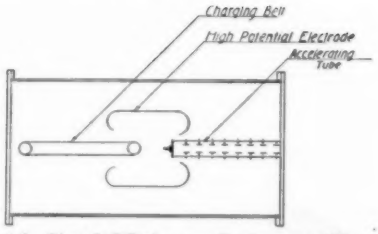


FIG. 1A. Sketch of the small electrostatic generator developed at the laboratory. Because of the short length of the accelerating tube and the comparatively large diameters of the steel tank and the high potential electrode, the tube operates satisfactorily without shielding.

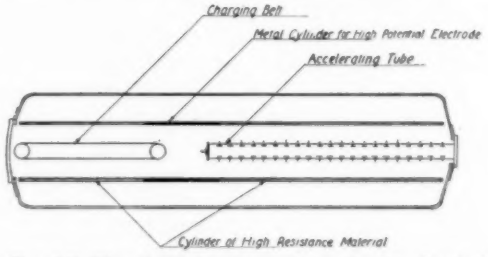


FIG. 1B. The electrode system shown in this sketch, if experimentally realizable, would be ideal for the large generator both to give a breakdown potential and to provide a satisfactory potential distribution along the charging belts and the accelerating tube. Cylinders of high resistance material were thought, however, to be impractical.

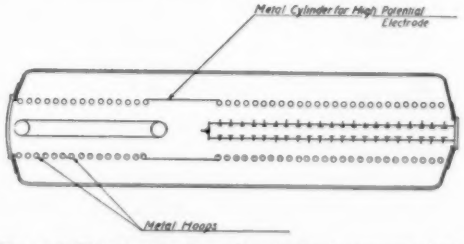


FIG. 1C. This sketch shows the electrode system adopted for the large generator. The hoop system was thought to provide the closest practical approach to the theoretically ideal arrangement shown in *B*.

## Design of High Potential Electrode System

A length of about 11 feet was considered necessary for the accelerating tube to assure satisfactory performance at the maximum potential expected of the generator. Because of the great length of accelerating tube compared with the $2\frac{3}{4}$-foot radius of the surrounding tank, a

[1] R. G. Herb, D. B. Parkinson and D. W. Kerst, R. S. I. 6, 261 (1935).

[2] We are indebted to The Chicago Bridge and Iron Works from whom the tank was purchased for their generous cooperation in working out the details of its construction.

high potential electrode similar to that used on the small pressure generator (*A*, Fig. 1) would be unsatisfactory, since it provides no shielding for the accelerating tube and a corona discharge would surely take place between high potential sections of the tube and the wall of the tank. Another reason for departing from the usual electrode design is given by a consideration of the inner electrode system which will give a potential distribution most nearly like the potential distribution given by two concentric cylinders infinite in length. Perhaps the closest approach to this ideal potential distribution would be given by an arrangement as shown in *B*, Fig. 1, with a conducting cylinder which is at the highest potential being continued at both ends by a cylinder of high resistance material down which a leakage current flows to give a gradual drop in potential. Such an arrangement, if experimentally realizable, would probably give a breakdown potential close to the breakdown potential between cylinders of infinite length, but cylinders of high resistance material were thought to be impractical and the arrangement *C*, Fig. 1, was considered the best practical way to secure good potential distribution. The conducting hoops as shown in *C*, Fig. 1, must be insulated from one another with provision, however, for a small current from hoop to hoop which can be provided by a system of corona points or resistors of very high ohmage. With this arrangement the potential, which is highest on the main electrode of *C*, Fig. 1, will decrease from both ends of the electrode by a number of discrete steps and will reach ground potential at both ends of the enclosing tank.

In order to decide on the radius of the inner electrode system, use was made of the relation that, for concentric cylinders of infinite length, the radius of the inner cylinder should be given by $r=R/e$ for maximum breakdown potential, where $R$ is the fixed radius of the outer cylinder and $e$ is the base of the natural logarithmic system. This relation would determine a radius of 12.2 inches for the inner electrode system of the large electrostatic generator, but since the breakdown voltage is a slowly varying function of $r$ in the region of optimum $r$, the radius of the inner electrode system was chosen to be $14\frac{7}{8}$ inches. This larger value of the radius was chosen so as to give ample room for charging belts and a power plant for the ion source.

Simple calculations were made in order to determine reasonable values for the diameter of the tubing from which the hoops were to be made and the air gap between the hoops, assuming the hoops to be made of round metal tubing bent into a circular form. Taking into account only the axial field, these calculations showed that for a generator potential of 3 MV the air gap between hoops could be safely made less than one-half the tubing diameter without danger of sparking from hoop to hoop. To allow for the added effect of the radial field, the ratio of tubing diameter to air gap was finally chosen to be 1.2. With this ratio determined to eliminate axial sparking, the absolute diameter of the tubing for the hoops was chosen partly from a consideration of the size most likely to give a high radial breakdown potential, but principally for convenience of construction. It seemed reasonable to assume that the breakdown potential should improve as

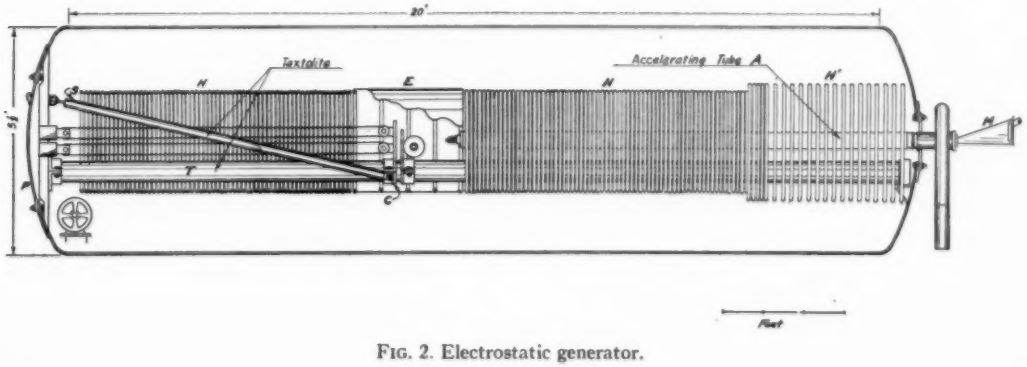


FIG. 2. Electrostatic generator.

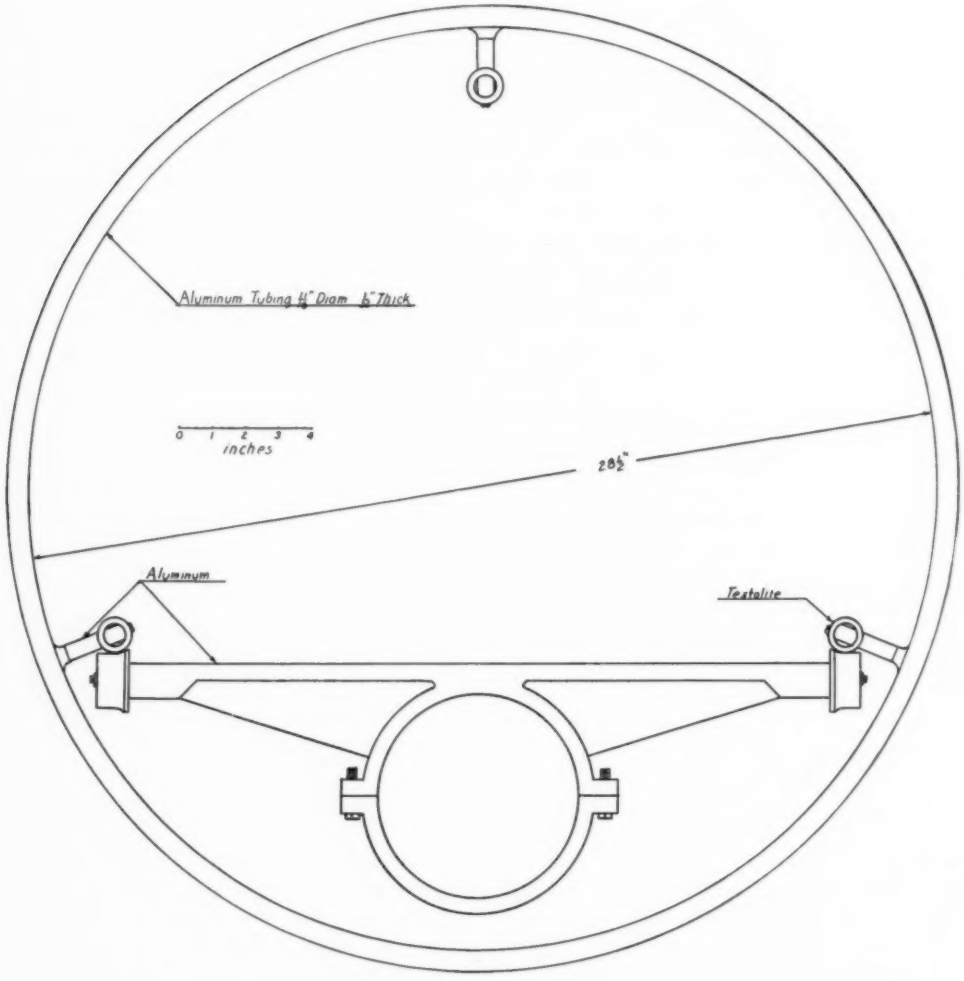


FIG. 3. Aluminum hoop and support.

the hoop tubing diameter and air gap become smaller, with their ratio held constant, since in the limit, with the hoop system degenerated into a system of closely spaced rings of fine wire, the potential distribution out a short distance from the system would be much like the potential distribution given by ideal cylinders of high resistance material. To best fulfill the conditions outlined above, of convenience of construction and high radial breakdown potential, the hoop tubing was chosen to have an outside diameter of $\frac{11}{16}$ inches and the hoops were spaced to have an air gap of $\frac{9}{16}$ inches.

## DETAILS OF CONSTRUCTION OF HIGH POTENTIAL ELECTRODE SYSTEM

In Fig. 2, the general arrangement of the high potential electrode system is shown, but to avoid confusion, many of the details are not included in the diagram. Mechanical support for all inner apparatus is provided by the textolite tube $T$ which has a 6-inch outside diameter and a $\frac{1}{4}$-inch wall thickness, and extends along the entire length of the tank. For additional rigidity, two textolite tension members $S$ with a $2\frac{1}{2}$-inch outside diameter and a $\frac{1}{4}$-inch wall thickness run parallel to each other from opposite sides of the

aluminum casting $C$ to an angle iron support at the end of the tank. These two textolite tubes are spaced $17\frac{1}{2}$ inches apart, from center to center, leaving sufficient free space for the charging belts.

The hoops are made from straight aluminum tubing, half-hard, $\frac{11}{16}$-inch outside diameter and $\frac{1}{32}$-inch wall thickness, bent into accurate circles and soldered with Kester aluminum solder. Each hoop is provided with 3 soldered studs as shown in Fig. 3 and by means of three small textolite tubes, the hoops are connected into rigid cylindrical sections with a total of 4 sections of hoops $H$ of Fig. 2. As a frame work for electrode $E$, Fig. 2, five aluminum hoops of the same size as those described above were mounted on 3 textolite tubes to form a section 30 inches long and over this frame, light weight galvanized sheet steel was bent and soldered.

To support electrode $E$ and the four hoop sections, aluminum castings fitted with Bakelite rollers, as shown in Fig. 3, are clamped to the large textolite tube $T$, Fig. 2. Eighteen of these castings are used, spaced evenly along the entire length of the textolite tube. The four hoop sections and electrode $E$ rest on these rollers and are ordinarily pinned together to form a rigid system with uniform hoop spacing. In order to have all apparatus inside the hoop system and the electrode easily accessible for adjustment or repair, the hoop section $H'$, Fig. 2, was made sufficiently large so that the smaller system $H$ can be telescoped into it. Thus by unpinning the system $H$, Fig. 2, in the proper place and telescoping it into section $H'$, a space four feet long is left uncovered wherever needed and is easily accessible. Section $H'$ is ordinarily clamped to the end of the tank but may be unclamped, and if the smaller hoop section has been telescoped inside, section $H'$ may be made to rest on it and may then be rolled out to have the inner apparatus at this end of the tank uncovered and accessible.

Each hoop is equipped with a needle point and a plate mounted so as to form a corona system with the corona gaps set at about $\frac{1}{2}$ inch and with the needles turned so as to be negative. As all electrical contacts of the hoop system and electrode $E$ with the inner apparatus are made automatically, the system can frequently be unpinned, an adjustment made on apparatus inside, and the system repinned, ready for operation in 3 or 4 minutes. The 3-foot opening in the end of the tank which may be covered by plate $P$, Fig. 2, provides room for an operator to enter the tank, and when inside, an operator with rubber soled shoes can walk without difficulty alongside of the inner electrode system on the sloping wall of the tank.

### Charging Belts and Pulleys

The two charging belts are each 13 inches wide and are made of rubberized fabric of the type used in hospitals for sheeting, with the splice formed by vulcanizing. Pulleys for the charging belts are made of steel tubing 3 inches in diameter and 14 inches long with steel end plugs brazed into place and turned down to form shafts. The pulleys have no crowning except for a 1° taper at the ends along a distance of $\frac{1}{2}$ inch. A one horsepower d.c. motor is used for each belt and the speed of the charging belt pulleys is about 3600 r.p.m. The needle system for charging the belts (not shown in Fig. 2) is similar to that used on the small pressure generator developed at this laboratory except that the pulleys in the high potential electrode are insulated from the electrode and can therefore be used as inductor plates for feeding negative charge to the outgoing belts.

### Accelerating Tube

Experience with an accelerating tube made up in short sections from straight glass cylinders

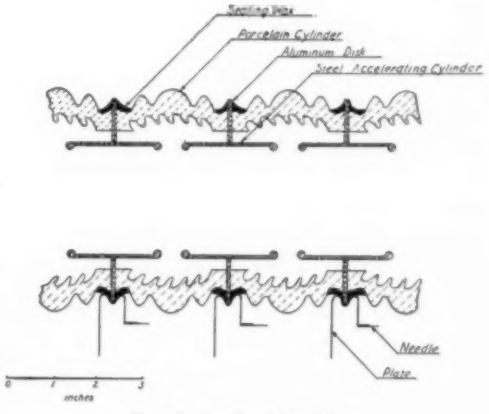


Fig. 4. Accelerating tube.

FIG. 5. Interior view of the generator showing the accelerating tube and the hoop system.

showed that the most serious factor limiting the voltage is a flash-over along the inner glass surface. Porcelain cylinders were therefore designed, corrugated inside and outside as shown in Fig. 4. A single porcelain section with electrodes as shown in the diagram withstood a potential of 100 kv satisfactorily. For the accelerating tube of the large generator 54 porcelain cylinders and metal electrodes were waxed together as shown in Fig. 4 using red sealing wax (American Express No. 2). The accelerating tube is supported inside the generator by heavy piano wire cradles at intervals of 15 inches along its entire length (Fig. 5) and sufficient flexibility to prevent strains and cracking is provided by a sylphon bellows and gimbal ring joint just next to the end plate of the tank. This tube has caused very little trouble due to leaks and when first mounted in the tank, it pumped down to a pressure of $2\times10^{-6}$ mm Hg.

While testing the performance of a single porcelain section in the small pressure generator, trouble was experienced with sparking along the external surface of the porcelain. This sparking occurred only when the porcelain section was evacuated and was practically unaffected by increasing the air pressure outside the section. Apparently charges on the inner surface of the porcelain caused irregular gradients on the external surface and consequent flash-over. This external sparking was later eliminated by wrapping a fine mesh brass gauze around the metal disk at each end of the porcelain cylinder. The explanation of this behavior is probably as follows: points on the fine mesh gauze cause a small corona current through the air close to the surface of the porcelain which prevents the development of high potential gradients. Further tests showed that the gauze could be replaced by three needle points spaced evenly around the metal disk at the end of each porcelain cylinder. The accelerating tube was therefore equipped with a corona system as shown in Fig. 4 and Fig. 5 which serves two separate purposes. First, it gives a uniform potential drop from section to section along the entire length of the tube; and second, the corona current along the surface of each porcelain cylinder prevents the development of high gradients on the surface and thus prevents sparking. By a simple system of automatic contacts, the accelerating tube is connected electrically to the surrounding hoop system at intervals of 15 inches. Over the period of a few months during which the generator has been in operation, the accelerating tube has performed satisfactorily at all generator potentials.

## PRODUCTION, FOCUSING AND MAGNETIC ANALYSIS OF POSITIVE IONS

Power for the ion source is provided by a 500-watt, 125-volt, self-excited a.c. generator driven from the inner pulley of the lower charging belt. By means of an RCA 866 rectifier tube and an 83 rectifier tube with the necessary transformers and condensers, d.c. potentials are supplied at 3000 volts and at 200 volts to run an ion source similar to that used by Tuve, Hafstad and Dahl. The rectifier tubes have operated without trouble with the air pressure in the tank up to 100 lb. and electric light bulbs of the ordinary type have also withstood the pressure satisfactorily except for one or two failures.

Focusing is accomplished by an adjustable corona gap across the first section of the accelerating tube. With the accelerating cylinders as shown in Fig. 4, no satisfactory focus could be obtained and the fluorescent spots formed by the ions on a quartz plate at the end of the magnetic analyzer were poorly defined. As these accelerating cylinders have a length of $2\frac{1}{8}$ inches and an inside diameter of about $2\frac{1}{4}$ inches, it

seemed probable that cylinders having a smaller inside diameter compared to their length would give better results. The first six accelerating cylinders at the high potential end of the tube were therefore made with the same length of $2\frac{1}{8}$ inches but were reduced to a diameter of one inch. After making this change, the ion beam has been well focused and, generally, by adjusting the corona gap across the first section of the tube, the fluorescent spots formed by the ions at the end of the magnetic analyzer can be brought down to a diameter of about 3 mm. In the brass box $M$ of Fig. 2, the ion beam is separated into its mass spectrum by means of an electromagnet, and the ions to be studied are shot into the target chamber.

Hydrogen pressure in the ion source, filament heating current for the ion source, and the corona gap for ion focusing can all be adjusted from outside the tank by controls working through packing glands. A window in the wall of the tank and a mirror properly placed inside the tank enable operators to read meters inside the high potential electrode. The pumping system for evacuation of the accelerating tube consists of three brass diffusion pumps using Apiezon oil, and a Cenco Hypervac. The diffusion pumps are of the same type as those used for the high voltage work at the Department of Terrestrial Magnetism of the Carnegie Institute of Washington and were made up from drawings generously furnished by Dr. M. A. Tuve.

## Measurement of Voltage

Voltage is measured by means of a generating voltmeter mounted on the side of the tank with the sectored spinning disk flush with the wall, in an opening just opposite the high potential electrode. The alternating current generated by the spinning disk is rectified by means of a commutator and measured with a Leeds and Northrup galvanometer, sensitivity $2.99\times10^{-10}$ amp./mm. A calibration of this voltmeter was made in the following way. With the small electrostatic generator which had been carefully calibrated by a method recently described in *The Physical Review*,[3] a series of runs were taken on the gamma-rays emitted by lithium bombarded by protons. Using two thick targets of pure evaporated lithium and two thin targets, nine separate runs were taken giving values for the peak of the gamma-ray resonance varying from 433 kv to 450 kv with an average at about 440 kv. This value of the resonance voltage agrees with the results of Hafstad, Heydenburg and Tuve, recently reported.[4] With the large generator, four runs were then taken on the gamma-rays from lithium bombarded by protons using both thick and thin targets, and by assuming that the average value thus determined for the resonance peak was at a potential of 440 kv, the sensitivity of the generating voltmeter was determined.

The generating voltmeter was shown to have a linear scale by a study of the deflections of the proton beam and the hydrogen diatomic ion beam in the magnetic analyzer. With the voltage at $V_1$, the magnetic field was adjusted to bring the proton beam through a $\frac{3}{16}$-inch hole into the target chamber where it impinged on a glass plate and formed a fluorescent spot. Then, with the magnetic field held constant, the voltage was lowered until the diatomic ions entered the target chamber. If $V_2$ is this second voltage, its value, provided the voltmeter is linear, should be given by $V_2=V_1/2$. By choosing a number of values for $V_1$, the voltmeter was shown to be linear to within about 5 percent over the entire voltage range of the generator. A more accurate check was not possible because the spots formed by the ion beams at the time these tests were made were at some voltages larger than the $\frac{3}{16}$-inch defining hole at the entrance to the target chamber.

## Additional Apparatus

### Compressor

Air is delivered to the tank up to the required pressure by a Quincy compressor, air-cooled, with a capacity of about 20 cubic feet per minute. For drying ingoing air, a steel cylinder filled with sodium hydroxide sticks is connected into the pipe line.

[3] R. G. Herb, D. B. Parkinson and D. W. Kerst, Phys. Rev. **48**, 118 (1935).

[4] L. R. Hafstad, N. P. Heydenburg and M. A. Tuve, Phys. Rev. **49**, 866 (1936).

**Cooling System**

An air blast from a vacuum cleaner blower provides cooling for the ion source. The blower is mounted on grounded angle iron supports near the motors which drive the charging belts, and the textolite tube *T*, Fig. 2, serves as a pipe line to deliver air to the ion source.

### Upper Voltage Limit of Generator

With the tank at atmospheric pressure, the highest usable generator voltage is generally about 500 kv although the peak voltage is not sharply defined and often the generator can be held above 600 kv for short periods of time. As the air pressure is increased, the upper voltage limit becomes even less sharply defined than at low pressures so that a study of peak voltages as a function of pressure is not very satisfactory. Experience over a period of a few months, during which considerable data have been taken on proton induced reactions, definitely shows that the maximum usable potential of the generator does not increase linearly with air pressure. For a short period of time, the generator has been held at 2500 kv but up to the present time the highest potential at which reliable data have been obtained is 2160 kv. This maximum usable potential could probably be increased somewhat by a careful overhauling and a thorough cleaning of the apparatus.[5]

During the first high voltage trials with the tank at high pressure, the potential was limited to about 1.7 MV by sparking along the textolite tubes *S*, Fig. 2. The sparking distance along these tubes is about 7 feet whereas the radial distance from the high potential electrode to the wall of the tank is only 18 inches. Sparking such as this, along the surface of insulators, has also been experienced in the small generator and in all cases an increase of air pressure gave no improvement in the sparking potential. This behavior indicates that on long insulators irregular surface charges accumulate which may give a sufficiently high gradient at some point to initiate a discharge. The surface discharges along the textolite tubes, *S*, were eliminated by a corona system similar to that used on the accelerating tube to prevent accumulation of charges. Strips of fine brass gauze about $\frac{1}{4}$ inch wide were wrapped around the tubes at intervals of $2\frac{1}{2}$ inches, and at intervals of 15 inches, the gauze systems were connected to the surrounding hoops. Although these gauze systems draw very little current (probably less than 5 microamperes), they have successfully eliminated surface sparking.

Trouble has also been caused by surface sparking down the charging belts when large charging currents are being used at high potentials, but these can be avoided by keeping the charging current below about 200 microamperes when working at high generator potentials. As this current limitation is not serious for work with positive ions, no effort has been made to increase the usable charging current, but to adapt a generator of this type to high voltage x-ray production for which currents of several milliamperes are needed, further development work would be necessary.

After eliminating the surface sparking along the belts and the textolite supports, the upper voltage limit was determined by radial sparking between the high potential electrode and the wall of the tank with the sparks generally occurring at the ends of the electrode.

### Voltage Control

Charge is put on the belts by a kenotron rectifier set and thus, by varying the resistance in the primary of the kenotron transformer, the generator voltage can be changed. When taking a run during which a steady generator potential is desired at some particular value, changes will occasionally occur so that the kenotron voltage must be varied to bring the electrostatic generator

[5] Some increase in the potential of an electrostatic generator can be obtained by the addition of $CCl_4$ vapor to the air. This effect was noticed by one of us (R. G. H.) three years ago while working with the small electrostatic generator and was then studied in considerable detail. A saturated vapor pressure of $CCl_4$ in air at atmospheric pressure was found to give a breakdown potential of about 1.7 times the breakdown potential of ordinary air. These results with air at atmospheric pressure were verified later by two different observers using an apparatus consisting of an adjustable sphere gap in a small pressure tank. A thorough investigation was then made using $CCl_4$ vapor in air at several different pressures up to a maximum of 75 lb. Publication was delayed because it was intended to look for similar effects caused by other vapors but details of the work will be published soon. In a recent issue of Compte rendus **202**, 291 (1936), Joliot, Feldenkrais and Lazard report the discovery of this effect. They find that an electrostatic generator operated in air containing a high vapor pressure of $CCl_4$ gives a maximum potential twice as high as when operated in ordinary air.

back to the desired potential. Recently a control has been devised utilizing corona current from the high potential electrode and an amplifying system for automatically varying the kenotron voltage to keep the electrostatic generator at a constant potential. Generally during a run, the automatic control keeps the voltage of the generator constant to within about 1 percent and often to 0.5 percent. As improvements are still being made in the amplifying circuit, a complete description of the apparatus will be postponed until a later time.

High frequency fluctuations of the generator voltage cannot be detected with the generating voltmeter because of the long period of the galvanometer used. A study of high frequency fluctuations was therefore made utilizing corona current to a needle sticking through a hole in the wall of the tank. The only periodic voltage fluctuation detected had a magnitude of about 0.5 percent and as its frequency was the same as that of the charging belts, it was probably caused by the splice in the belts.

## Discussion

As the success of the electrostatic generator described in this paper, both for development of high potential and for utilization of that high potential, depends to a large extent on the arrangement of the inner electrode system, a brief discussion will be given of the advantages of this electrode design. The hoop system gives a uniform, axial field along the accelerating tube and along the belts. The distance provided for the tube and the belts is great compared with the radial distance from the high potential electrode to the wall of the tank and therefore when the generator is at its maximum potential, the field inside the hoop system is far below the breakdown value. Metal castings and wires inside the hoop system cause no trouble if kept approximately parallel to the plane of the hoops and the accelerating tube with its metal electrodes and its corona system is operating under ideal conditions. As the high potential electrode ($E$, Fig. 2) may be left open at both ends, the space available for charging belts and the accelerating tube is limited only by the diameter of the cylinder.

A similar system could be used for an electrostatic generator in a large room at atmospheric pressure or in an upright pressure tank. Instead of the usual sphere mounted on insulating supports, a cylindrical column of hoops could be used, capped by a hemisphere. Ample room would then be available inside the hoop system for supports, belts and accelerating tubes.

From a consideration of the performance of the two generators developed at this laboratory it would seem that to obtain a further increase in potential an increase in the dimensions of the apparatus would be the safest way to proceed. Higher pressures might also give considerable improvement but the nonlinear increase of usable potential with pressure up to a pressure of 100 lb. makes the effectiveness of still higher pressure difficult to predict.

We wish to express our indebtedness to the late Professor C. E. Mendenhall and to Professor H. B. Wahlin for advice and generous support. We also wish to express our appreciation to Mr. J. P. Foerst and Mr. J. A. Johnson for their work on the construction of apparatus and to Mr. J. L. McKibben for valuable work in the development of the generator. We are indebted to the Wisconsin Alumni Research Foundation and the Bowman Cancer Foundation for generous financial assistance.

# On the Capture of Orbital Electrons by Nuclei

C. MØLLER
*Universitetets Institut for Teoretisk Fysik, Copenhagen, Denmark*
(Received November 9, 1936)

ACCORDING to the theory of $\beta$ decay put forward by Fermi[1] a nucleus of charge $Z$ can, provided the process is energetically possible, be transformed into a nucleus of charge $Z-1$ in two different ways: by the emission of a positron or by the absorption of an orbital electron. In a paper to appear shortly.[2] I have calculated the probability of the latter process and have found that for heavy elements the capture of a $K$ electron is in most cases much more probable than the emission of a positron. The total probability per second for the emission of a positron is in the case of "allowed" transitions given by

$$\lambda^+ = |M|^2 G^2 \kappa F(Z, W_0), \qquad \kappa = \frac{4(2\rho)^{2S} mc^2}{\Gamma(3+2S)^2 \hbar};$$
$$S = (1-(Z\alpha)^2)^{\frac{1}{2}} - 1. \quad (1)$$

Here $\alpha(=1/137)$ is the fine structure constant, $\rho$ is the radius of the nucleus divided by $\hbar/mc$, $m$ is the mass of the electron and $W_0$ is the energy difference between the initial nucleus of charge $Z$ and the final nucleus of charge $Z-1$, $mc^2$ being taken as unit energy. $F(Z, W_0)$ is a function of $Z$ and $W_0$, whose form depends on what assumption is made about the interaction between heavy and light particles. If we take the (0, 0) interaction proposed in Fermi's original paper and put $Z=82.2$ we get for different values of $W_0$ the $F$ values given in the second column of Table I. The corresponding $F$ values for the case of the (0, 1) interaction proposed by Konopinski and Uhlenbeck[3] are given in the fourth column. $G$ in (1) is a dimensionless constant related to the universal constant $g$ in Fermi's theory. To account for the decay periods found experimentally of the ordinary $\beta$-ray emitters we must put

$G=1.1\times10^{-13}$ in the case of (0, 0) interactions, (2)

$G=0.1\times10^{-13}$ in the case of (0, 1) interactions.

$|M|$ in (1) is the matrix element of the Fermi theory, a quantity which by definition cannot be larger than unity. The experimental data on the decay constants and on the upper limits of the ordinary $\beta$-ray spectra show that the matrix elements $|M|$ for heavy nuclei are in general several times smaller than the matrix elements of the light elements.

For the probability per second of a $K$ electron being absorbed by the nucleus we found the expression

$$\lambda_K = |M|^2 G^2 \kappa F_K(Z, W_0) \quad (3)$$

for "allowed" transitions, where $F_K$ in the case of (0, 0) interactions is given by

$$F_K = \pi\Gamma(3+2S)(Z\alpha)^{3+2S}(W_0+1)^2.$$

For (0, 1) interaction the factor $(W_0+1)^2$ is replaced by $(W_0+1)^4$. The values of $F_K$ for $Z=82.2$ and for the two kinds of interactions are given in the third and fifth columns of Table I. It can be seen that $F_K$ is certainly considerably larger than $F$ so that the probability of the capture of a $K$ electron is much larger than the probability of the emission of a positron.

This result seems to be essential for the interpretation of the experiments of Cork and Lawrence[4] who bombarded platinum with deuterons and found that among other things a radioactive substance was found which emitted positrons. They assumed that $_{78}Pt^{192}$ is trans-

TABLE I. *Values of $F(Z, W_0)$ and of $F_K(Z, W_0)$.*

| | (0, 0) INTERACTION | | (0, 1) INTERACTION | |
|---|---|---|---|---|
| $W_0$ | $F(Z=82.2)$ | $F_k$ | $F(Z=82.2)$ | $F_k$ |
| 0 | 0 | 1.2 | 0 | 1.19 |
| 1 | 0 | 4.8 | 0 | 19.0 |
| 1.40 | $<6\times10^{-4}$ | 6.8 | $<10^{-5}$ | 39.4 |
| 2.29 | 0.02 | 12.9 | 0.008 | 139.3 |
| 3.20 | 0.25 | 21.0 | 0.38 | 369.9 |
| 4.11 | 1.2 | 31.0 | 3.8 | 810.6 |
| 5.03 | 3.9 | 43.2 | 20.7 | 1572 |
| 7.09 | 26.5 | 77.8 | 318.2 | 5092 |

[1] E. Fermi, Zeits. f. Physik **88**, 161 (1934).
[2] Physik. Zeits. Sowjetunion.
[3] E. J. Konopinski and G. E. Uhlenbeck, Phys. Rev. **48**, 7 (1935).
[4] J. M. Cork and E. O. Lawrence, Phys. Rev. **49**, 788 (1936).

formed by the bombardment into $_{78}Pt^{193}$, which can emit a positron and go over to $_{77}Ir^{193}$. The upper limit of the positron spectrum lies in the neighborhood of 2.1 MV, which corresponds to $W_0=5.1$. The decay period is 49 min. corresponding to a decay constant $\lambda=3.4\times10^{-4}$ sec.$^{-1}$.

For $Z=78$ and $W_0=5.1$ we get the following values for $F$ and $F_K$ (in the neighborhood of $Z=82.2$ $F_K$ varies approximately as $Z^{8-2\times0.2}$ while $F$ is practically constant)

$$\begin{aligned} F&=4.2, \quad F_k=37.8 \quad \text{for (0, 0) interaction} \\ F&=30.8, \quad F_k=1440 \quad \text{for (0, 1) interaction.} \end{aligned} \tag{4}$$

From (1) we get, using (2)

$$\begin{aligned} \lambda^+&=2.6\times10^{-4}|M|^2, \quad (0,0) \text{ interaction,} \\ \lambda^+&=3.1\times10^{-5}|M|^2, \quad (0,1) \text{ interaction.} \end{aligned}$$

Even if we give $|M|^2$ its maximum value of unity these values are smaller than the experimental decay constant $\lambda=3.4\times10^{-4}$, which shows that there must exist some other process, in addition to the positron emission, whereby $_{78}Pt^{193}$ can be transformed into $_{77}Ir^{193}$. If we take into account the possibility of a $K$ electron being captured, we have $\lambda=\lambda^+ + \lambda_K$. Using (1), (2) and (3) we get for the two different types of interaction

$$\lambda=\lambda^+ + \lambda_K = \begin{cases} 26.2\times10^{-4}|M|^2 \\ 14.8\times10^{-4}|M|^2 \end{cases}$$

which can be brought into agreement with the experimental value by choosing a suitable value for $|M|^2$. This gives $|M|^2\sim\frac{1}{8}$ which is of the same order of magnitude as has been found for the matrix elements of other heavy elements.

While the total decay constant $\lambda^+ + \lambda_k$ is about the same for both types of interaction, the ratio $\lambda_k/\lambda^+ = F_K/F$ between the probabilities of the two processes depends very much on the assumption made about the interaction. As can be seen from (4) we have

$$\frac{\lambda_K}{\lambda^+}=\frac{F_K}{F}=\begin{cases} 9 & \text{for (0, 0) interaction,} \\ 47 & \text{for (0, 1) interaction.} \end{cases}$$

From a theoretical point of view it would therefore be of great value if this ratio could be determined experimentally. Since the capture of a $K$ electron will always be followed by the emission of a quantum belonging to the characteristic x-ray spectrum of the element formed by the process, the ratio $\lambda_K/\lambda^+$ is equal to the ratio between the number of x-rays and the number of positrons emitted in a given time interval.

Finally in using the output of positrons after saturation has been obtained, to calculate the cross section for the formation of $_{78}Pt^{193}$ by the bombardment of $_{78}Pt^{192}$ with deuterons, we must take into account the fact that the number of active nuclei formed per second is $(F+F_K)/F$ times the number of positrons emitted per second. Allowing for the abundance of $_{78}Pt^{192}$ in platinum being smaller than 3 percent[5] we find from the data on the output of positrons given in the paper of Cork and Lawrence that this cross section is of the order of at least $10^{-28}$ cm$^2$ on the assumption of (0, 0) interaction. On the (0, 1) interaction assumption this cross section is even larger, being in fact of the order of $7\times10^{-26}$ cm$^2$ at the lowest.

[5] B. Fuchs und H. Kopfermann, Naturwiss. **23**, 372 (1935).

# A Study of Kinetic Energies of Atomic Ions Formed by Electron Impact in Nitric Oxide and Hydrogen Chloride

ELMO E. HANSON
*Department of Physics, University of Minnesota, Minneapolis, Minnesota*
(Received June 6, 1936)

A study was made of the kinetic energy of the atomic ions formed by electron impact in NO and HCl. Their energy distribution was measured as a function of the electron energies at impact, and their ionization potentials were determined. The most probable values of the heats of dissociation of the molecules and of the molecular ions were calculated. Negative ions possessing up to 2.5 volts kinetic energy were observed in NO, and the electron affinity of oxygen was calculated. Negative ions found in HCl had less than 0.5 volt energy. The following is a summary of the results and the probable processes:

| PROBABLE PROCESS | KINETIC ENERGY OF IONS | HEAT OF DISSOCIATION |
|---|---|---|
| $NO^+ \rightarrow N^+ + O(^1D_2)$ | 0 to 6 VOLTS | |
| $NO^+ \rightarrow N + O^+$ | | 9.3±0.2 VOLTS |
| $NO \rightarrow N + O$ | | 5.3±0.2 |
| $NO + e \rightarrow N + O^-$ | 1 to 2.5 | ELECTRON AFFINITY OF O = 2.1±0.5 |
| $HCl^+ \rightarrow H^+ + Cl(^2P)$ | 0 to 10 | |
| $HCl^+(^2\Pi) \rightarrow H + Cl^+$ | | 4.8±0.2 |
| $HCl^+ \rightarrow H^+ + Cl$ | 2 to 6 | EXCITATION ENERGY OF Cl ≦ 11.6 |
| $HCl \rightarrow H + Cl$ | | 4.7±0.2 |
| $HCl \pm e \rightarrow H + Cl^-$ | LESS THAN 0.5 | ELECTRON AFFINITY OF Cl ≦ 4.0 |


## INTRODUCTION

IT was predicted by the quantum mechanics[1–4] that in hydrogen positive ions which would have kinetic energies much greater than the normal thermal energies could be formed by dissociation following electron impact. This was experimentally verified by Bleakney and Tate[5, 6] and later by Lozier,[7] who made a detailed study of the phenomenon.

Tate and Lozier,[8] and Lozier[9–11] have shown that such ions are also formed in all the molecular gases which they studied. Besides hydrogen the gases which have been studied are $N_2$, CO and $O_2$. Furthermore, it was shown that when negative ions are formed as dissociation products, they also might have several volts energy.

The formation of high energy ions is interpreted as arising from a transition to an unstable electronic state of the molecule. When this occurs, dissociation takes place, and the molecular components fly apart with velocities determined by: (1) the energy absorbed by the normal molecule, (2) the final states of the dissociation products and (3) the masses of the products. Thus in the process, $AB^+ \rightarrow A^+ + B$, the kinetic energy of the ion, $A^+$, is[8]

$$V_F = M_B/(M_A + M_B)[V_i - (U_2 - U_1)]. \quad (1)$$

$M_A$ and $M_B$ are the masses of the component atoms $A$ and $B$, respectively, $V_i$ is the energy absorbed by the normal molecule in its transition to the unstable state (i.e., the "ionization potential"), and $(U_2 - U_1)$ is the difference in potential energy between the final and the initial states of the molecule. Since the above formula was derived simply from considerations of the conservation of energy and of momentum it is, therefore, also applicable to the case of negative ions.

The heat of dissociation of the normal molecule and of the molecular ion may be calculated[8] if $(U_2 - U_1)$ is determined from measurements of $V_F$ and $V_i$, and if the masses and the excitation energy of the products are known. The heat of dissociation of the normal molecule is given by

[1] Heitler and London, Zeits. f. Physik **44**, 455 (1927).
[2] Burrau, Kgl. Dansk. Selsk. Math. Fys. **7**, 14 (1927).
[3] Morse and Stuekelberg, Phys. Rev. **33**, 932 (1929).
[4] Condon, Phys. Rev. **35**, 658 (1930).
[5] Bleakney and Tate, Phys. Rev. **35**, 658 (1930).
[6] Bleakney, Phys. Rev. **35**, 1180 (1930).
[7] Lozier, Phys. Rev. **36**, 1285 (1930).
[8] Tate and Lozier, Phys. Rev. **39**, 254 (1932).
[9] Lozier, Phys. Rev. **43**, 776 (1933).
[10] Lozier, Phys. Rev. **44**, 575 (1933).
[11] Lozier, Phys. Rev. **46**, 268 (1934).

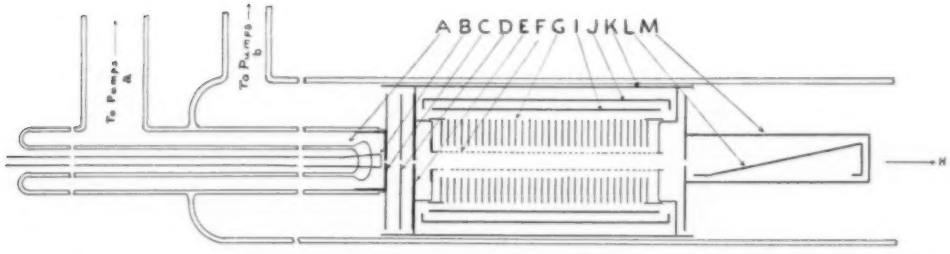


FIG. 1. The experimental tube. The filament chamber *A* is formed by closing the Pyrex tube with a snugly fitting spun copper cup. A 0.5 mm diameter hole in the center of this cup allows electrons to pass and be accelerated to the desired energy by controlled potentials placed between the disks *C*, *D* and *E*. After passing down the axis of the tube (in the direction of a collimating magnetic field *H*) these electrons are collected in the trap *LM*. The cylindrical wire gauze *F* is connected to *E* to give a field free region of ionization. The disks *G* allow only those ions to pass whose velocity is 98 percent perpendicular to the electron beam. The ions which qualify in direction of travel and which have sufficient energy to penetrate the differences of potential which may be placed between the elements *F*, *G* and *I* are collected on the cylinder *I*. *J* is a guard ring, while *K* is an electrical shield.

the formula,

$$D(AB) = (U_2 - U_1) - I_A - E,$$

where $I_A$ is the ionization potential of atom $A$ (assuming that $A$ comes off charged) and $E$ is the total excitation energy of the products. The heat of dissociation of the normal molecular ion, $AB^+$, is given by

$$D(AB^+) = (U_2 - U_1) - I_m - E, \qquad (2)$$

where $I_m$ is the ionization potential of the molecular ion. Similarly, if negative ions having large kinetic energies are formed in the gas, the electron affinity of the atom may be calculated. Thus, if $B^-$ ions having kinetic energy are formed, the electron affinity of $B$ is

$$E(B) = D(AB) - (U_2 - U_1) - E. \qquad (3)$$

Thus, aside from showing the presence of unstable electronic levels in the ionized molecule, a study of the formation of high velocity ions by electron impact is valuable in that it gives values for heats of dissociation and electron affinities.

## APPARATUS

The experimental tube, a modification of Tate and Lozier's apparatus,[8] was built entirely from copper, tungsten and Pyrex. Because NO and HCl are easily dissociated by a hot tungsten filament, it was necessary to employ differential pumping to maintain as low a pressure as possible around the filament while the pressure in the remainder of the tube was high enough to allow accurate measurements to be made. The leads *a* and *b* (Fig. 1) go to the same set of pumps; a difference in the rates of effusion through the two leads is effected by the difference in their diameters. A mercury cut-off in series with *b* can be used to lower its effusion rate still more.

In all cases the apparatus was baked out first in a quartz furnace at 800°C under a vacuum, and later in the Pyrex tube for thirty hours at 360°C.

The flow method was used to admit the gas to the apparatus, the pumps being run continuously while the gas leaked in through a capillary tube. The pressure behind the capillary was adjusted to give a working pressure in the experimental tube of about $5 \times 10^{-5}$ mm of Hg.

The nitric oxide was prepared by the action of nitric acid on electrolytic copper and purified by being passed through water and over potassium hydroxide and by being fractionally distilled. A mass-spectrograph analysis by Dr. A. L. Vaughan showed the only measurable impurity was $N_2O$ in concentration less than one percent.

The sample of hydrogen chloride was prepared by the action of $H_2SO_4$ on NaCl. It was dried over $P_2O_5$, and fractionally distilled in the usual manner. A mass-spectrograph analysis run in collaboration with Mr. A. O. Nier showed no measurable impurities.

A vacuum tube electrometer[12] was used to measure the ion currents. When used with an input resistor of $2.3 \times 10^{10}$ ohms, the maximum

[12] Distad and Williams, Rev. Sci. Inst. **5**, 289 (1934).

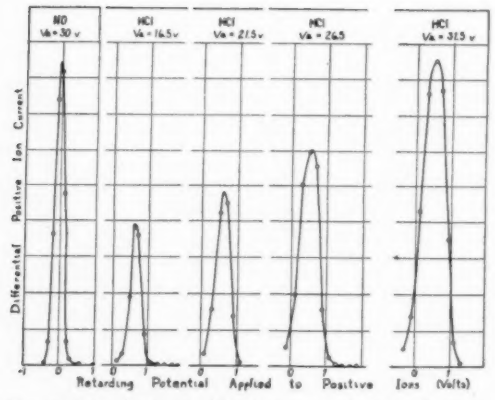


FIG. 2. Distribution in kinetic energy of molecular ions.

current sensitivity available was $3.3\times10^{-16}$ amp./mm with random fluctuations of less than 2 mm.

## METHOD

Two types of data were obtained: (1) the minimum electron energy $V_i$ necessary to form an ion having a kinetic energy $V_F$, and (2) the kinetic energy distribution of ions for various electron energies.

The velocity distribution of the ions was found by the retarding potential method. The ions, in traversing the region from gauze to defining disks to collector, lost or gained an energy equal to the algebraic sum of the voltages applied between these elements. It was customary in the work on positive ions to apply a drawing out potential of 3 volts in the gauze-grid region, while this potential plus the retarding potential was applied in the opposite direction in the grid-collector region. With the electron energy fixed at some value $V_a$, the retarding potential $V_R$ was changed in steps of $\Delta V_R$ and the corresponding change in positive ion current $\Delta I^+$ was measured. $\Delta I^+$ was, then, proportional to the number of ions having energies between $V_R-\Delta V_R/2$ and $V_R+\Delta V_R/2$. A plot of $\Delta I^+$ *vs.* $V_R$ gives the kinetic energy distribution of the ions. In practice $\Delta V_R$ was 0.4 volt for NO and 0.2 volt for HCl. To make it possible to utilize a high sensitivity in the amplifier, the potential drop across the input resistor was balanced by a potentiometer between the input grid and the positive end of the resistor. The sensitivity utilized in the amplifier was then $10^{-14}$ amp./mm.

When a retarding potential $V_R$ will just prevent an ion from reaching the collector, the ion must have started from the electron beam with a kinetic energy equal to $V_R$ unless there were other fields present or if there were a magnetic field present to curve the path of the ions. Since a magnetic field of 158 oersteds parallel to the tube axis was used, the ions must have started with an energy $(300b^2eH^2)/(8mC^2)$ volts[7] greater than the retarding potential. To measure the contact potentials and the space charge that might exist in the tube, use was made of the fact that the most abundant ions, the molecular ions, have only thermal velocities of a few hundredths of a volt. Velocity distribution curves of these ions are given in Fig. 2. Their maxima should within experimental error appear at $V_R=0$ volts; their measured position gives the value of the inherent potentials in the tube and therefore the

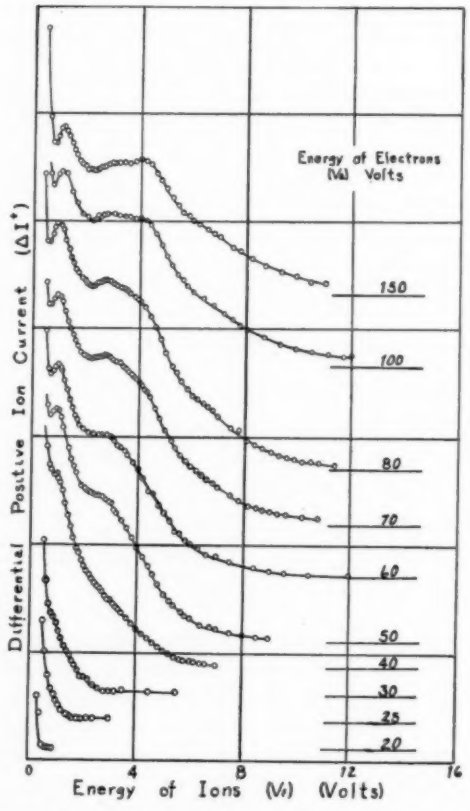


FIG. 3. Distribution in kinetic energy of positive ions formed in NO at various electron energies.

corrections to be applied to $V_R$. Space charge in the tube appeared to be negligible since the position of the maxima in Fig. 2 did not vary with pressure or electron current.

To measure the minimum electron energies $V_i$ necessary to produce ions having kinetic energies $V_F$ the following method was used: With the retarding potential set to give the desired $V_F$, the energy $V_a$ of the electrons was varied and the ion currents were recorded. An upward break in the curve thus obtained gave the onset potential of the ion having the kinetic energy $V_F$. The voltage scale for the electrons was calibrated from the observed onset potential of the molecular ion and from the known ionization potential of the molecule. (Drawing-out potentials in the gauze-grid-collector regions served to sweep the molecular ions into the collector.) For the work on NO, Tate and Smith's value[13] of 9.5 volts was used for the ionization potential; for the work on HCl the ionization potential used was 12.9 volts from the work of A. O. Nier and the author.[14]

Negative ions were studied in much the same way as the positive ions. In addition the relative efficiency of formation of the total number of negative ions was measured as a function of the electron energy.

## Results and Conclusions

### Nitric oxide

The distribution in kinetic energy of the positive ions is given in Fig. 3. The increments in ion current have been reduced to the same pressure and electron current. As one might expect, the ions of higher velocity become relatively more abundant as the incident electron energy is increased. We note that the curves have two maxima, a broad maximum at about 3 volts kinetic energy, and a very sharp peak at about 1 volt. The sharp peak, which is present in all the curves above 30 volts electron energy, is probably due to ions formed by the dissociation of $NO^+$ (excited) from a flat repulsive potential energy curve. The ions in the broad peak must be due to a dissociation of $NO^+$ from a rather steep potential energy curve, there being a rise of about 10 volts in the Frank-Condon region.

[13] Tate and Smith, Phys. Rev. **39**, 270 (1932).
[14] Nier and Hanson, Phys. Rev. **48**, 477 (1935).

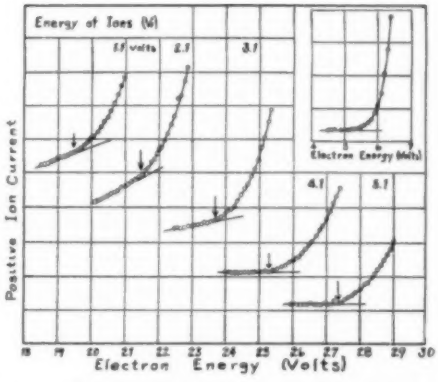


FIG. 4. Ionization potentials of positive ions having kinetic energy in NO.

In Fig. 4 we have a sample of the curves used to determine the onset potentials, $V_i$, of ions having kinetic energies, $V_F$. The curve in the inset is for the onset of $NO^+$, and it is used to calibrate the electron voltage scale. The mass-spectrograph studies of Hogness and Lunn,[15] and of Tate, Smith and Vaughan[16] have shown that both $N^+$ and $O^+$ are formed in NO. Vaughan[17] has also shown that the amount of $O^+$ formed was less than 5 percent of the $N^+$ formed. The upward breaks in the above curves were therefore assumed to be due to the onset of $N^+$ ions. This assumption gives good agreement with the experimental value of the slope of the $V_i$ *vs.* $V_F$ curve given in Fig. 5. From Eq. (1) we note that $V_F$ is a linear function of $V_i$. The experimental values of these quantities are plotted in Fig. 5 and a straight line of the theoretical slope 16/30 is drawn through the points. The closed circles are from data taken earlier on another sample of gas. The intercept gives $(U_2-U_1)=21.7$ volts as the weighted mean. It is to be noted that Hogness and Lunn[15] and also Tate, Smith and Vaughan[16] give 22.0 volts for the ionization potential of $N^+$. One would expect the mass-spectrograph value to be higher inasmuch as the kinetic energy carried by the ions is not corrected for. To calculate the probable observational error, $(U_2-U_1)$ was calculated for each of the 21 observations and the probable error obtained from the method of least squares. The value so

[15] Hogness and Lunn, Phys. Rev. **30**, 26 (1927).
[16] Tate, Smith and Vaughan, Phys. Rev. **48**, 525 (1935).
[17] Vaughan, Thesis, Univ. of Minn. (1934).

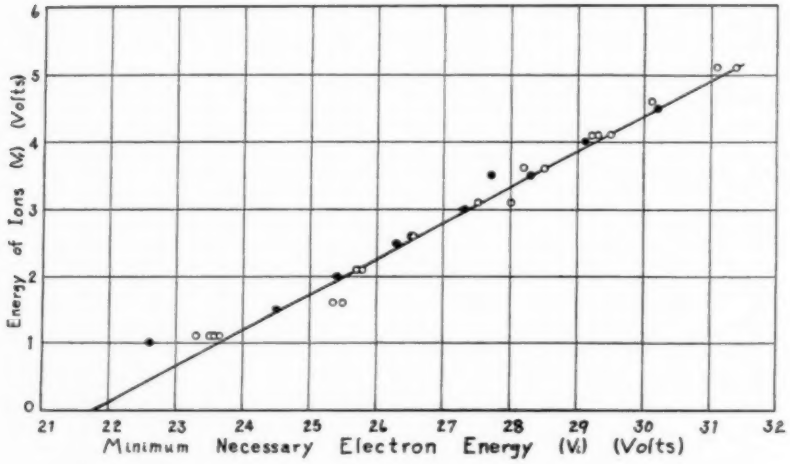


FIG. 5. Kinetic energies *vs.* ionization potentials of positive ions in NO.

obtained was $\pm 0.03$ volt; however, it was felt that a safer estimate for the probable systematic error would be $\pm 0.2$ volt.

If one assumes the process for forming these kinetic energy ions in NO to be $NO^+ \rightarrow N^+ + O$, the heat of dissociation of NO would be $D(NO) = 21.7 - 14.48 = 7.22$ volts, where 14.48 volts is the spectroscopic value for the ionization potential of atomic nitrogen. Kaplan,[18] however, has shown from band spectra that $D(NO) \leqq 6.1$ volts. We must therefore assume that one of the products is in an excited state. In Table I are given the possible states of excitation[19] of $N^+$ and O with the corresponding values of $D(NO)$. The only reasonable values for $D(NO)$ are those obtained from the combinations $N^+(^1D_2) + O(^3P_0)$ and $N^+(^3P_0) + O(^1D_2)$. From Lozier's work[10, 11] it appears that it is more probable for the uncharged dissociation product to be excited. Also if $N^+$ were excited, it would involve a double electron jump, which is perhaps unlikely.[20] The difference between the two possible values of $D(NO)$ is only 0.06 volt, which is well within our probable error.

Using our value of 5.27 volts for $D(NO)$, and the known value for $D(O_2)$ in the thermochemical equation,

$$(1/2)D(N_2) + (1/2)D(O_2) - 0.94 = D(NO),$$[21]

we obtain for $D(N_2)$ the value 7.32 volts. The latest value given by Kaplan[22, 23] from the band spectra is 7.4 volts, with which our value is in very good agreement.

A limit may be sent on $D(NO^+)$. The mass-spectrographic work mentioned above[15, 16] showed that $O^+$ was formed about one volt lower than $N^+$. For the process, $NO^+ \rightarrow N + O^+$, $(U_2 - U_1)$ should be less than the corresponding value for the process $NO^+ \rightarrow N^+ + O$ by the difference in the ionization potentials of N and O, i.e., by $14.48 - 13.55 = 0.93$ volt. Therefore, $(U_2 - U_1)$ for the first process above is $21.7 - 1.95 - 0.93 = 18.82$ volts, and $D(NO^+) = 18.82 - 9.5 = 9.3$ volts, where 9.5 is the ionization potential of NO.

TABLE I. *Possible states of excitation of $N^+$ and O and the corresponding heats of dissociation.*

| State | $N^+$ Term Value (electron volts) | State | O Term Value (electron volts) | $D(NO)$ (electron volts) |
|---|---|---|---|---|
| $^3P_0$ | 0 | $^3P_0$ | 0 | 7.22 |
| $^3P_0$ | 0 | $^1D_2$ | 1.95 | 5.27 |
| $^3P_0$ | 0 | $^1S_0$ | 5.27 | 3.05 |
| $^1D_2$ | 1.89 | $^3P_0$ | 0 | 5.33 |
| $^1D_2$ | 1.89 | $^1D_2$ | 1.95 | 3.48 |
| $^1S_0$ | 4.03 | $^3P_0$ | 0 | 3.19 |

[18] Kaplan, Phys. Rev. **37**, 1410 (1931).
[19] Bacher and Goudsmit, *Atomic Energy States* (McGraw-Hill Book Company, 1932).
[20] Mulliken, Phys. Rev. **46**, 144 (1934).
[21] Landolt Bornstein **2**, 1495 (1923).
[22] Kaplan, Phys. Rev. **45**, 898 (1934).
[23] Lozier, Phys. Rev. **46**, 268 (1934).

This value is independent of the ionization potential of NO since it was also used to calibrate the electron voltage scale. We can only set a limit on $D(NO^+)$ since $r_e$, the internuclear equilibrium distance, is not known.

### Negative ions in NO

In Fig. 6 is given the relative efficiency of production of negative ions in NO. The shape of the curve and the position of the maxima agree in general with the curve given by Tate and Smith.[13] These ions, which have been identified as $O^-$,[16] have an appreciable amount of kinetic energy. The ionization potentials of the kinetic energy ions are given in Fig. 7. The currents that were measured were very small, which accounts for the points not falling very well on a smooth curve. In Fig. 8 is given the straight line of the theoretical slope 14/30 obtained by plotting $V_1$ *vs.* $V_F$. For values of $V_F$ lower than 1.1 and greater than 2.1 volts, the points deviate consistently from a straight line. The intercept of the line gives $U_2-U_1=3.2$ volts, with a systematic error estimated to be less than $\pm 0.5$ volt. If the process is $NO+e\rightarrow N+O^-$, the electron affinity of oxygen is $E(O)=D(NO)-3.2=2.1 \pm 0.5$ volt. This is in good agreement with Lozier's value[11] of 2.2 volts. It is not likely that the nitrogen atom comes off excited in the process since this would make the value of $E(O)$ greater than 4.4 volts. This would mean that in Lozier's experiment $O^-$ would have to possess at least 2.2 volts excitation energy. The little that is known about excited states in negative ions seems to indicate that they are for the most part unstable.[11]

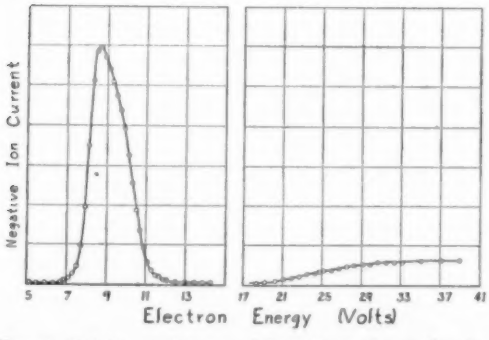


FIG. 6. Relative efficiency of formation of negative ions in NO.

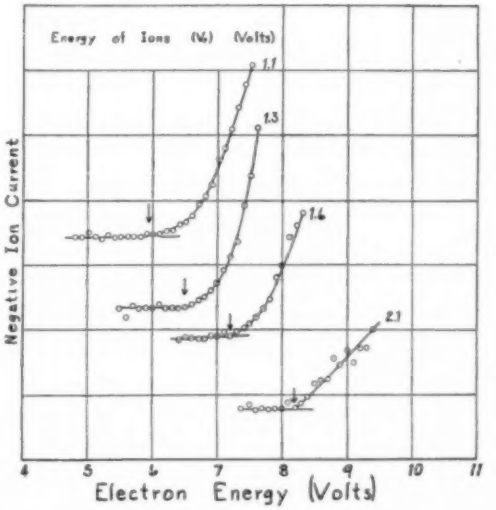


FIG. 7. Ionization potentials of negative ions having kinetic energy in NO.

By an empirical method of extrapolation, Glockler[24] has estimated the value of $E(O)$ to be 3.8 volts. To reconcile our value to this would require $O^-$ to have 1.7 volts excitation energy, a value that seems high from the standpoint of stability. Since Glockler's extrapolation was rather long, the discrepancy is not as serious as it might appear.

### Hydrogen Chloride

In Fig. 9 are given the kinetic energy distribution curves for positive ions in HCl. It is obvious that these ions are $H^+$ ions since from momentum and energy considerations neither $HCl^+$ nor $Cl^+$ could possess such velocities. That these ions were $H^+$ was confirmed by Nier and the author[14] by using a mass spectrograph. The most prominent features of the curves in Fig. 8 are the three sharp maxima that become evident above 40 volts electron energy. The sharpness of these peaks indicates that the repulsive potential energy curves which describe the dissociation process must be rather flat in the Franck-Condon region. The most likely process for the formation of the ions of the peaks is $HCl^{++}\rightarrow H^+ + Cl^+(^3P)$. To form an $H^+$ ion having 6 volts kinetic energy by this process would require 37 volts electron

[24] Glockler, Phys. Rev. **46**, 268 (1934).

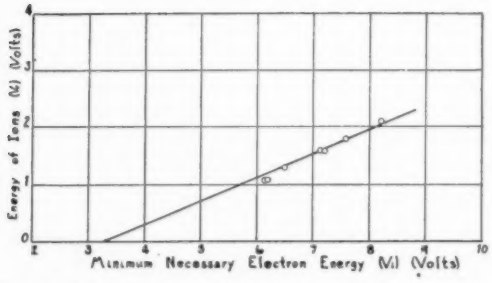


FIG. 8. Kinetic energy *vs.* ionization potentials of negative ions in NO.

energy, while if the $Cl^+$ were excited to the next energy level it would require 48.5 volts energy to form such an ion. To explain the triplet structure of the peaks we might assume that there exists for each $J$ value of $Cl^+(^3P)$ an unstable potential energy curve. Since the separation in energy of the three peaks is much greater than the corresponding differences in the triplet levels of $Cl^+(^3P)$, the highest potential energy curve must be the steepest and the highest energy peak should be the broadest. It is of interest that this is true. Mulliken[25] has tentatively constructed such triplet repulsive potential energy curves for the process $HCl^+ \rightarrow H + Cl^+(^3P)$. The above data are evidence in favor of the existence of such states for the doubly charged molecular ion.

In Fig. 10 are given samples of the ionization potential curves for kinetic energy ions. In the inset is given the corresponding curve for the onset of $HCl^+$; it is used as a calibration curve for the electron voltage scale. The readings for these curves were staggered, the open circles being for one sequence of readings, while the closed circles are for another sequence. The negative slope of the base lines of these curves was probably due to negative ions from a small amount of NO which existed as an impurity in the tube. These small negative currents did not interfere with the measurement of the positions of the breaks in the ionization curves.

For the $V_F$ *vs.* $V_i$ graph of Fig. 11 the mean straight line was drawn with the theoretical slope 35/36. The intercept gives for $U_2 - U_1$ the value 18.35 volts. The appearance potential of $H^+$ ions in the mass-spectrograph[14] study was $18.6 \pm 0.3$ volts; this is higher as one would expect if all the $H^+$ ions carried some kinetic energy. From a calculation on the deviation of $U_2 - U_1$ from its mean for each individual observation on the basis of least squares the probable observational error is 0.002 volt; we feel

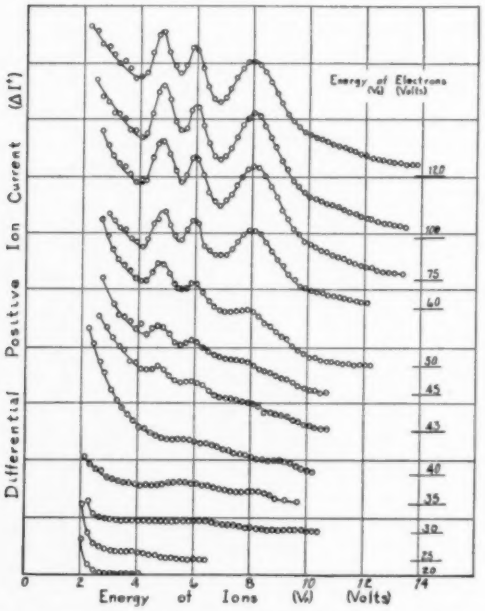


FIG. 9. Distribution in kinetic energy of positive ions formed in HCl.

[25] Mulliken, Rev. Mod. Phys. 4, 6 (1932).

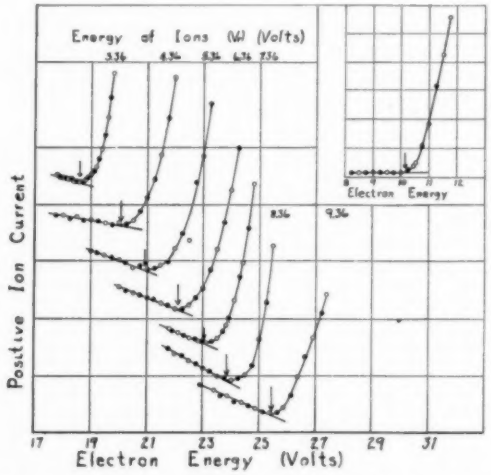


FIG. 10. Ionization potentials of positive ions having kinetic energy in HCl.

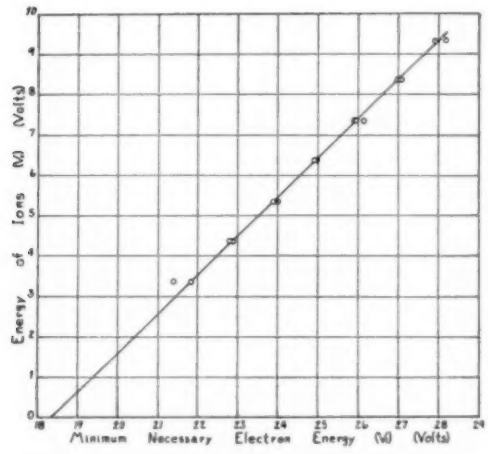


FIG. 11. Kinetic energies *vs.* ionization potentials of positive ions in HCl.

certain that the systematic error must be less than 0.2 volt.

Assuming that the process for the formation of these ions is $HCl^+ \rightarrow H^+ + Cl(^2P^0_{3/2})$, we get for $D(HCl)$ the value $18.35 - 13.54 = 4.8 \pm 0.2$ volts, which is 0.4 volt higher than the rather reliable chemical value.[26] The only other possible process would be $HCl^+ \rightarrow H^+ + Cl(^2P^0_{1/2})$; if we assume this process, $D(HCl) = 4.7 \pm 0.2$ volts, which still does not agree within the probable error with the chemical value of 4.42 volts. The explanation for this may be that the ionization potential of HCl, upon which our value for $U_2 - U_1$ depends, is actually lower than the value used. It should be pointed out that the values for the ionization potential of HCl given previous[27, 28] to the work of Nier and Hanson[14] would give for $D(HCl)$ a value 0.9 volt still higher.

The heat of dissociation of $HCl^+$ may be calculated. Two stable states for $HCl^+$ have been observed from band spectra,[29, 30] a $^2\Pi$ and a $^2\Sigma^+$ state. The $^2\Sigma^+$ state when dissociated gives $H^+ + Cl$; the $^2\Pi$ state is made up of $H + Cl^+$. Therefore, the horizontal asymptote of the $^2\Pi$ potential energy curve must lie below the

[26] Landolt Bornstein **2**, 1489 (1923); Frank, Trans. Faraday Soc. **21**, 536 (1926).
[27] Knipping, Zeits. f. Physik **7**, 328 (1921).
[28] McKaye, Phys. Rev. **24**, 319 (1925).
[29] Brice and Jenkins, Nature **123**, 944 (1929).
[30] Kulp, Zeits. f. Physik **67**, 7 (1931).

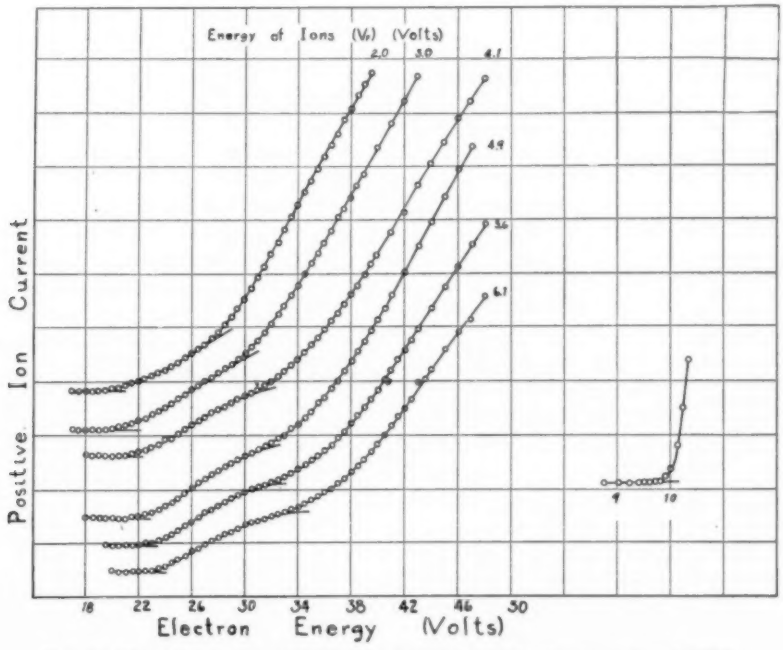


FIG. 12. The first and second ionization potentials of kinetic energy ions in HCl.

asymptote of the $^2\Sigma^+$ curve by the difference in the ionization potentials of atomic hydrogen and atomic chlorine, i.e., by 0.58 volt. Subtracting the ionization potential of HCl from $U_2-U_1-0.58$ we get $D(HCl^+\,^2\Pi)=4.76$ volts. This value is independent of the ionization potential of HCl since that quantity is contained in $U_2-U_1$ as an additive constant. Since $r_e$ is nearly the same for $HCl^+(^2\Pi)$ as it is for HCl,[30] we can do more than set a limit on $D(HCl^+\,^2\Pi)$.

When the curves for the determination of the ionization potentials of high velocity $H^+$ ions were continued to higher electron energies, a second break was found in the curves. In Fig. 12 are given a few such curves. In Table II is given a summary of the results and the calculated values of $U_2-U_1$ for the process. Within experimental error $U_2-U_1$ is constant and equal to 29.5 volts in the region $V_F=3.0$ to 6.1 volts. This indicates that the process is $HCl^+\rightarrow H^++Cl$ (excited), where the excitation energy of Cl is 11.6 volts. We note that there are several energy levels in Cl near this value, notably the so called 4° level at 11.6 volts.[19] The excitation energy is too low to give the process $HCl^{++}\rightarrow H^++Cl^+$.

### Negative ions in HCl

Negative ions, which have been identified as $Cl^-$,[14, 31] were observed. The kinetic energy of these ions was definitely less than 0.5 volt.

TABLE II. *The second ionization potentials of positive ions with kinetic energy in HCl.*

| $V_F$ | $V_i$(corrected) | $U_2-U_1=V_i-36/35V_F$ |
|---|---|---|
| 2.0 volts | 30.3 volts | 28.2 volts |
| 3.0 | 32.5 | 29.4 |
| 4.1 | 33.6 | 29.4 |
| 4.9 | 34.5 | 29.45 |
| 5.6 | 35.4 | 29.6 |
| 6.1 | 35.9 | 29.6 |
| 7.1 | 38.1 | 30.8 |
| 8.2 | 38.8 | 30.3 |
| 9.5 | 40.8 | 31.3 |

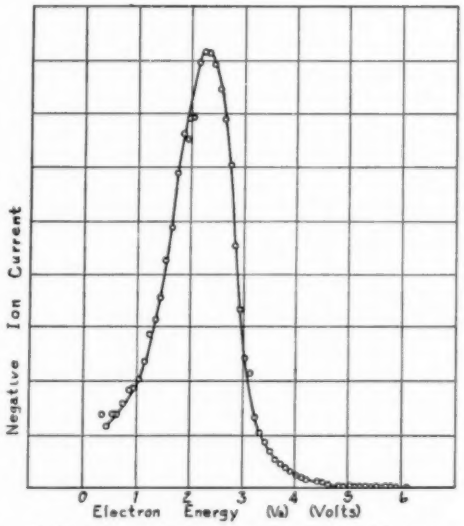


FIG. 13. Total negative ion current per unit electron current in HCl.

In Fig. 13 is given the relative efficiency of production of these ions. The curve exhibits the characteristic sharp peak usually observed for negative ions. Because the electron and the ion currents became very small in the region near an electron energy of zero, it was not possible to determine whether the relative efficiency became zero for $V_e>0$. When we extrapolate the symmetrical portion of the curve to zero efficiency, we get 0.4 volt for the onset potential. This makes the electron affinity of Cl equal to or greater than $D(HCl)-0.4=4.0$ volts. In view of our long extrapolation, the agreement with the value 3.7 volts cited by Glockler[24] is good.

The author wishes to express his gratitude to Professor John T. Tate, under whose direction the work was performed.

[31] Aston, *Isotopes* (Longmans Green & Co., 1924), p. 65.

# On the Structure of the Nuclei Between Helium and Oxygen

E. FEENBERG* AND E. WIGNER†
*University of Wisconsin, Madison, Wisconsin*
(Received October 10, 1936)

In order to test the present assumptions on nuclear forces, the theory is applied to the nuclei in which the first $p$ shell of protons and neutrons is being built up, i.e., to the nuclei with masses between 5 and 16. The Hartree-Fock approximation is used for the numerical calculations, but the more qualitative results are independent to a large degree of the approximations used. The angular momenta of the ground states appear to be given correctly by the theory. Although the wave functions used do not correspond to preformed alpha-particles, the first-order energies exhibit a marked four-shell structure. The experimental energy difference between the nuclear pairs $(N, N+1)$, $(N+1, N)$ may possibly be somewhat larger than the difference in the electrostatic energies. Support for the use of spin exchange (Heisenberg) forces to account for the singlet-triplet separation in the deuteron is found in the singlet-triplet separation inferred from the $Li^6-He^6$ normal state energy difference. However, the $B^{10}-Be^{10}$ and $N^{14}-C^{14}$ normal state differences do not fit the simple theory which is adequate for the singlet-triplet spacing in the two and six particle problems.

## I. INTRODUCTION

IT is generally accepted now that the explanation of the binding energies and scattering properties of the nuclei $n$, $H^1$, $H^2$, $H^3$, $He^3$, $He^4$ requires several kinds of forces.[1] The forces which are generally assumed at present between a proton and a neutron ("between unlike particles") are: (1) a "Majorana force" involving an exchange $P$ of the Cartesian coordinates of the two particles and (2) a "Heisenberg force" involving the product of a Cartesian coordinate exchange $P$ and a spin coordinate exchange $Q$. The Heisenberg force has about $\frac{1}{4}$ the depth of the Majorana force and the same range of action. For all present calculations the exact dependence of the potential on distance seems to be relatively unimportant and we shall use, for the sake of convenience, the usual

$$(1-g)A_{rr}e^{-r^2/r_0^2}P=(1-g)A_{rr}e^{-\alpha r^2}P \quad (1a)$$

for the Majorana force and

$$gA_{rr}e^{-\alpha r^2}PQ \quad (1b)$$

for the Heisenberg force between unlike particles. Here $A_{rr}=72\ mc^2$, $r_0=2.25\cdot10^{-13}$ cm, $g=0.22$ and $\alpha=16$ if $r$ is measured in units of $\hbar/c(Mm)^{\frac{1}{2}}=8.97\cdot10^{-13}$ cm.

The forces between like particles are less well known. Between pairs of protons and pairs of neutrons one assumes a potential with a depth $A_{rr}=41\ mc^2$ and the same width as between unlike particles.[1] This force is either assumed to involve an exchange $P$ of the Cartesian coordinates

$$A_{rr}e^{-\alpha r^2}P \quad (2a)$$

or else the scalar product of their spin operators:

$$-\tfrac{1}{3}A_{rr}e^{-\alpha r^2}(\sigma_1\cdot\sigma_2). \quad (2b)$$

The latter possibility can be considered, because of Dirac's identity for antisymmetric wave functions[2]

$$-\tfrac{1}{3}(\sigma_1\cdot\sigma_2)=\tfrac{1}{3}+\tfrac{2}{3}P_{12}, \quad (3)$$

as the sum of an ordinary and an exchange force. It is undecided, at present, which of the two forms of interaction deserves preference. In fact it has been proposed[3] to assume interactions which would give equal attractions between pairs of like and unlike particles in the singlet state. We obtain a problem having this property by assuming for the interaction between like particles the same forces as between unlike particles:[4]

$$(1-g)A_{rr}e^{-\alpha r^2}P+gA_{rr}e^{-\alpha r^2}PQ. \quad (2c)$$

* Now at the Institute for Advanced Study.
† Now at Princeton University.
[1] E. Feenberg and J. K. Knipp, Phys. Rev. **48**, 906 (1935). E. Feenberg and S. S. Share, Phys. Rev. **50**, 253 (1936).
[2] Cf. P. A. M. Dirac, *Quantum Mechanics* (Oxford, 1935), §19, §61; J. H. Van Vleck, Phys. Rev. **48**, 367 (1935).
[3] G. Breit and E. U. Condon, private communications.
[4] The assumption that the forces between all kinds of particles are the same was first put forward by L. A. Young, Phys. Rev. **47**, 972 (1935).